Gait Analysis and Biomechanical Modelling of Walking with a Reciprocating Gait Orthosis

Towards Improved Exoskeleton-Assisted Walking for Individuals with Spinal Cord Injury

TM30004: MSc Thesis Report

Linde Zegwaard

Delft University of Technology, Rijndam Rehabilitation Centre and Erasmus MC

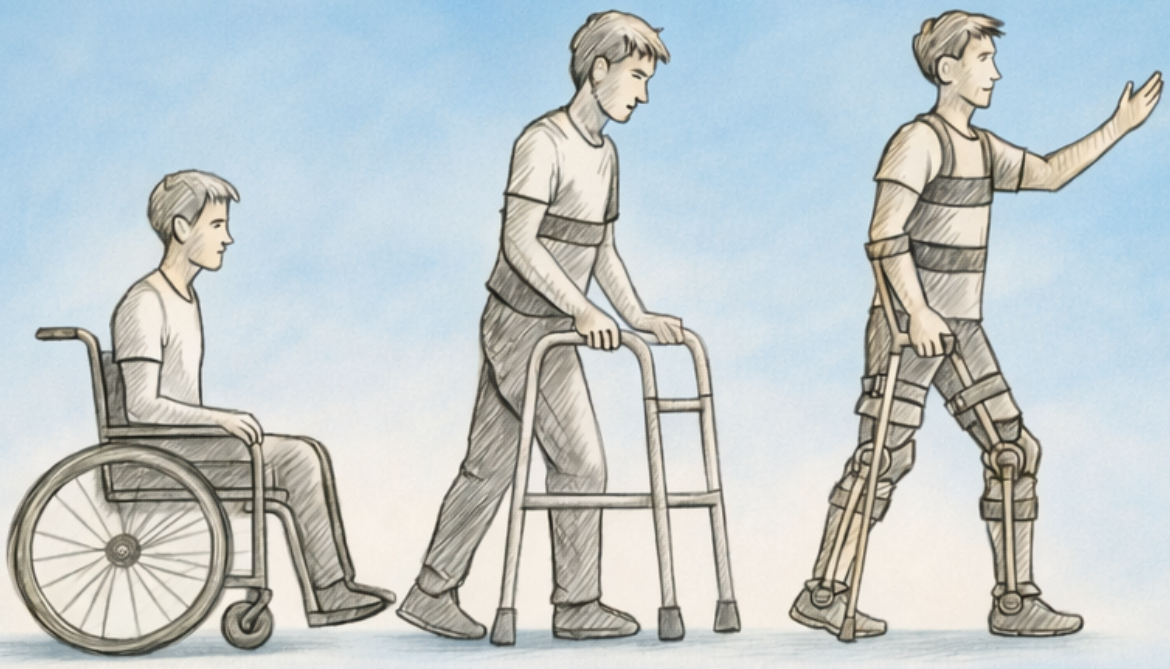

TU Delft

RIJNDAM VERBAAS JEZELF

Erasmus MC

Gait Analysis and Biomechanical Modelling of Walking with a Reciprocating Gait Orthosis

Towards Improved Exoskeleton-Assisted Walking for Individuals with Spinal Cord Injury

by

Linde Zegwaard

Student number: 4779673

Defence date: 16/01/2026

Medical Supervisor:	R. Osterthun
Technical Supervisor:	G. Smit
Project Duration:	February, 2025 - January, 2026
Department:	Rehabilitation, Spinal Cord Injury and Surgery
Institutions:	Rijndam Rehabilitation Centre and Erasmus MC
Faculty:	Mechanical Engineering, TU Delft

Cover: Generated with the assistance of generative AI (OpenAI Chat-GPT). The assistive devices and human silhouettes were inspired by reference imagery from Enabling Devices' article "Hope for Spinal Cord Injury Treatment" (https://enablingdevices.com).

TU Delft

Summary

Introduction
In individuals with spinal cord injury (SCI), wheelchair use is the primary means of mobility and is often associated with a sedentary lifestyle and an increased risk of secondary health complications. Although increasing physical activity can mitigate some of these effects, achieving sufficient activity levels remains challenging. Upright standing and walking remain important rehabilitation goals for individuals with SCI and may contribute to increased physical activity, while also being associated with improvements in body image.

Various exoskeletal systems have been developed to enable upright ambulation. However, many powered devices rely on heavy and bulky actuators, limiting their practicality in daily life. Passive orthotic devices, such as the (Advanced) Reciprocating Gait Orthosis ((A)RGO), allow walking with crutches but are associated with high physical effort and substantial upper-body demands. The Cloudwalker project aims to make exoskeleton-assisted ambulation accessible to a broader population of individuals with SCI, in part by reducing the effort required during RGO-assisted walking. This study supports its development by characterising ARGO Walker–assisted gait and developing a simplified biomechanical model to enable future simulation-based evaluation of assistive strategies and design choices aimed at reducing walking effort.

Aim
The aim of this study was to characterise ARGO Walker–assisted gait in terms of joint kinematic and kinetics, and to use these insights to develop an initial, simplified biomechanical model of ARGO-assisted gait in OpenSim.

Methods
A healthy participant performed ARGO Walker–assisted walking trials using crutches while motion capture and ground reaction forces from both feet and crutches were recorded. Joint angles and joint moments were computed from the experimental data in OpenSim using inverse kinematics and inverse dynamics. In addition, a simplified ARGO Walker model was developed in OpenSim Creator and qualitatively evaluated by prescribing experimental motion and visually inspecting human–exoskeleton alignment.

Results
ARGO Walker–assisted walking was substantially slower than healthy gait, with a mean walking speed of 0.34 m/s and a stance-dominated gait cycle (66.9% stance, 33.1% swing). Kinematic analysis revealed clear effects of the mechanical constraints imposed by the device across multiple joint kinematics, with particularly a pronounced posterior pelvic tilt and increased lumbar flexion throughout the gait cycle. Joint kinetic analysis showed markedly increased net joint moments compared with healthy reference data, particularly for hip flexion, knee extension, and lumbar extension moments.

In addition, the simplified ARGO Walker model moved largely in synchrony with the human body during walking. However, remaining misalignments between the human and exoskeleton and with experimental observations indicate that further refinement is required before simulation-based analyses can be performed.

Conclusion
ARGO Walker–assisted gait differs substantially from healthy walking due to the mechanical constraints of the device, resulting in restricted distal joint motion and increased reliance on proximal joints and crutch support. This walking strategy is associated with elevated joint moments, particularly at the lumbar region, indicating increased mechanical demands during ARGO-assisted gait. Furthermore, the developed simplified OpenSim model provides an initial framework for future simulation-based investigations of assistive strategies and design adaptations, but requires further refinement before it can be used to reliably evaluate approaches aimed at improving accessibility of ARGO-assisted walking.

Contents

1

Introduction

1.1. Spinal cord injury

Walking is a key component of human mobility, and the impact of its loss is profound. In spinal cord injury (SCI), the spinal cord's function as the pathway for motor and sensory communication between the brain and the body is disrupted, resulting in impairments below the lesion level. According to the World Health Organization (2024), over 15 million people worldwide are living with SCI, which corresponds to approximately 1 in 550 individuals[1].

Paraplegia is a common consequence of SCI and is characterized by the impairment or loss of motor and/or sensory function in the thoracic, lumbar or sacral segments of the spinal cord. In paraplegia, arm function is preserved, while the trunk, legs and pelvic organs may be affected, depending on the level of injury[2].

Individuals with SCI also experience a wide range of secondary health conditions, including pain, spasticity, and bladder and bowel dysfunction[3]. Because paralysis severely limits their ability to move independently, people with SCI typically have a markedly reduced level of physical activity compared to able-bodied individuals[4]. The resulting sedentary lifestyle, commonly observed in this population, further increases the risk of secondary health complications such as cardiovascular disease[5], type 2 diabetes [6][7], pressure ulcers[8] and ultimately, reduced life expectancy[9]. Prolonged immobilization additionally contributes to osteoporosis[10][11] and muscle atrophy[12]. Improving physical activity is therefore an important factor in maintaining health and mitigating secondary complications in individuals with SCI. Previous studies have shown that regular exercise is associated with improvements in physical capacity and muscular strength in individuals with SCI[13]. More recent evidence suggests that regular physical activity may improve glucose metabolism and cardiorespiratory fitness in this population[14].

1.2. Mobility aids and rehabilitation approaches

Mobility aids play an essential role in supporting independence after SCI. The wheelchair is the primary means of mobility for individuals with SCI and lower-limb paresis[15], and it still allows for upper-body-based physical activity, which offers important health benefits. Nevertheless, despite these benefits, many manual wheelchair users with SCI find it challenging to achieve sufficient levels of physical activity[16]. Moreover, a 2008 survey showed that walking remains a top recovery priority for individuals with SCI, regardless of injury severity, time since injury, or age at onset[17]. Moreover, technologies that enable individuals with SCI to stand or walk have been shown to improve body image and sense of well-being[18].

This has motivated the development of assistive rehabilitation approaches and mobility aids aimed at enabling upright mobility and promoting active participation in walking-related exercise. Rehabilitation approaches aiming at enabling upright mobility include body weight-supported treadmill training, orthoses, and robotic exoskeletons. Because these approaches provide external support for standing

and stepping, they allow individuals with SCI to practice walking movements in an upright position.

Despite their potential, current orthotic and exoskeletal systems still face limitations in terms of usability, adaptability, and accessibility. Many wearable exoskeletons remain heavy and bulky due to their rigid structures, actuators and batteries required for powered movement[19], reducing their practicality in everyday use.
Furthermore, several systems rely on predefined movement trajectories[19], which limit adaptability and user-driven control. As a result, users may become passive participants, rather than active contributors to the walking motion. Current systems often do not sufficiently engage the user's remaining musculature. In addition, high device costs and limited availability restrict access to these technologies for many individuals. Together, these limitations highlight the need for more lightweight, accessible, and user-engaging mobility solutions.

1.3. (Advanced) Reciprocating Gait Orthosis and the Cloudwalker

Because of the limitations of existing orthotic and exoskeletal systems, the Cloudwalker project was initiated. The Cloudwalker is a passive, lightweight exoskeleton developed by Erasmus MC, Rijndam Rehabilitation, and TU Delft, enabling exoskeleton-assisted ambulation in individuals with spinal cord injury (SCI). The device is based on the principle of the (Advanced) Reciprocating Gait Orthosis ((A)RGO), which has been developed to allow standing and ambulation in paraplegic patients through the use of walking aids such as crutches.
The ARGO consists of a hip-knee-ankle-foot orthosis that stabilizes the lower limbs and trunk while enabling reciprocal gait through a mechanically coupled connection between the two hip joints. By controlling hip extension and assisting reciprocal hip flexion, the device allows forward progression while maintaining stability [20]. The ARGO is a passive orthotic device, meaning that it does not contain motors or electrical actuators and that movement is generated entirely by the user's own effort in combination with the mechanical elements of the device. As a result, the upper body provides the main driving force during walking, and the intended users are individuals with a spinal cord lesion at approximately the thoracic level T6–T7 or lower, who retain sufficient upper-body function for moving themselves forward and walking with crutches. As a consequence of this passive, upper-body-driven gait strategy, walking with an (A)RGO requires considerable physical effort. Several studies have reported that (A)RGO systems are frequently abandoned or only minimally used in daily life, with the high energy cost and metabolic demand during ambulation identified as key contributing factors [20, 21].

The Cloudwalker project therefore aims to make exoskeleton-assisted walking accessible to a broader population of individuals with spinal cord injury by reducing the energy demand associated with ambulation, alongside other improvements.

The Cloudwalker's design focuses on being safe, lightweight, affordable, and user-friendly. The current prototype includes hinged hip joints that are connected by a flexible coupling mechanism using a Bowden cable. In contrast to the ARGO Walker, which employs a high-stiffness push–pull cable resulting in a displacement-coupled system in which motion at one hip directly enforces equal displacement at the contralateral side, the Cloudwalker incorporates elastic elements such as springs within the hip coupling. Since the Cloudwalker is not yet CE-approved, the experimental walking trials in this study were performed using the ARGO Walker. The ARGO Walker serves as the basis for the Cloudwalker and is approved for clinical use. In addition, it operates according to similar mechanical principles and walking behaviour. For these reasons, the ARGO Walker was used in this study during the experimental trials and data collection, and the term ARGO Walker is used throughout this thesis instead of Cloudwalker.

1.4. Functional Electrical Stimulation

A potential strategy to reduce the high physical effort associated with (A)RGO-assisted walking is the integration of functional electrical stimulation (FES) to activate lower-limb muscles in individuals with SCI. In particular, enabling knee flexion during swing may reduce the need for compensatory upper-body strategies for foot clearance and limb advancement. FES is a technology which uses electrical currents delivered through electrodes to induce muscle contractions, thereby activating one's own paralyzed muscles, which can replace the natural signal that should be coming from the brain[22]. When combined with orthotic devices, FES may support joint stabilization and contribute to more efficient

forward progression during gait[23]. In addition, FES has been associated with broader therapeutic benefits in individuals with SCI, including reductions in spasticity[24] and preservation of bone mass [25].

Previous studies investigating hybrid systems combining FES with orthoses have reported variable results on energy expenditure during walking. While some early work suggested reductions in upper-body effort during short distances of walking [26], a subsequent study did not demonstrate consistent reductions in energy expenditure during prolonged ambulation [27]. Moreover, a study combining FES with a powered exoskeleton suggests that FES may increase cardiorespiratory demand, indicating that its primary contribution in such contexts may lie in enhancing training intensity rather than improving walking efficiency [28].

A major limitation of FES-based assistance is the rapid onset of muscle fatigue in individuals with SCI, particularly given the high prevalence of muscle atrophy in this population. This restricts its applicability for sustained functional ambulation and currently limits its use primarily to therapeutic or experimental settings [29, 30]. Consequently, the potential of FES within RGOs continues to be investigated in several studies.

The systematic literature review conducted as part of this thesis (Appendix A) showed that experimental studies combining FES with fully passive orthotic systems are currently lacking. Existing work mainly consists of theoretical models, which suggest technical feasibility and describe design and optimized control strategies intended to share joint moment requirements between electrically stimulated muscles and the orthotic structure. Experimental studies combining FES with semi-passive systems, which include minimal motorised assistance alongside FES, have demonstrated that synchronized stimulation and mechanical support can enable stepping and short walking trials, although performance is limited by rapid muscle fatigue.

At the same time, the effectiveness of such systems is influenced by orthosis design and FES control strategies, indicating that improved coordination between mechanical support and stimulation may help mitigate some of these limitations.

This motivates the need for a biomechanical characterization of ARGO-assisted gait, which can subsequently be used as a basis for simulation-based exploration of FES-assisted gait within passive exoskeletal systems such as the Cloudwalker. Therefore, this study establishes a biomechanical baseline of ARGO-assisted gait and develops a corresponding simplified model, which together form prerequisites for evaluating whether and how FES, alternative assistive control strategies, or design modifications could be integrated to reduce physical effort during walking and serve as a reference for future theoretical simulations.

1.5. Aim of Study

The aim of this study is to characterize ARGO Walker–assisted gait by examining joint kinematics and kinetics arising from the mechanical characteristics of the device, and to use these insights to develop an initial, simplified biomechanical model of ARGO Walker–assisted gait in OpenSim.

Research question:
How can ARGO Walker–assisted gait be characterized in terms of joint kinematics and kinetics, in relation to the mechanical characteristics of the ARGO Walker?

Sub questions:

1. How does ARGO Walker–assisted gait differ from normal gait in terms of joint angles, joint moments and spatiotemporal parameters?
2. How can a simplified biomechanical model of the human-ARGO Walker system be developed in OpenSim?

2

Background

This chapter provides the medical and technical theoretical background required for this thesis, including gait cycle definitions, spinal cord injury characteristics, kinematic terminology, and inverse kinematics and dynamics. In addition, the mechanical characteristics of the ARGO Walker are described to provide context for the OpenSim model developed later in this thesis.

2.1. Gait Cycle

A gait cycle is a succession of coordinated lower-limb movements that occur during walking. It is defined as the interval between two successive heel strikes of the same foot and is also referred to as a stride[31]. Each gait cycle consists of two main phases: the stance phase and the swing phase, which alternate between the left and right leg (Figure 2.1).

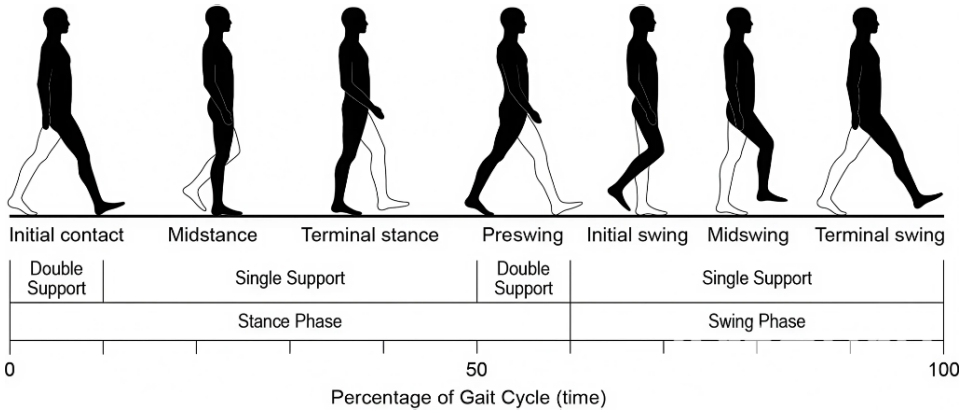

Figure 2.1: Gait cycle [32]

The stance phase comprises the period from heel strike to toe-off, during which the foot remains in contact with the ground, and typically represents approximately 60% of the gait cycle. The remaining 40% corresponds to the swing phase, which begins at toe-off and ends with the next heel strike of the same foot.

Within the gait cycle, periods of single support (only one foot in contact with the ground) and double support (both feet simultaneously in contact with the ground) can be identified, occurring as the stance phases of the left and right legs overlap in time [31]. An overview of the full gait cycle is shown in Figure 2.1.

2.2. Kinematic Terminology

2.2.1. Overview

Throughout this thesis, several body movements are analysed and presented. To ensure clarity and consistency in terminology, this section provides a visual overview of the several movements discussed in the following chapters.

2.2.2. Lower body kinematics

Hip movements

In this study, three degrees of freedom of the hip are considered: flexion/extension, adduction/abduction, and internal/external rotation. Internal rotation refers to medial rotation of the femur, whereas external rotation refers to lateral rotation, as illustrated in Figure 2.2c.

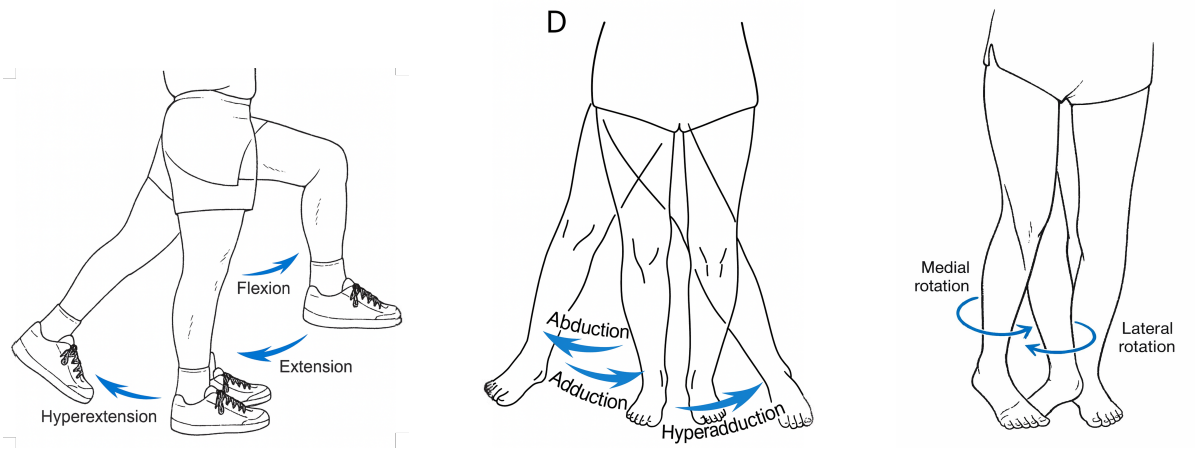

(a) Hip flexion/extension **(b)** Hip adduction/abduction **(c)** Hip internal/external rotation

Figure 2.2: Overview of hip movements[33].

Knee and ankle movements

The movements analysed in this study for the knee and ankle are shown in Figure 2.3. For the knee, flexion and extension are considered. For the ankle, dorsiflexion and plantarflexion are considered and represent the movement of the feet upwards and downwards.

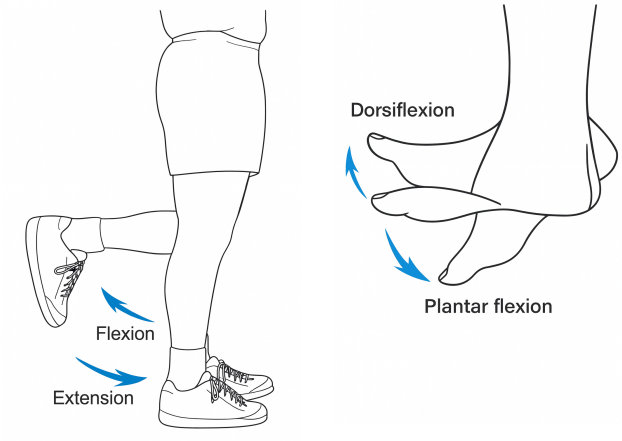

(a) Knee flexion/extension **(b)** Ankle movements (dorsiflexion/plantarflexion)

Figure 2.3: Overview of knee and ankle movements[33].

2.2.3. Pelvic and lumbar kinematics

Pelvis movements

The pelvis movements referred to in this thesis are illustrated in Figure 2.4a. Figures A and B show forward and backward pelvic tilt. Figures C and D illustrate sideways motion, also referred to as pelvic list. Left pelvic list corresponds to a drop on the left with a simultaneous hike on the right side, and right pelvic list represents the opposite pattern. Figures E and F show pelvic rotation, defined as rotation to the left or to the right. In this study, pelvic motion is expressed relative to the global reference frame.

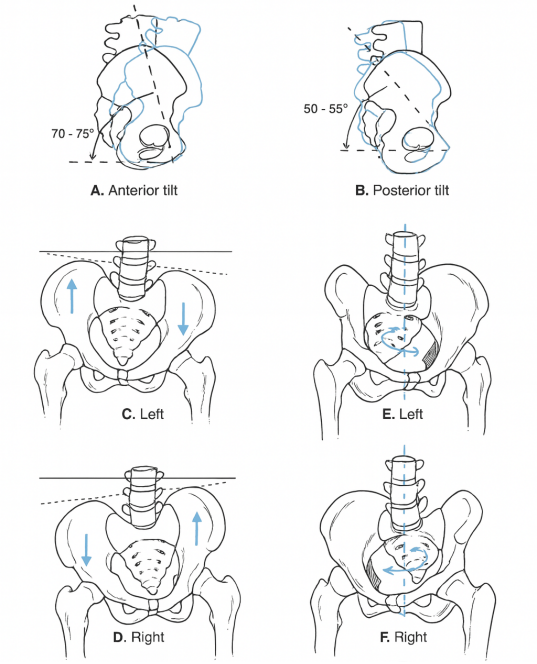

(a) Overview of pelvis movements [33].

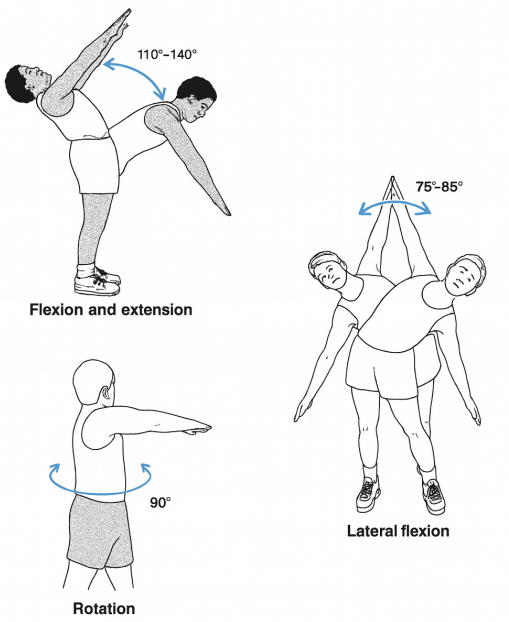

(b) Overview of lumbar movements [33].

Figure 2.4: Illustration of pelvis (left) and lumbar (right) movements considered in this thesis.

Lumbar movements

Lumbar movements refer to the motion of the lumbar spine (L1–L5), as seen in Figure 2.5.

In this thesis, lumbar motion is described using three types of movement, as shown in Figure 2.4b. The lumbar spine can bend forward and backward, which is referred to as flexion and extension. It can also bend to the left or right, and it can rotate around its vertical axis, turning the trunk to the right or to the left.

2.3. Target population for the ARGO Walker

The target population for the ARGO Walker consists of patients with a spinal cord injury at the T6–T7 level or lower.

The “T” refers to the thoracic region of the spinal column, which contains twelve vertebrae in total; T6 and T7 are located approximately in the middle of this region, as shown in Figure 2.5. Patients with lesions at or below this level typically retain enough trunk control and upper-limb strength to operate the ARGO Walker, although this also depends on individual factors such as physical fitness, strength, and age. In contrast, individuals with higher-level thoracic or cervical lesions often lack the necessary core stability and arm strength to ambulate within the ARGO Walker. Both complete and incomplete spinal cord injuries can be eligible, as long as sufficient trunk control and upper-limb strength are present, as typically observed in individuals with lesions at or below T6–T7.

As shown in Figure 2.5, the T6 level lies within the green-coloured thoracic region, corresponding to the mid-trunk area. Thoracic spinal nerves primarily contribute to trunk control, temperature regulation, and abdominal muscle control. Therefore, part of these functions is expected to be preserved in the

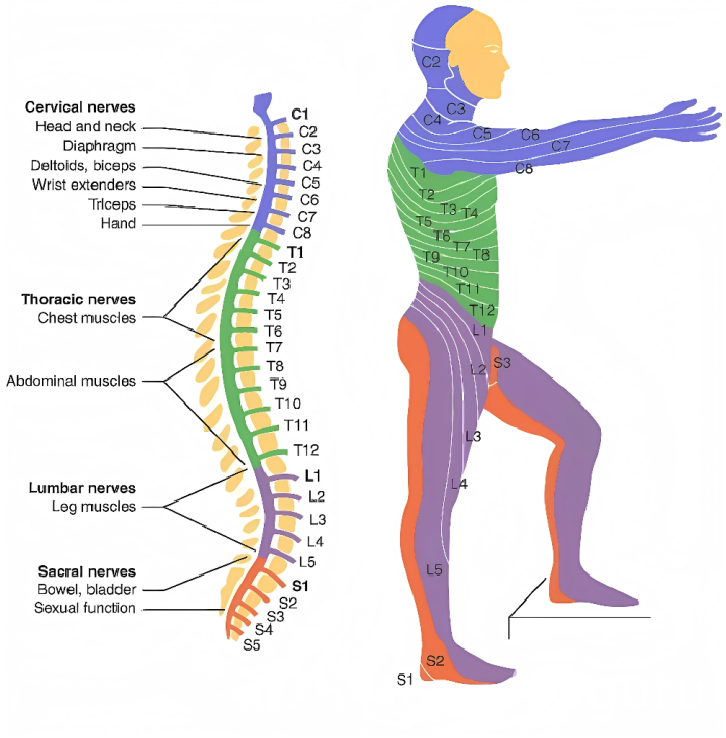

Figure 2.5: Organization of the spinal cord (with cervical, thoracic, lumbar, and sacral segments), spinal vertebrae, and a broad representation of major segmental muscles and functions of the spinal cord[34].

ARGO Walker's intended user group.

In contrast, lumbar spinal nerves are primarily responsible for lower-limb motor function, including hip, leg, and foot movement[35]. In individuals using the ARGO Walker, motor function at these levels is typically absent or impaired, requiring mechanical support for standing and ambulation.

2.4. Mechanical characteristics of the ARGO Walker

2.4.1. Overview

A detailed understanding of the mechanical design and functional principles of the ARGO Walker is essential for interpreting its gait characteristics and for subsequent modelling. These mechanical characteristics inform the definition of joint limits, coupling behaviour, and model properties implemented in the OpenSim model. The ARGO Walker is a passive RGO composed of rigid lower-limb segments connected via hip, knee, and ankle joints. Reciprocal motion between the legs is enforced by a Bowden-cable coupling at the hip joints. An overview of the ARGO Walker is shown in Figure 2.6a, with the positions of the Bowden cables at the hip and knee highlighted.

2.4.2. Hip joint coupling and motion

A Bowden cable is a flexible wire-driven transmission system consisting of an inner cable that slides within a hollow outer sheath. When the inner cable slides, mechanical force is transmitted through the system, most commonly pulling force, but pushing force can also be transmitted. Because the cable and housing are flexible, the mechanism can be routed along curved paths without losing its ability to transmit force[36].

In the ARGO Walker, the Bowden cable system is used at the hip joints to mechanically link the two legs. This means that when one leg moves forward, the other automatically moves backward, creating a reciprocal motion between the limbs. The Bowden cables at the knee joints facilitate knee flexion during donning and sit-to-stand transitions, while during walking the knee joints remain mechanically locked and are maintained in full extension throughout the gait cycle.

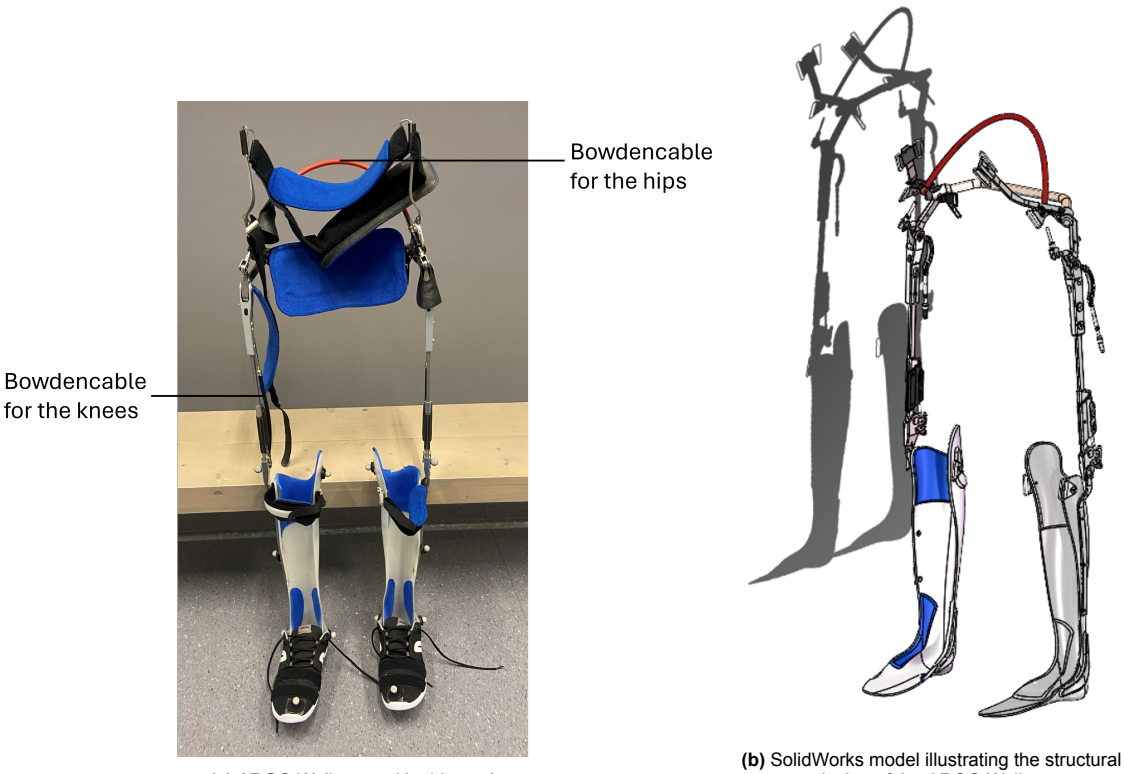

(a) ARGO Walker used in this study.

(b) SolidWorks model illustrating the structural design of the ARGO Walker.

Figure 2.6: Overview of the ARGO Walker.

The effective hip range of motion of the ARGO Walker is limited to approximately 15° of flexion and 15° of extension, as determined using a digital angle gauge. Within this range, reciprocal motion between the hips is enforced by the Bowden-cable coupling, such that forward motion of one hip induces an equal and opposite motion at the contralateral side, with no visually detectable slack or compliance. The hip coupling therefore behaves as a near-rigid mechanical connection over the functional range of motion.

2.4.3. Material assessment and structural design

The ARGO Walker is constructed from a combination of metallic and polymeric materials to provide structural rigidity while limiting overall weight. The primary materials used in the device include stainless steel, steel, aluminium, bronze, brass, and polypropylene.

The metallic components provide the required stiffness and load-bearing capacity of the orthosis, while polymer components are primarily used in the lower-leg and foot segments to reduce weight and introduce limited flexibility. An overview of the structural design of the ARGO Walker is shown in Figure 2.6b, based on the available SolidWorks model of the device.

2.4.4. Lower-leg and foot segment

As shown in Figure 2.7, the outer casing of the lower-leg segment is predominantly made of polypropylene, with varying thickness across the segment. Reinforcement around the ankle joint results in a relatively rigid connection, while the material becomes thinner toward the forefoot. This design allows a slight toe-off motion due to increased flexibility near the toe region.

2.5. OpenSim

2.5.1. Overview

For biomechanical modelling, OpenSim version 4.5 was used in this study[37]. OpenSim is an open-source software platform designed to create and analyze dynamic simulations of movement. It enables

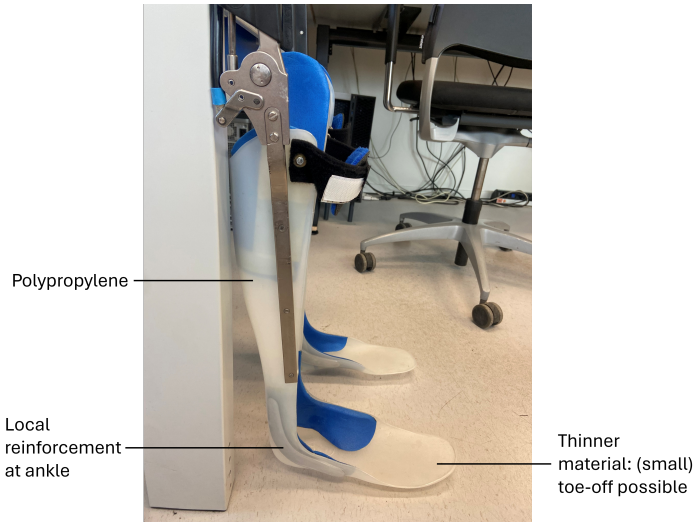

Figure 2.7: Lower-leg and foot segment of the ARGO Walker.

users to develop musculoskeletal models and perform dynamic simulations of a wide variety of movements. In this study, OpenSim was used to process motion capture and ground reaction force data. The workflow included model scaling, inverse kinematics (IK), and inverse dynamics (ID) analyses.

2.5.2. Kinematics and kinetics

In biomechanical analysis, human movement can be described using kinematics and kinetics. Kinematics refers to the description of motion without considering the forces that cause it, and includes quantities such as positions, velocities, and accelerations. Kinetics, or dynamics, on the other hand, relates motion to the forces and moments responsible for producing that motion, including joint moments and external forces such as ground reaction forces[33, 38].

In experimental gait analysis, kinematics are typically obtained from motion capture data, while dynamics are derived by combining kinematic information with external force measurements.

Figure 2.8: Illustration of inverse kinematics, showing the alignment of experimental marker data with a musculoskeletal model during walking[39].

2.5.3. Inverse kinematics

Inverse kinematics refers to the estimation of joint angles from experimentally measured marker trajectories. Unlike forward kinematics, where joint angles are prescribed to compute segment positions, inverse kinematics starts from measured marker trajectories and estimates the corresponding joint configurations.

In OpenSim, the Inverse Kinematics (IK) Tool processes each time frame of the experimental data and positions the musculoskeletal model in a pose that best matches the measured marker data at that time step. This is illustrated in Figure 2.8.

This best-fit pose is determined by minimizing the weighted sum of squared errors between the experimental and model marker positions[39].

2.5.4. Inverse dynamics

Inverse dynamics is used to compute the net joint moments required to produce an observed movement. In contrast to forward dynamics, where forces are prescribed to predict motion, inverse dynamics starts from measured kinematics and external forces to calculate the underlying joint moments responsible for the motion.

In OpenSim, the Inverse Dynamics (ID) Tool uses the model's kinematics together with measured external loads, such as ground reaction forces, to perform an inverse dynamic analysis. By solving the equations of motion derived from Newton's laws, which combine measured kinematics with external forces, the ID tool yields the net joint moments required to generate the observed motion[40].

3

Methods

This chapter describes the experimental protocol of the walking trials, data processing and gait analysis pipeline in OpenSim, and the development of the simplified ARGO Walker model used in this thesis.

3.1. Experimental walking trials

3.1.1. Ethical approval

Prior to data collection, approval for the study was obtained from the Human Research Ethics Committee (HREC) at TU Delft. During preparation of the ethical application, consultations were held with the Faculty Data Steward of the faculty of Mechanical Engineering and the TU Delft Privacy Team to determine the classification of the study and the required ethical assessments.

The study was classified as non-WMO research. Ethical approval covered both the protocol for an experienced ARGO Walker user with a spinal cord injury (SCI) and the protocol for a healthy participant. Written informed consent was obtained before participation from the participant who ultimately took part in the study.

3.1.2. Participant

The original aim was to conduct the experiment with an experienced ARGO Walker user with a spinal cord injury (SCI). Participants with SCI were eligible only if they already owned an ARGO Walker and were experienced users of the device. An eligible SCI participant was successfully recruited, and the full SCI protocol had been approved by the HREC. However, due to unforeseen circumstances, the experiment could not be carried out with this participant. Following the approved alternative plan, the study proceeded with a healthy participant.

The inclusion and exclusion criteria for the healthy participant are summarized in Table 3.1.

Table 3.1: Inclusion and exclusion criteria applied for the healthy participant in this study.

Inclusion criteria	Exclusion criteria
Must be an informed volunteer.	Has physical complaints that could affect safety or performance (e.g., balance disorders, musculoskeletal issues, back or arm pain).
Must have a height above 1.80 m.	Is unable to maintain a steady cadence over two step cycles after training sessions.
Must properly fit into the ARGO Walker after the fitting session, specifically having relatively small calf circumference.	
Must have no physical complaints that could affect the test or health.	

The participant included in this study met all eligibility criteria and was male, with a height of 194 cm and a body mass of 74 kg.

3.1.3. Laboratory setup

The walking trials were conducted in the Biomechatronics & Human-Machine Control Laboratory at TU Delft (Building 34). The laboratory is equipped with a multi-camera motion capture system comprising 12 Qualisys cameras that tracked passive reflective markers. Two additional video cameras recorded the lower body for visual validation: one focused on foot and crutch contacts with the force plates, and the other captured the overall walking pattern. Only the lower body was filmed, and participants' faces were not recorded. The system was operated using Qualisys Track Manager (QTM) software[41].

Ground reaction forces were measured using four force plates (Kistler Group, Winterthur, Switzerland, labeled A–D) [42], as shown in Figure 3.1. Plates A and B measured ground reaction forces from the right and left feet, respectively, while plates C and D measured the forces from the right and left crutches. Because the force plates are slightly elevated relative to the floor, raised platforms were placed around them to create a level walking surface.

Participants walked from one end of the setup and continued to the opposite side of the laboratory. Because additional leveling plates are not available beyond the force plates, the crutches landed on lower ground after contacting the force plates. For this reason, only the forward walking trials (from the starting side to the far end) were used for analysis, as walking in the reverse direction could alter crutch-ground contact dynamics and affect the measured ground reaction forces.

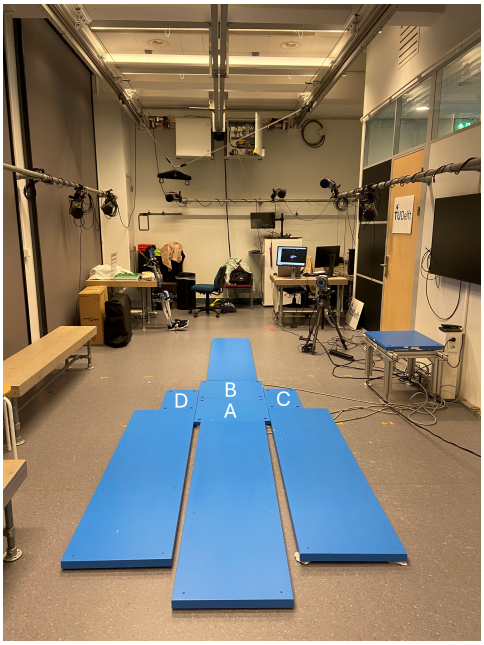

Figure 3.1: Experimental setup of the gait analysis laboratory.

3.1.4. Marker placement and static calibration

Overview

To capture the motion of the participant and the crutches, reflective markers were placed according to the Conventional Gait Model (CGM) 2.5 protocol[43], with several adaptations required for this study (Table 3.2 and Figure 3.2). Two types of markers were distinguished: anatomical markers, placed on palpable bony landmarks to define joint centres and support model scaling, and cluster markers, attached to body segments to ensure robust tracking during dynamic trials.

Adaptations to the CGM 2.5 protocol

The standard CGM 2.5 marker set was modified to meet requirements of this study, resulting in a total of 64 markers. Some markers were repositioned compared to the standard CGM 2.5 configuration. Specifically, the T2 marker was moved to the C7 location, and the T10 marker was replaced by a marker at T12. In addition, two upper arm markers on each side were renamed according to Barzyk et al. [44], resulting in the use of LUPA/RUPA and LFRM/RFRM markers. Additionally, one marker was added at the olecranon on each arm (LOLEC/ROLEC). Markers added or repositioned relative to the CGM 2.5 protocol are shown in red in Figure 3.2a.

Markers for the crutches and ARGO Walker

To track movement of the assistive devices, five markers were attached to each crutch, distributed over the cuff, handgrip, shaft, and crutch tip (Figure 3.2b). Two additional markers (LKNEE and RKNEE) were placed on the ARGO Walker, lateral to the anatomical knee markers (LKNE/RKNE). These were included to ensure continuous visibility of the knee joint during walking, as the metal frame of the ARGO Walker occasionally could obscure the anatomical knee markers during walking.

Static calibration trial

A static calibration trial was recorded with the participant standing upright inside the ARGO Walker, feet placed in neutral position and the crutches held in their usual standing posture with the crutch tips resting on the ground. This trial served as the reference for scaling the musculoskeletal model in OpenSim to the participant's anthropometry (i.e., body dimensions and segment proportions). All anatomical markers visible during this trial were used during scaling, whereas cluster and device markers were only used for dynamic tracking.

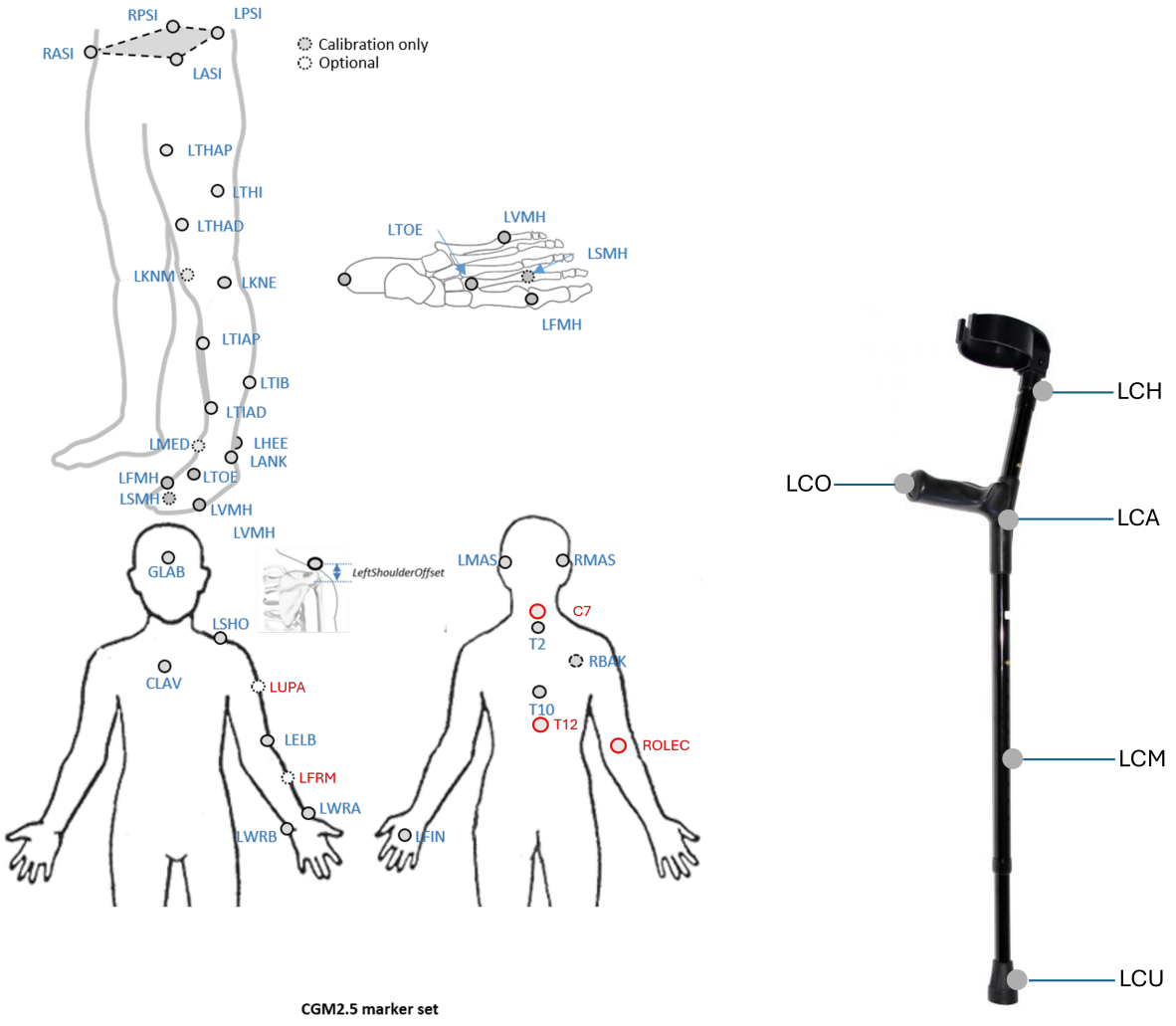

(a) Full-body marker placement (CGM 2.5)[43]

(b) Crutch marker placement.

Figure 3.2: Marker placement used in this study for motion capture.

Table 3.2: Overview of the markers used during the experiments. Cluster markers are underlined in the list of abbreviations, whereas anatomical markers are not [44, 45]. Markers placed on the crutches and the ARGO Walker are indicated with an asterisk (*).

Body part / mechanical part	Marker(s)	Explanation
Torso	CLAV	Between the clavicles, above the sternum
	LSHO/RHSO	Acromion
	C7	7th cervical vertebra
	T12	12th thoracic vertebra
	RBAK	Right back marker (for left-right orientation of the model)
Arms	LUPA/RUPA	Upper arm
	LELB/RELB	Elbow
	LOLEB/ROLEB*	Olecranon
	LFRM/RFRM	Forearm
	LWRA/RWRA	Wrist
	LWRB/RWRB	Wrist
Pelvis	LASI/RASI	Most prominent aspect of the iliac crest anteriorly
	LPSI/RPSI	Most prominent posterior aspect of the iliac crest
Legs (femur/tibia)	LTHAP/RTHAP	1/3 of the way down the center of the anterior thigh
	LTHI/RTHI	Half way down the lateral thigh
	LTHAD/RTHAD	2/3 of the way down the centre of the anterior thigh
	LKNE/RKNE	Lateral epicondyle of the femur
	LKNM/RKNM	Medial epicondyle of the femur
	LTIAP/RTIAP	Tibial tubercle: Prominence on the superior anterior tibia
	LTIB/RTIB	Half way down the lateral lower leg
	LTIAD/RTIAD	Half way down the lower leg on the crest of the tibia
Feet	LHEE/RHEE	Calcaneus: heel bone
	LANK/RANK	Lateral malleolus
	LMED/RMED	Medial malleolus
	LTOE/RTOE	2nd metatarsal-cuneiform joint
	LVMH/RVMH	5th metatarsophalangeal joint
	LFMH/RFMH	1st metatarsophalangeal joint
	LSMH/RSMH	2nd metatarsophalangeal joint
ARGO Walker	LKNEE/RKNEE*	On the ARGO Walker lateral to the knee joint
Crutches	LCH/RCH*	Upper part near the forearm cuff
	LCA/RCA*	At the shaft, just below the handgrip
	LCO/RCO*	Lateral side of the handgrip
	LCM/RCM*	Middle of crutch shaft
	LCU/RCU*	At the crutch tip (rubber end)

3.1.5. Walking trials and data collection

Prior to the measurement day, the participant completed familiarization sessions to learn how to walk with the ARGO Walker. During these sessions, the participant practiced advancing both crutches simultaneously, shifting body weight and extending the upper body to drive the ARGO mechanism, and allowing the ARGO mechanism to guide the swing phase. Breaks and feedback moments were provided as needed until a consistent gait pattern was achieved. A fitting session was performed beforehand to ensure proper alignment and comfort within the exoskeleton.
On the measurement day, the experimental session consisted of four phases: donning the ARGO Walker, marker placement, a static calibration trial, and dynamic walking trials. The static trial was recorded after all markers were positioned and served as the reference for scaling the OpenSim model.

During the dynamic trials, the participant walked back and forth over approximately 6 meters at a self-selected walking speed while motion capture and ground reaction force data were collected. Participants were allowed to rest at any moment, and marker positions were checked and adjusted between trials when necessary. At least ten complete gait cycles (right heel strike to subsequent right heel strike) were collected.

The specific activities and durations of the training and measurement sessions for the participant are summarized in Tables 3.3 and 3.4.

Table 3.3: Training session for the healthy participant.

Activity	Duration [min]
1. Walking trial	
Familiarization	10
Break and feedback	5
Practice walk	10
Second break and review	5
Initial data recording	5

Table 3.4: Test session for the healthy participant.

Activity	Duration [min]
1. Preparation	
Donning the ARGO Walker and preparation	5
Marker placement	20
2. Calibration trial	
Static trial	1
3. Walking trial	
Familiarization	5
Initial motion capture	10
Break and possible marker adjustment	5
Data collection	20

3.1.6. Data pre-processing

After completion of the walking trials, all motion capture recordings were stored on the laboratory computer and processed using Qualisys Track Manager (QTM). The preprocessing phase consisted of

assigning correct marker labels across the entire recording, checking for gaps or swaps of markers, and preparing the processed trajectories for use in OpenSim.

The labelled motion capture data were exported from QTM as `.c3d` files for further biomechanical analysis. During export, unidentified and empty trajectories were removed to reduce noise and missing marker artefacts. The resulting `.c3d` files were then converted to `.trc` and `.mot` files using a custom Python script. The `.trc` file contains the 3D marker trajectories used for inverse kinematics, whereas the `.mot` file contains the ground reaction forces, moments, and centres of pressure recorded by the force plates.

Ground reaction force (GRF) signals were baseline-corrected using the first 10 frames of each trial to compensate for any static offset in the force plates. Forces below 10 N were thresholded to zero to remove background noise and ensure accurate stance-phase detection.

Marker trajectories were exported in millimetres and subsequently converted to metres during preprocessing to match the unit conventions used in OpenSim.

To determine which parts of the data could be used for analysis, gait cycles were selected with the help of video recordings that were made during the experimental trials. Each walking trial was visually inspected to identify trials in which both feet and both crutches fully contacted the force plates, excluding trials with only partial contacts with the plates. For each suitable trial, the start and end timestamps of the walking sequence (approximately 10 seconds per trial) were noted, and only these segments were analysed in OpenSim. In total, ten walking trials were selected for analysis.

3.2. Gait analysis and data post-processing

3.2.1. Overview

Before gait of the ARGO Walker could be analysed, some previous steps were implemented in OpenSim. These steps are elaborated in this section and consisted of selecting and scaling a musculoskeletal model to the participant's anatomy, adding crutches, and performing inverse kinematics and inverse dynamics. The inverse analyses presented in this study were performed on the human biomechanical model without the exoskeleton and with the muscles removed. A schematic overview of the pipeline is provided in Figure 3.3.

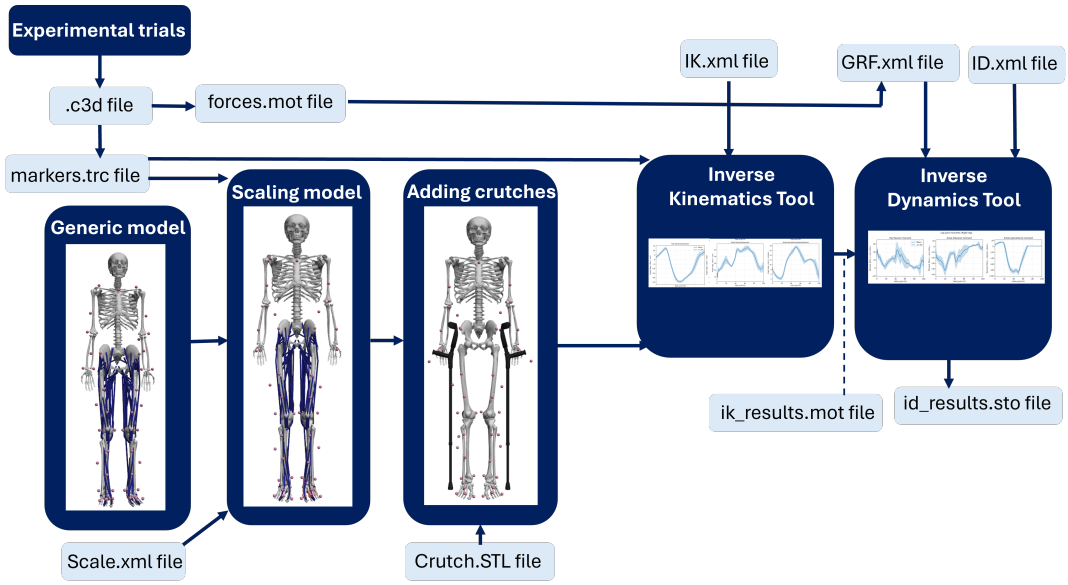

Figure 3.3: Flowchart of the OpenSim analysis workflow used in this study.

3.2.2. Base model selection

For this study, the musculoskeletal model RajagopalLaiUhlrich2023.osim was used, which integrates the improvements on, amongst others, muscle properties introduced by Lai et al. (2017)[46] and Uhlrich

et al. (2022)[47] into the original Rajagopal2016 model[48].

The model provides a full-body representation with 33 degrees of freedom including both upper- and lower-limb segments. Although upper-body muscles are absent, the model was selected because it is often used for simulating human gait and, unlike models that include only the lower limb(s), allows analysis of upper-body motion as well.

Since the target user group consists of individuals with spinal cord injury, the lower-limb muscles of the model were removed. These muscles are typically non-functional in this population and would therefore not contribute to movement generation. To enable lower-limb motion in the absence of muscles, coordinate actuators were added for each available degree of freedom.

Additionally, the original RajagopalLaiUhlrich2023 model does not include wrist flexion and wrist deviation degrees of freedom. These DOFs were added to accurately capture the upper-limb kinematics required for modelling crutch-assisted gait.

The subsequent modelling of the ARGO Walker exoskeleton, including the addition of segments, joints, constraints, and attachments, was performed primarily using OpenSim Creator[49], an open-source software for creating and modifying OpenSim models.

3.2.3. Scaling to participant anthropometry

The model was scaled to the participant using the OpenSim Scale Tool and a custom `scale.xml` configuration file. Marker trajectories from the static calibration trial (`.trc`) were used to adjust segment lengths and marker positions.

Marker weights were iteratively refined to minimise the influence of less accurately placed markers, achieving a maximum anatomical marker error below 2 cm, which was considered acceptable for a good fit between the model and the participant's anatomy and for subsequent kinematic analyses.

To evaluate the quality of each scaling run, the `reportMarkerErrors.m` script was used to inspect marker errors. Based on these results, scaling parameters were iteratively refined until satisfactory accuracy was achieved.

3.2.4. Integration of crutches into the model

The participant's crutches were modelled as rigid bodies imported into OpenSim from `.stl` geometry files, which were obtained from the instrumented crutch models developed by Febrer-Nafría et al. [50].

Each crutch was attached to the corresponding hand segment using a `WeldJoint`, reflecting the physical fixation of the participant's forearm within the crutch cuff. During walking, the crutches made intermittent contact with the ground. Ground reaction forces acting at the crutch tips were directly measured using two force plates placed under the crutches, and these forces were applied to the model during the inverse dynamics analysis.

3.2.5. Inverse kinematics

After scaling the model to the participant, inverse kinematics (IK) was performed using the OpenSim Inverse Kinematics Tool and a custom `IK.xml` configuration file. Marker weights in the inverse kinematics tool were assigned to prioritise anatomical markers, including the pelvis markers (ASIS and PSIS) and trunk markers such as C7, T12, and the clavicula marker (CLAV), while cluster markers (underlined in Table 3.2) were assigned lower weights to reduce the influence of soft tissue artefacts. For some individual markers, weights were further adjusted based on the participant's posture and individual characteristics. Because the participant adopts a slightly forward-hanging shoulder posture, which differed from the pose of the generic model, the corresponding markers on both acromion (RSHO/LSHO) were assigned a lower weight compared to the clavicula, C7, and T12 markers.

The IK analysis generated an `ik_results.mot` file containing time series of joint angles representing hip, knee, and ankle kinematics, as well as pelvic and lumbar motion. These outputs were subsequently post-processed and visualised using custom Python scripts.

3.2.6. Inverse dynamics

Inverse dynamics (ID) was performed using the OpenSim Inverse Dynamics Tool with a custom `ID.xml` setup file. Joint moments were computed from the inverse kinematics–derived kinematics and the external forces measured at the feet and crutches, and were stored in the resulting `id_results.sto` file. The ID outputs were subsequently post-processed and visualised using custom Python scripts. These processed results were used to evaluate joint moment patterns during ARGO-assisted gait.

3.2.7. Data post-processing and spatiotemporal gait parameter extraction

Prior to visualisation of the results in Python, the OpenSim outputs were post-processed to enable gait analysis. Key gait events, including heel strike and toe-off of both the left and right foot, were identified based on the magnitude of the ground reaction forces. Foot contact was defined as a ground reaction force exceeding a threshold of 50 N for at least 10 consecutive samples to reduce the influence of noise. Heel strike was defined as the onset of such a contact period, whereas toe-off was defined as the end of the contact period.

Because consecutive heel strikes of the same foot could not be measured directly, as only one force plate was available per foot, the gait cycle was not defined from heel strike to heel strike measured by the force plates. Instead, for the right leg, the gait cycle was defined to start at the first right heel strike on the force plate and to end after a stride duration estimated from successive peaks in right hip flexion obtained from inverse kinematics. This approach allowed the start (0%) and end (100%) of each gait cycle to be determined for normalisation and visualisation of the data. Heel strike and toe-off events of both feet were indicated in the resulting plots.

Crutch–ground contact was also visualised in the plots. Complete crutch contact could not be identified from the force data, as each crutch contacted the ground twice within a gait cycle, while only one force plate was available per crutch. Consequently, only the first crutch–ground contact per gait cycle was captured in the force data. Crutch contact was therefore identified from marker kinematics rather than from ground reaction forces, assuming ground contact when the forward velocity of the lowest crutch marker approached zero. In the figures in the Results section, the yellow shaded regions indicate the mean timing of crutch–ground contact across multiple gait cycles, with darker shading representing more frequent contact and lighter shading representing less frequent contact.

To characterise the overall walking pattern, spatiotemporal gait parameters were extracted from the processed data. These parameters included step length, stride time, cadence, stance-to-swing ratio, and walking speed, and were calculated using a custom Python script. Spatiotemporal parameters were computed within selected time segments of approximately 10 seconds per trial, for a total of ten trials, centred around stepping on the force plates. Step time was defined as the time interval between consecutive contralateral heel strikes, and cadence was calculated as steps per minute based on the step time. Stride duration was estimated from successive peaks in right hip flexion obtained from inverse kinematics, as described above. Right stance percentage was defined as the proportion of the right gait cycle from right heel strike until right toe-off, while swing percentage was defined as the remaining part of the cycle. Step length was estimated from the change in centre-of-pressure position between consecutive contralateral heel strikes. Walking speed was estimated as the mean ratio of step length to step time.

3.3. Biomechanical modelling of the ARGO Walker

3.3.1. Overview

In this section, the development of the ARGO Walker exoskeleton model in OpenSim is described. The aim of this model was to create a simplified representation of the ARGO Walker that could be integrated with a skeletal model to study ARGO-assisted gait, rather than to capture every mechanical detail of the device. The modelling approach therefore focused on capturing the key functional characteristics of the ARGO Walker through the definition of design requirements, segment geometries, joint structures, and attachment strategies used to integrate the device with the skeletal model. An overview of the main modelling steps is shown in Figure 3.4. These steps are described in more detail in the following subsections.

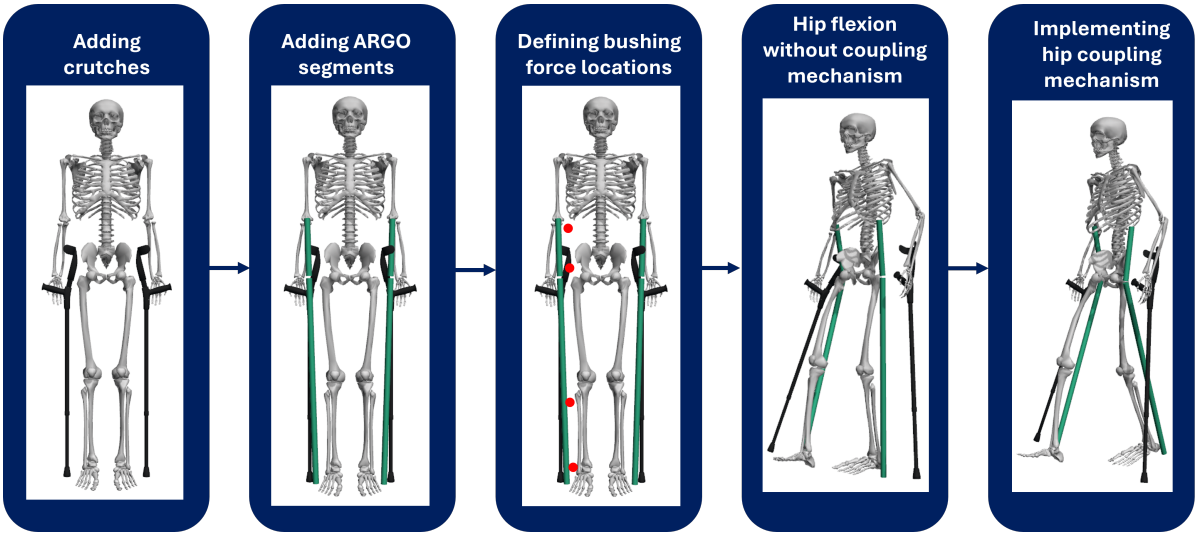

Figure 3.4: Overview of model development steps in OpenSim, including crutch integration, ARGO segment definition, bushing force locations, hip flexion evaluation, and implementation of the hip coupling mechanism.

3.3.2. Design requirements and modelling assumptions

To model the ARGO Walker in OpenSim, the device was simplified into four rigid, cylindrical segments, two on each side of the body. As shown in Figure 3.5a, the two red circles indicate the mechanical joint locations in the ARGO Walker device. Because the knee joint of the ARGO Walker is mechanically locked during walking, this joint was not modelled, and the upper and lower leg were combined into a single segment. The upper red circle in the figure corresponds to the attachment point connecting the trunk segment (L1/R1) to the leg segment (L2/R2). This is modelled as the BallJoint, as seen in Figure 3.5b. Each side of the ARGO Walker was therefore represented by a trunk segment and a leg segment.

The red arrows highlight the strap locations, which represent the contact interfaces between the exoskeleton and the human body.

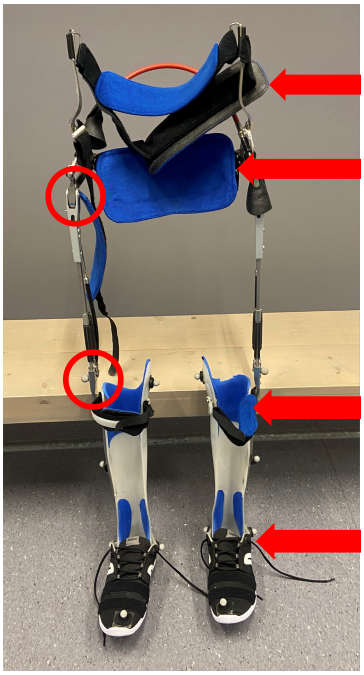

(a) The ARGO Walker showing joint locations (circles) and human–exoskeleton attachment points (arrows).

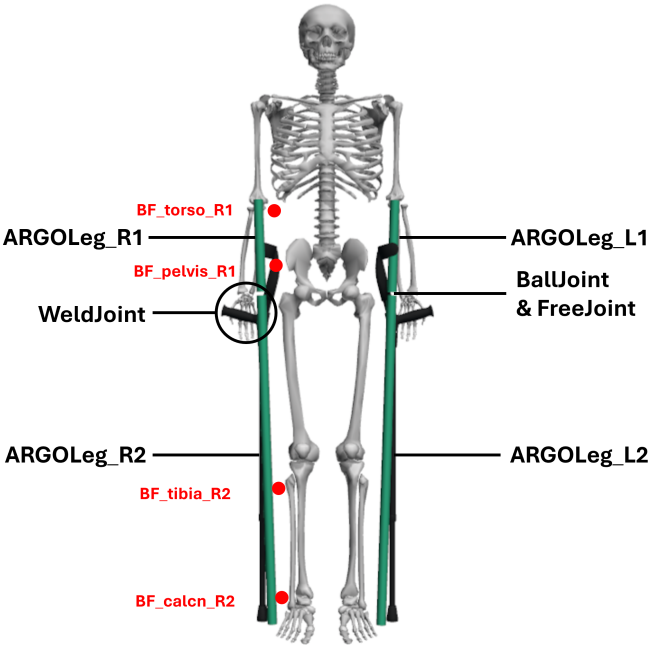

(b) ARGO Walker representation in OpenSim Creator, including segment definitions and joint types. The red dots indicate the approximate locations where the bushing forces were applied.

Figure 3.5: The physical ARGO Walker and the simplified model.

3.3.3. ARGO Walker components and joint modelling

Table 3.5 provides an overview of the ARGO Walker components that were implemented in the OpenSim model.

In the OpenSim model, the ARGO Walker was represented using rigid segments whose geometries were simplified to homogeneous cylindrical shapes. In OpenSim Creator, each segment was defined by its mass, length, radius, and mass moment of inertia. The segment masses were assigned based on the estimated weight distribution obtained from the SolidWorks model. As the mass moments of inertia of the physical ARGO Walker components were not available, the inertial properties of the simplified exoskeleton segments were calculated using the corresponding formulas[51]. Each segment was modelled as a solid cylinder with its centre of mass located at the geometric centre. The resulting inertia tensor was computed based on the assigned segment mass and the corresponding length and radius of the cylindrical geometry. In OpenSim, the inertia properties are specified as $[I_{xx}\ I_{yy}\ I_{zz}\ I_{xy}\ I_{xz}\ I_{yz}]$, defined about the segment's centre of mass. The coordinate frames of the ARGO Walker segments were aligned with the longitudinal axis of each cylindrical segment, which aligned with the y-axis. Consequently, the products of inertia I_{xy}, I_{xz}, and I_{yz} were assumed to be zero. The moment of inertia about the longitudinal axis (I_{yy}) was computed using

$$I_{\parallel} = \frac{1}{2} m r^2, \tag{3.1}$$

where m is the segment mass and r is the cylinder radius. The moments of inertia about the two axes perpendicular to the longitudinal axis (I_{xx} and I_{zz}) were computed using

$$I_{\perp} = \frac{1}{12} m \left(3r^2 + L^2\right), \tag{3.2}$$

where L represents the length of the cylindrical segment.

Both the length and radius of the ARGO Walker segments used for inertia calculations were estimated from the dimensions of the corresponding cylindrical segments in the model. The actual lengths of the cylindrical segments were 0.312 m and 0.945 m, which closely match the model dimensions. A segment radius of 0.015 m was assumed in the model.

Table 3.5 summarises the implemented components, their masses, and the joints through which they connect to the rest of the model.

Table 3.5: Overview of ARGO Walker exoskeleton components implemented in OpenSim.

Component	Mass [kg]	Length (model) [m]	$[I_{xx}\ I_{yy}\ I_{zz}]$ $[\mathrm{kg\,m^2}]$	Connected via joint(s)
ARGOLeg_R1/L1 (trunk segment)	0.9	0.282	[0.006015, 0.000101, 0.006015]	BallJoint (with R2/L2)
ARGOLeg_R2/L2 (leg segment)	2.0	1.01	[0.170129, 0.000225, 0.170129]	FreeJoint (with ground)
Crutch segments	0.55	-	-	WeldJoint (with hands)

To accurately represent the mechanical behaviour of the ARGO Walker, the joint types between the exoskeleton segments were defined based on the range of motion measured in the physical device and the range of motion seen during the walking trials (Table 3.6). The relative motion between the trunk segment (L1/R1) and the leg segment (L2/R2) was implemented using a BallJoint. This joint determines how the trunk segment (L1/R1) moves with respect to the leg segment (L2/R2). The joint centre was aligned with the anatomical hip joint in the skeletal model so that both the human and exoskeleton hips act around the same location.

The connection between the exoskeleton and the environment was modelled using a FreeJoint between the leg segment (L2/R2) and ground. This joint provides the global placement and rotational freedom required for the exoskeleton to move within the OpenSim environment. The rotation joint centre point was again positioned at the same height as the hip joint.

Some modelling choices, particularly those related to joint ranges of motion and allowed degrees of freedom, were informed by the kinematic data obtained during the experimental walking trials, which are presented in the Results section. Inspection of this data revealed some deviations from the ranges that were expected based on inspection of the ARGO Walker.

For the flexion–extension motion of the exoskeletal legs, a mechanical range of motion of approximately ±15° was measured directly on the device. However, analysis of the experimental kinematics (Figure 4.1) shows that the hip flexion–extension angles ranged approximately from 13° of flexion to −25° of extension. These angles are defined relative to the pelvis, which exhibited substantial tilt during the gait cycle, as also seen in Figure 4.1, thereby explaining the larger apparent range of motion. In the ARGO Walker model, the range of motion of the exoskeletal legs was therefore still limited to ±15° in forward and backward rotation (flexion/extension movement), despite the larger hip flexion–extension angles observed experimentally. In OpenSim Creator, joint ranges of motion are specified in radians and were converted from degrees using the following relation:

$$\theta_{\mathrm{rad}} = \theta_{\mathrm{deg}} \cdot \frac{\pi}{180} \tag{3.3}$$

Accordingly, the range of motion was defined from −0.262 rad to 0.262 rad.

The hip joint of the physical ARGO Walker was identified as a hinge joint, indicating that abduction and adduction were not intended motions of the device. Nevertheless, a small range of motion was observed during the experimental trials, with values of approximately 5° of adduction to 12° of abduction. These motions are also reported in Table 3.6. To accommodate these experimentally observed movements, a BallJoint was therefore selected instead of a HingeJoint for the hip joint representation of the ARGO Walker. In the ARGO Walker model, lateral hip motion of the exoskeletal legs was therefore constrained to a range of −8° (adduction) to +15° (abduction), consistent with the experimentally observed values. The corresponding range of motion was defined from −0.140 rad to 0.262 rad.

Finally, the internal–external rotation degree of freedom at the joint between the upper and lower exoskeletal leg segments is disabled. Although small internal–external rotation angles at the hips were observed in the experimental kinematic data, these rotations are most likely attributed to motion of the user's legs within the ARGO Walker rather than to rotation of the exoskeletal structure itself. Despite being secured by straps, some relative movement between the user's legs and the exoskeleton is expected. The ARGO Walker is therefore assumed to be mechanically constrained in this rotational direction, and no axial rotation of the exoskeletal leg segments relative to the upper exoskeleton is expected based on the device design.

Table 3.6: Joint definitions and mechanical properties of the ARGO Walker model. F/E=flexion/extension. A/A=abduction/adduction. ROM=range of motion.

Joint	Type	DOF	ROM of ARGO legs (theoretical)	ROM of hip joint (experimental)	Parent frame	Child frame
ARGO hip joint (L/R)	BallJoint	3	F/E: -15° to $+15^\circ$, A/A: 0° to 0°	F/E: -25° to $+15^\circ$, A/A: -5° to $+12^\circ$	ARGOLeg_L2/R2	ARGOLeg_L1/R1
Rotation w.r.t environment	FreeJoint	6	-	-	ground	ARGOLeg_R2/L2
Crutch–hand connection	WeldJoint	0	none (rigid)	none	hand_r / hand_l	crutch_r / crutch_l

3.3.4. Bowden cable coupling

The Bowden cable was modelled as a reciprocal coupling between the left and right exoskeleton legs. A `CoordinateCouplerConstraint` was used to enforce a functional relationship between the hip rotation angles of both sides, such that the motion of one leg directly drives the opposite leg. The coupling was defined using a `SimmSpline` function that implements a linear mapping from the right-leg hip rotation, `ARGOHip_R2_rz`, (independent coordinate) to the left-leg hip rotation, `ARGOHip_L2_rz`, (dependent coordinate). The `rz` coordinate denotes rotation about the local z-axis and represents forward and backward rotation of the exoskeleton hip joints. The resulting mathematical relationship is:

$$\theta_{\text{left}} = -\theta_{\text{right}}. \tag{3.4}$$

This relationship indicates that a forward swing of one leg produces an equal and opposite rotation of the other leg, mimicking the passive reciprocal action of the Bowden cable.

3.3.5. Attachment of the exoskeleton to the human model

To integrate the ARGO Walker with the skeletal model, local human–exoskeleton interaction interfaces were defined at the physical attachment locations between the user and the exoskeleton. These mechanical interactions between the user and the exoskeleton were represented using OpenSim's BushingForce elements. A BushingForce models the connection between two bodies as a three-dimensional spring–damper system, generating forces and moments in response to relative translational and rotational deviations between two frames. This formulation allows compliant behaviour at the human–exoskeleton interface and is used to approximate deformation of soft tissue and attachment straps in simulations as the user moves relative to the exoskeleton [52]. BushingForces are most suitable for strap-based attachments, where only limited relative motion between the exoskeleton and the body is expected. This approach is therefore commonly used in musculoskeletal simulations to represent compliant contact between the human body and orthotic or assistive devices. The red dots in Figure 3.5b illustrate the locations where bushing forces were applied on the right side of the model. Corresponding mirrored locations were defined on the left side.

Implementing bushing forces requires information on the relative motion between the user and the exoskeleton, which can be obtained from motion capture markers placed on the exoskeleton and the user, as well as stiffness and damping parameters that are typically derived from mechanical testing of the connecting straps or literature. In the present study, only a single reflective marker per exoskeleton side was available, which was insufficient to reconstruct relative motion between the user and the exoskeleton during gait. As a result, compliance parameters of this contact could not be derived from the experimental data.

Therefore, representative bushing parameters were adopted from the literature. Sahetapy (2024) experimentally quantified stiffness, damping and migration of exosuit cuffs, which are soft attachment elements such as straps or bands that connect an exosuit to the body, to study how deformation at the contact interface affects muscle activation in a passive shoulder exosuit [53]. In that study, stiffness and damping were identified by fitting a linear spring-damper model to force–displacement and force–velocity relationships obtained from the experimental data.

Using these values as a basis, translational bushing stiffness and damping in the present model were scaled according to the expected strength of the mechanical coupling at each attachment location. Lower values were assigned at the pelvis and torso to reflect greater soft-tissue compliance, whereas higher values were used at the lower leg and foot to represent a tighter mechanical coupling. Rotational stiffness and damping were chosen to permit small relative rotations between the exoskeleton and the body, without causing unstable behaviour of the simulation.

Table 3.7: Bushing stiffness and damping parameters used to model the mechanical coupling between the human body and the ARGO Walker exoskeleton. Values were informed by literature-reported cuff compliance ranges [53] and scaled according to attachment location.

Attachment location	Translational stiffness [N/m]	Translational damping [Ns/m]	Rotational stiffness [Nm/rad]	Rotational damping [Nm/(rad/s)]
Pelvis-L1/R1	2140	124	1500	15
Torso-L1/R1	2140	124	1500	15
Tibia-L2/R2	6000	120	2500	25
Calcaneus-L2/R2	6000	120	2500	25

For this part of the model, several modelling choices were again revised based on insights obtained from the experimental kinematic data. Initially, a bushing force was defined at the level of the pelvis, as one of the ARGO Walker straps is located approximately at pelvic height (Figure 3.5a). However, the kinematic data revealed substantial pelvic tilt during walking, as illustrated in the lower-right plot of Figure 4.1. When this pelvic bushing force was combined with the other three attachment points, the model would become numerically unstable, resulting in large relative displacements and unrealistically high interaction forces, and preventing the simulation from converging to a feasible solution. For this reason, the pelvic bushing force was disabled in the model. Its location and parameter definitions remain included.

3.3.6. Evaluation of the model in OpenSim

The model was qualitatively evaluated to assess whether the ARGO Walker followed the motion of the human model in a realistic manner. The relative alignment between the exoskeleton and the human body was visually inspected at different phases of the gait cycle.

The MATLAB script `prescribeMotionInModel.m`, provided in the OpenSim documentation, was adapted for use with the current model and motion files. The script was modified such that the simulation start time matched the start time of the motion file instead of being set to zero. In addition, the ARGO-specific coordinates were excluded from the prescribed motion to allow these degrees of freedom to respond to the model dynamics rather than being prescribed.

The adapted script was then run using the final OpenSim model and a motion file obtained from inverse kinematics. This resulted in a `Prescribed.osim` model, which was subsequently run in a forward-dynamics simulation and visually inspected in OpenSim Creator at several points in the gait cycle.

4

Results

This chapter presents the results of the experimental gait analysis, focusing on lower- and upper-body joint kinematics and kinetics during walking with the ARGO Walker, compared with healthy reference gait. In addition, the behaviour of the developed ARGO Walker model is qualitatively evaluated across the gait cycle.

4.1. Gait analysis and data post-processing

4.1.1. Model scaling results

In the final scaled model, the RMS (Root Mean Square) marker error after running Inverse Kinematics was 1.36 cm, meeting the predefined target of an RMS error below 2 cm. This indicates that the model was scaled appropriately and could be used reliably for subsequent Inverse Kinematics and Inverse Dynamics analyses.

4.1.2. (Joint) kinematics

Overview

In this section, the spatiotemporal parameters and the lower- and upper-body joint kinematics during gait with the ARGO Walker are presented.

Spatiotemporal parameters

Table 4.1: Spatiotemporal gait parameters during ARGO Walker gait compared to normative reference values[54, 55].

Parameter	Mean (ARGO gait)	SD (ARGO gait)	Healthy reference gait
Cadence (steps/min)	36.0	2.1	111
Speed (m/s)	0.34	0.03	1.56
Stride time (s)	3.41	0.15	1.09
Stance/Swing (%)	66.9/33.1	2.3	60/40
Step length (m)	0.56	0.03	0.7

The spatiotemporal parameters show that walking with the ARGO Walker is substantially slower than healthy reference gait. Cadence (36 steps/min) and speed (0.34 m/s) are both markedly reduced compared to normative values. Stride time is more than twice as long as in healthy reference gait, indicating a slower stepping rhythm. The stance-to-swing ratio shifts toward prolonged stance (66.9%/33.1%).

Static pose joint angles

The joint angles measured in the static pose, corresponding to the participant standing upright in the exoskeleton with the crutches in contact with the ground, are presented in Table 4.2 and provide context for the dynamic kinematic results presented in the following sections.

Table 4.2: Static pose angles for various joint movements.

Variable	Angle in static pose
Hip flexion/extension	$\sim -10°$
Hip adduction/abduction	$\sim 0°$
Hip internal/external rotation	$\sim 0°$
Knee flexion/extension	$\sim 15°$
Ankle dorsiflexion/plantar flexion	$\sim 10°$
Pelvis tilt	$\sim 10°$
Pelvis list	$\sim 0°$
Pelvis rotation	$\sim -5°$
Lumbar flexion/extension	$\sim -25°$
Lumbar bending	$\sim 0°$
Lumbar rotation	$\sim 0°$

In the static pose, the most pronounced deviation from neutral is observed in lumbar flexion, with an angle of approximately 25°. The pelvis exhibits a posterior tilt of approximately 10°, while the hips are positioned at around 10° of extension relative to the pelvis. In addition, the knees are flexed with approximately 15°, and the ankles are positioned in dorsiflexion of approximately 10° during static standing.

Lower body kinematics

In Figure 4.1, the mean joint kinematics (±1 SD) of the right hip, knee, ankle, and pelvis are shown across ten gait cycles. To illustrate deviations from normal gait, dashed red curves represent reference kinematics from healthy, unassisted walking. These reference data were taken from the normal.mot file included in OpenSim's Gait2392 Tutorial 1 dataset [56, 57]. The dataset was generated by the OpenSim team based on experimental gait data reported in two previously published studies [58, 59].

To assess how representative these reference kinematics were, they were qualitatively compared with healthy gait data reported in other studies, including the dataset by Camargo et al. (2021) [60]. While the Camargo dataset showed some clear differences in magnitude for several parameters, comparison with additional literature indicated that the OpenSim reference kinematics aligned more closely with reported values from other studies. Based on this qualitative comparison, the OpenSim reference dataset was selected as the most appropriate reference dataset for illustrating general differences between ARGO-assisted and healthy gait.

Table 4.3 summarises the percentages in the gait cycle of the main gait cycle events shown in the figures.

Table 4.3: Gait events in the gait cycle of the right foot

Gait event	Mean percentage in gait cycle	SD
Right heel strike	0%	0%
Right toe-off	66.9%	2.3%
Left heel strike	49.1%	1.7%
Left toe-off	11.7%	4.5%

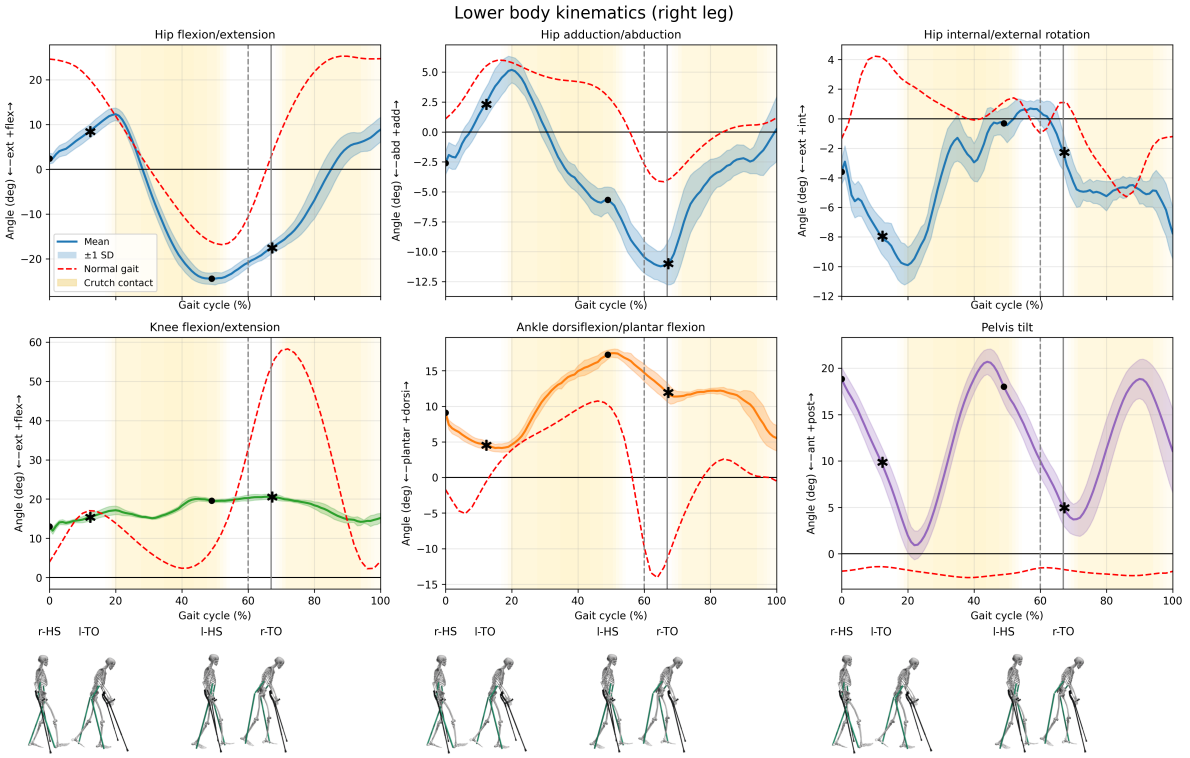

Figure 4.1: Lower-body kinematics of the right leg during gait with the ARGO Walker exoskeleton. Solid coloured lines show the mean joint angles across ten gait cycles, with shaded areas indicating ±1 SD. Dashed red curves represent reference kinematics from a healthy gait dataset. Vertical grey lines indicate right-foot toe-off, marking the transition from stance to swing (reference: 60%, experimental: ~67%). Black dots denote right and left heel strikes (r-HS, l-HS), and black asterisks indicate left and right toe-off events (l-TO, r-TO). Yellow shading indicates periods of crutch–ground contact.

Hip kinematics

For hip flexion and extension, the experimental data show an asymmetric pattern, with peak hip flexion of about 13° and peak hip extension up to 25°. In contrast to healthy gait, hip flexion does not decrease immediately after heel strike, but elevates during early stance before progressing toward extension during mid-stance.

Hip adduction-abduction exhibits greater variability than reference gait. In particular, increased hip abduction is observed, while overall hip adduction is reduced throughout the gait cycle.

Hip internal–external rotation differs from reference gait, with the hip remaining externally rotated throughout the gait cycle.

Knee kinematics

Knee flexion is strongly restricted during ARGO-assisted gait, with less than 10° of residual motion throughout the gait cycle. As a result, the characteristic knee flexion peak during swing observed in healthy gait is absent, consistent with the knee-locking mechanism of the exoskeleton.

Ankle kinematics

Ankle motion during ARGO-assisted gait is markedly restricted compared to reference gait. The ankle remains dorsiflexed throughout stance and swing, with no plantarflexion observed during late stance and early swing, a phase that in healthy gait is characterised by a plantarflexion peak associated with push-off. During early and mid-swing, ankle angles remain relatively constant, in contrast to the larger variations seen in healthy gait.

Pelvic kinematics

Pelvic motion during ARGO-assisted gait is characterised by a pronounced posteriorly tilted orientation throughout the gait cycle, with pelvic tilt fluctuating between approximately 0° and 20°. In contrast, healthy gait typically shows only a small anterior tilt with minimal variation.

Upper body kinematics

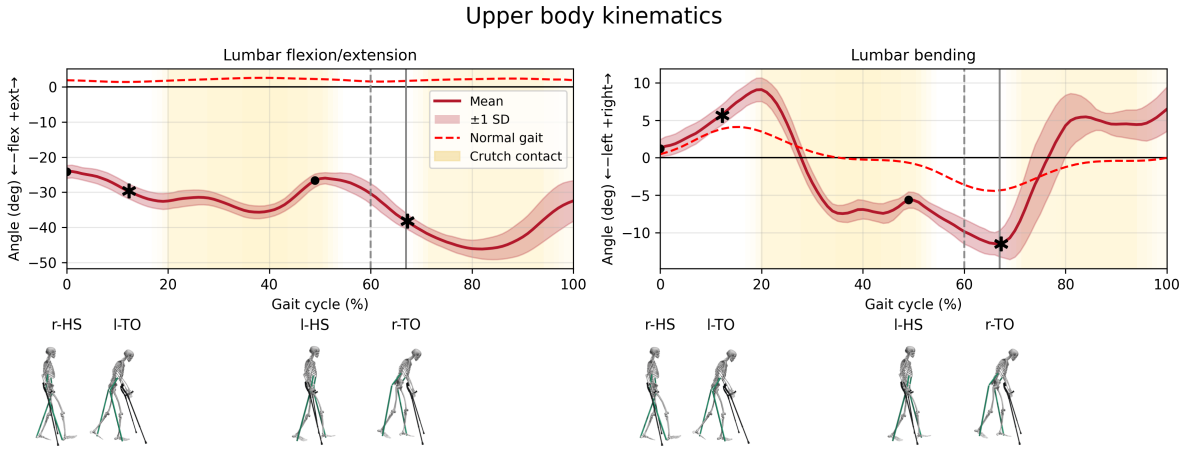

Figure 4.2: Upper-body kinematics during gait with the ARGO Walker exoskeleton. Solid coloured lines show the mean joint angles across ten gait cycles, with shaded areas indicating ±1 SD. Dashed red curves represent reference kinematics from a healthy gait dataset. Vertical grey lines indicate right-foot toe-off, marking the transition from stance to swing (reference: 60%, experimental: ~67%). Black dots denote right and left heel strikes (r-HS, l-HS), and black asterisks indicate left and right toe-off events (l-TO, r-TO). Yellow shading indicates periods of crutch–ground contact.

In Figure 4.2, the mean joint kinematics (±1 SD) of the lumbar region are shown.

Lumbar kinematics

Lumbar kinematics during ARGO-assisted gait show pronounced deviations from reference gait. Lumbar flexion is consistently increased throughout the gait cycle, ranging from approximately 25° to 50°, whereas for healthy gait remains slightly extended, with only minor deviations. Reductions in lumbar flexion occur shortly after heel strike and once the crutches are lifted off the ground. In addition, substantial lumbar lateral bending (lateroflexion) is observed, fluctuating up to approximately 10° to both the left and right over the gait cycle.

4.1.3. Joint kinetics

Overview

In this section, the lower- and upper-body joint kinetics during gait with the ARGO Walker are presented in Figures 4.3, 4.4, and 4.5. The figures show the mean joint moments (±1 SD) across ten gait cycles. The dashed red curves represent reference joint moments from the open-source dataset of Camargo et al. (2021)[60], which includes lower-limb biomechanics of healthy adults.

Because joint moments are strongly influenced by factors such as body mass, segment lengths, and particularly gait speed, these reference curves should be interpreted with caution. To allow a more meaningful comparison with the slow ARGO-assisted gait speed (0.34 m/s), the slow-speed condition of the Camargo dataset was selected as reference. This slow condition (0.88 ± 0.19 m/s) remains considerably faster than ARGO-assisted gait, and the corresponding reference joint moments are therefore expected to be higher than those that would occur when walking at 0.34 m/s.

For the reference gait plots shown in the figures, data from subjects AB06–AB15 (N = 10) and the slow walking condition of the dataset were included. The corresponding subject characteristics of this reference group are summarised in Table 4.4.

Table 4.4: Physical characteristics of subjects AB06–AB15 (N = 10) for the reference kinematics.

Parameter	Mean	SD
Age (years)	21.1	1.37
Height (m)	1.71	0.01
Mass (kg)	72.7	13.6
Gender (M/F)	8 / 2	–

Lower body kinetics

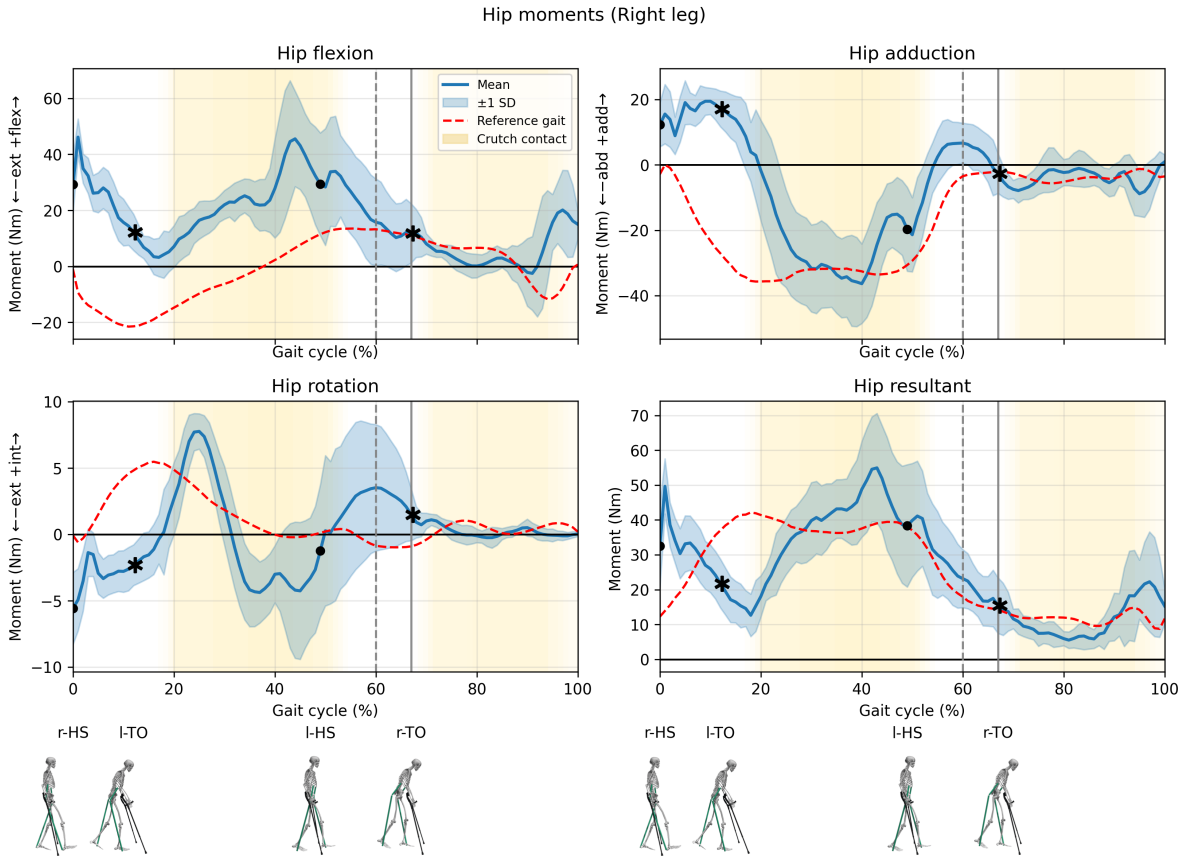

Figure 4.3: Hip joint kinetics of the right leg during gait with the ARGO Walker exoskeleton. Solid coloured lines show the mean joint angles across ten gait cycles, with shaded areas indicating ±1 SD. Dashed red curves represent reference kinematics from a healthy gait dataset. Vertical grey lines indicate right-foot toe-off, marking the transition from stance to swing (reference: 60%, experimental: ~67%). Black dots denote right and left heel strikes (r-HS, l-HS), and black asterisks indicate left and right toe-off events (l-TO, r-TO). Yellow shading indicates periods of crutch–ground contact.

Hip kinetics

Figure 4.3 presents the mean hip joint moments (±1 SD) of the right leg across ten gait cycles during ARGO-assisted gait, together with slow-speed reference curves from the Camargo dataset.

For hip flexion and extension, hip joint moments during ARGO-assisted gait are predominantly flexion-directed throughout stance. This contrasts with the reference pattern, which exhibits an extension moment during early stance that gradually transitions into a flexion moment toward late stance. Overall, hip flexion moments during ARGO-assisted gait are substantially larger than those observed during normal walking, with peak values approximately three times higher.

In ARGO-assisted gait, hip moments are additionally observed in adduction and external rotation, which

are (mostly) absent in healthy walking, alongside the abduction and internal-rotation moments present in both gait patterns. The resultant hip moment is increased, with peak values around mid-stance approximately 10–15 Nm higher than the reference.

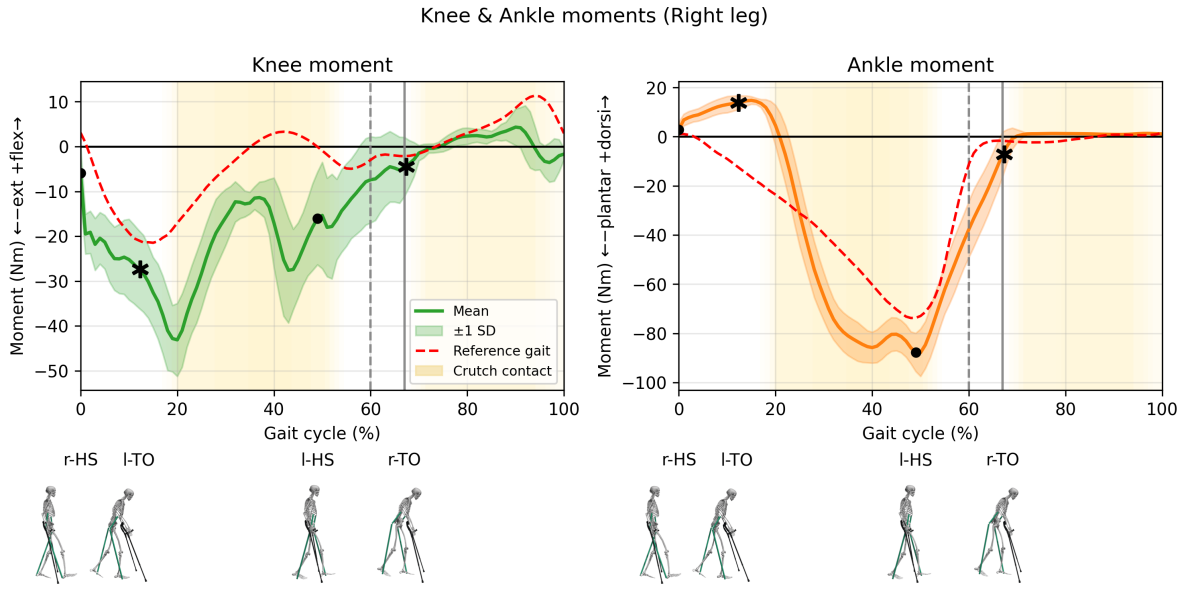

Figure 4.4: Knee and ankle joint kinetics of the right leg during gait with the ARGO Walker exoskeleton. Solid coloured lines show the mean joint angles across ten gait cycles, with shaded areas indicating ±1 SD. Dashed red curves represent reference kinematics from a healthy gait dataset. Vertical grey lines indicate right-foot toe-off, marking the transition from stance to swing (reference: 60%, experimental: ~67%). Black dots denote right and left heel strikes (r-HS, l-HS), and black asterisks indicate left and right toe-off events (l-TO, r-TO). Yellow shading indicates periods of crutch–ground contact.

Knee kinetics

Figure 4.4 shows that both ARGO gait and the slow reference gait are dominated by knee extension moments throughout most of the gait cycle. However, the ARGO knee moment is substantially larger, with peak magnitudes during mid-stance approximately twice those observed in healthy gait.

Ankle kinetics

Figure 4.4 shows that ankle joint kinetics during both ARGO-assisted gait and the slow reference condition are dominated by plantarflexion moments during stance. During ARGO-assisted gait, the plantarflexion moment increases more steeply and reaches slightly larger peak values compared to the reference gait. During mid- and late stance, the plantar flexion moment reaches a plateau before returning toward neutral in early swing.

Pelvis kinetics

Pelvic tilt and pelvic list moments during ARGO-assisted gait exhibit greater variability and larger amplitudes than the reference pattern, as shown in Figure 4.5. Pelvic rotation moments remain within a similar magnitude range as the reference data, although with a reduced peak value. Compared with the reference pattern, the resultant pelvic moment during ARGO-assisted gait exhibits a markedly lower peak magnitude and reduced overall values.

Upper body kinetics

Lumbar kinetics

Lumbar joint kinetics during ARGO-assisted gait differ markedly from reference gait. ARGO-assisted gait is characterised by large extension-directed lumbar moments, reaching peak values of approximately 100 Nm, with prominent peaks occurring during mid-stance and around the transition to swing. These extension moments decrease around the timing of crutch–ground contact. In contrast, reference gait predominantly exhibits flexion-directed lumbar moments, with flexion moments remaining smaller throughout the gait cycle, with peak values of 50 Nm.

Both ARGO gait and the reference gait show clear left–right oscillations in lumbar lateral bending moments, with similar magnitudes. A reduction in bending moment magnitude is observed following crutch

contact.

Lumbar rotation moments and the resultant lumbar moment during ARGO-assisted gait are increased compared to the reference pattern, with larger fluctuations observed in the rotation moments.

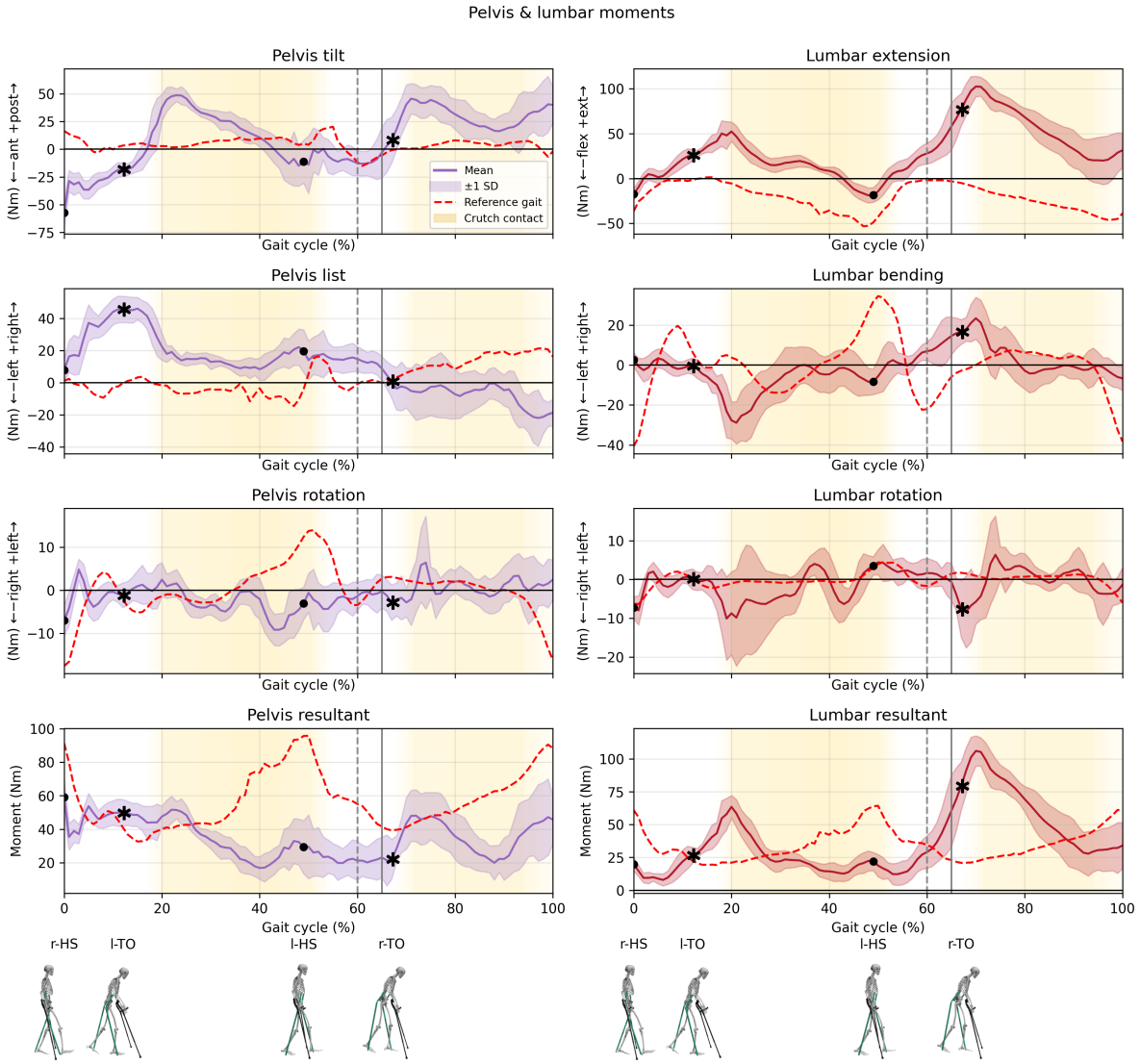

Figure 4.5: Pelvis and lumbar joint moments across the gait cycle. Solid coloured lines show the mean joint angles across ten gait cycles, with shaded areas indicating ±1 SD. Dashed red curves represent reference kinematics from a healthy gait dataset. Vertical grey lines indicate right-foot toe-off, marking the transition from stance to swing (reference: 60%, experimental: ~67%). Black dots denote right and left heel strikes (r-HS, l-HS), and black asterisks indicate left and right toe-off events (l-TO, r-TO). Yellow shading indicates periods of crutch–ground contact.

4.2. Biomechanical modelling of the ARGO Walker

After running the model, the motion of the ARGO Walker relative to the body was visually inspected at different moments of the gait cycle. This is illustrated in Figure 4.6.

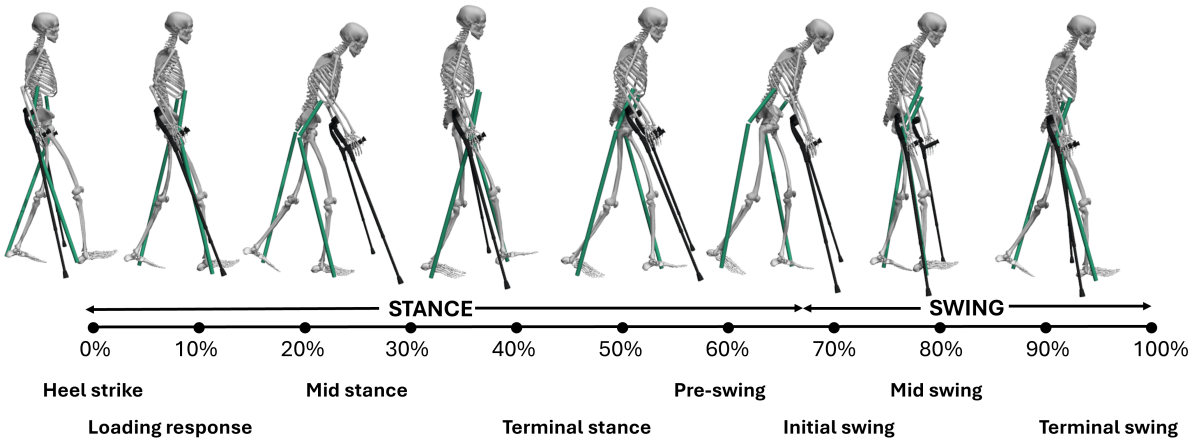

Figure 4.6: The ARGO Walker model in the subsequent gait cycle phases

Across the gait cycle, variations are observed in the relative positioning between the ARGO Walker and the lower limb. During heel strike and particularly around toe-off of the right foot (around pre-swing), the distance between the ARGO Walker and the leg is largest, most notably at the location of the knee bushing force. During other phases of the gait cycle, this distance is reduced. In these phases, the ARGO Walker foot segment is positioned more anteriorly, closer to the midfoot, rather than near the heel region around the calcaneus, which is primarily observed at heel strike.

Additionally, the position of the ARGO Walker hip BallJoint centre varies throughout the gait cycle. During terminal swing, the BallJoint centre is closely aligned with the hip joint centre of the skeletal model, occurring during a more upright posture of the model. During pre-swing and initial swing, the ARGO Walker BallJoint centre is located posterior to the anatomical hip joint centre, while the skeletal model exhibits increased forward trunk flexion. In contrast, between mid-stance and terminal stance, the BallJoint centre is positioned anterior to the hip joint centre, during phases in which the model adopts a more extended posture.

Finally, the two upper components of the ARGO Walker, R1 and L1, move in synchrony during parts of the gait cycle, with no visible relative motion between them. In other phases, however, independent motion between these components is observed. This is most evident during heel strike, where the two components are oriented in opposite directions.

5

Discussion

5.1. Study overview

This study examined the gait pattern and walking strategy during ARGO Walker-assisted gait and used these insights to develop an initial model of the exoskeleton in OpenSim. The model is highly simplified and requires significant further refinement before it can be used effectively. However, this study serves as an exploratory first step in creating a preliminary model. With further improvements, the model could eventually serve as a foundation for simulations that may inform design and control adaptations for the CloudWalker exoskeleton, as discussed in the Outlook section.

5.2. Gait analysis in the ARGO Walker

5.2.1. Overall gait strategy

Walking with the ARGO Walker is characterized by a substantially slower gait compared to typical healthy gait. Walking speed was more than four times lower than during normal gait. This reduced speed was accompanied by a markedly lower cadence, approximately three times lower, and a substantially prolonged stride duration, approximately three times higher, while step length was moderately reduced and the stance phase slightly prolonged. Together, these spatiotemporal characteristics reflect a strongly stability-oriented gait strategy, which is expected when ambulating with a rigid, passive orthosis in combination with crutches.

5.2.2. Biomechanics under ARGO constraints

Overview

The ARGO Walker imposes strong mechanical constraints on gait, which shape the observed kinematic and kinetic patterns. Joint moments are therefore interpreted in relation to these constraints and are considered in the context of gait velocity and crutch loading when compared with healthy reference data. Joint moments in the healthy reference data are reported at substantially higher walking speeds than those observed during ARGO-assisted gait. Since joint moment magnitudes are known to increase with gait velocity, the reference joint moments are expected to be higher than those that would occur during healthy walking at comparable speeds. In addition, healthy reference data were obtained during walking without crutches, whereas ARGO-assisted gait involves crutches with upper-limb support, which may further contribute to differences in joint loading patterns. Furthermore, the measured motion reflects the combined behaviour of the human user and the exoskeleton. Accordingly, the reported joint moments represent net internal moments required to reproduce the observed motion and arise from both biological contributions (muscle activity and passive tissues) and mechanical contributions from the device (joint constraints and reaction forces). These contributions cannot be separated in the present analysis.

Several characteristic gait patterns can be directly linked to the mechanical characteristics of the ARGO system, most notably the reciprocating hip coupling, the locked knee and limited ankle mobility. These restrictions alter normal swing mechanics and shift demands elsewhere in the kinematic chain, as

discussed in the following sections. In addition, upper body contributions are discussed, together with a closer examination of the kinetic demands.

Hip driving mechanism

Hip motion in the ARGO Walker is indirectly driven through the reciprocating mechanism that couples both hips via a Bowden cable. As a result, hip flexion and extension emerge from upper body movements rather than from lower-limb actuation.

For hip flexion/extension, the intended range of motion of the ARGO Walker is approximately –15° (extension) to 15° (flexion), as described earlier. However, the experimental data reveal an asymmetric hip flexion–extension pattern, characterised by larger peak extension than flexion. This asymmetry can partly be attributed to the static posterior pelvic tilt imposed by the exoskeleton and fixation straps, which results in an offset toward hip extension in the static pose. To maintain full foot contact with the ground, the legs therefore extend relative to the pelvis. In addition, hip joint angles are defined relative to the pelvis rather than to the global reference frame, meaning that pelvic orientation directly influences the measured hip kinematics. The substantially larger pelvic tilt excursions observed during ARGO Walker–assisted gait, compared with healthy gait, further amplify this asymmetry across the gait cycle.

Hip moment patterns provide additional insight into the role of the hip during ARGO Walker–assisted gait. In contrast to healthy gait, where a clear hip extension moment is present during early stance to control weight acceptance, ARGO Walker–assisted gait is dominated by flexion-directed hip moments throughout the gait cycle. The absence of an early-stance hip extension moment can be attributed to the mechanical constraints of the system, including the locked knee and limited ankle mobility, which substantially reduce the need for shock absorption and stabilisation by the hip. Compared with healthy gait, a pronounced hip flexion moment is observed during ARGO-assisted gait, with peak values occurring in late stance, just prior to swing initiation, when the hip approaches its maximum extension angle. This moment primarily serves to initiate limb advancement. Because the knee cannot flex and ankle push-off is limited, the limb cannot shorten or receive an effective propulsive impulse. Consequently, the hip must generate a substantial flexion moment to accelerate the stiff, extended limb into swing.

Locked knee mechanism

The locked knee in the ARGO Walker eliminates normal swing-phase knee flexion, requiring alternative strategies to achieve foot clearance. To compensate for the absence of knee flexion, a small increase in hip abduction is observed in comparison with healthy gait, however primarily during stance and to a smaller extent during swing, consistent with a small circumduction-like motion. In addition, due to the rigid foot segment of the exoskeleton, the foot is maintained in a dorsiflexed posture throughout the gait cycle, thereby facilitating toe clearance during swing and preventing toe drag.

In the experimentally derived kinetic data, a pronounced extension-directed net knee moment is observed, most prominently during early stance. In ARGO-assisted gait, this elevated knee extension moment reflects the need to counter external knee-flexion moments generated by the ground reaction force during weight acceptance. Because the knee is mechanically locked, it cannot flex to provide normal shock absorption, preventing a reduction of the external knee moment through controlled knee flexion and causing load acceptance to be shifted to other segments and to the crutches. As a result, stability depends on a large knee extension moment, generated by body weight and by reaction moments from the knee-lock mechanism of the exoskeleton.

Limited ankle mobility

In healthy gait, the ankle transitions from dorsiflexion into plantarflexion during late stance, enabling a smooth heel-to-toe rollover and an effective push-off. In contrast, during ARGO-assisted gait the ankle dorsiflexion angle decreases only slightly and does not transition into plantarflexion.

This behaviour is a direct consequence of the largely rigid ankle–foot segment of the ARGO Walker, imposed by the exoskeleton structure and stiff foot shell. As a result, controlled dorsiflexion during stance and active plantarflexion during push-off are restricted, limiting the contribution of the ankle to forward propulsion during walking. Consequently, forward progression of the body is increasingly generated by more proximal segments, with greater reliance on hip motion and compensatory lumbar movements during ARGO-assisted gait.

These mechanical constraints are reflected in the ankle moments. In normal gait, the plantarflexion moment gradually increases as the ankle dorsiflexes under body weight and reaches a clear peak during push-off, just prior to toe-off. In ARGO-assisted gait, a steeper rise in the plantarflexion moment is observed during stance, followed by a sustained plateau rather than a peak. This pattern reflects the transmission of ground reaction forces through a stiff foot–ankle structure, leading to a rapid increase in the external moment arm about the ankle rather than active ankle control. Because the ankle angle changes little after heel-to-forefoot load transfer and remains in a dorsiflexed orientation during late stance, the plantarflexion moment does not translate into effective push-off, but instead represents a sustained internal moment.

Upper-body and pelvic compensation during crutch-assisted gait

The kinematic data show a persistently forward-inclined trunk posture, achieved through a combination of lumbar flexion and hip-pelvis positioning throughout the gait cycle. This posture facilitates weight transfer onto the crutches while maintaining balance during stance.

The experimentally derived kinetic data reveal pronounced lumbar extension moments during ARGO-assisted gait, substantially exceeding those observed in healthy walking. These elevated moments indicate an increased demand on the lumbar region to stabilise the body when the lower limbs cannot effectively contribute to load absorption. Importantly, lumbar extension moments decrease at the instant of crutch contact, demonstrating that crutch loading partially supports the trunk and reduces the demand on the lumbar extensors.

Crutch support also influences side-to-side control of the lumbar region. Increased lumbar lateral bending is observed during the gait cycle. However, once the crutches contact the ground, the lumbar bending angle returns toward a more neutral position. The associated lumbar lateral bending moments decrease accordingly, suggesting that side-to-side stabilisation is partly transferred from the lumbar region to the crutches.

Lumbar rotation moments are increased compared with healthy walking. This likely reflects a greater involvement of trunk rotation in facilitating forward progression of the body during walking when lower-limb mobility is restricted and limb advancement relies more strongly on upper-body motion.

Pelvic kinematics show a consistent posterior tilt throughout the gait cycle, in contrast to the small anterior pelvic tilt typically observed during healthy gait. Correspondingly, pelvic tilt moments are shifted toward posterior-tilt directions and, similar to the lumbar extension moments, decrease when the crutches bear load.

Pelvic list moments are increased compared with healthy gait. This likely reflects the trunk-driven weight-shifting strategy required to advance the limbs under the mechanical constraints of the exoskeleton.

Pelvic rotation moments are reduced during ARGO-assisted gait, with minimal excursions around neutral. Whereas healthy walking shows a distinct internal rotation moment during late stance, this peak is largely absent in ARGO-assisted gait. This reduction is consistent with the mechanical constraints imposed by the exoskeleton, in which the lower limbs are fixed within rigid shells that restrict femoral rotation relative to the pelvis. This restriction is also reflected in the, mostly, externally rotated hip posture observed throughout the gait cycle, particularly during stance, in contrast to the internal hip rotation typically seen in healthy gait during this phase.

Kinetic demands

Across the hip, knee, ankle, and lumbar region, ARGO-assisted gait is characterised by substantially higher joint moments compared with healthy reference gait, reflecting the increased kinetic demands. When considering peak joint moments, the largest increases were observed at the knee, lumbar region, and hip. Ankle moments showed only small increases, whereas resultant pelvic joint moments were reduced compared with healthy gait.

The healthy reference data were collected at substantially higher walking speeds than those observed during ARGO-assisted gait. Since joint moment magnitudes are known to increase with gait velocity, the reported differences likely underestimate the true discrepancy that would be present if healthy walking

were evaluated at walking speeds comparable to those achieved with the ARGO Walker. At matched walking speeds, joint moment differences would therefore be expected to be even larger.

For the lower-limb joints, the elevated joint moments can primarily be attributed to the mechanical constraints imposed by the exoskeleton, including the locked knee and restricted ankle motion. These constraints alter load transmission through the lower limbs. The inability of the knee and ankle to flex limits shock absorption, requiring larger internal extension moments in the knee to counteract external loads and maintain stability under the influence of ground reaction forces.

As the walking trials in this study were performed by a healthy participant, biological contributions from the human musculoskeletal system are also present. However, because inverse dynamics returns net joint moments, it is not possible to distinguish between moments generated by the human body and reaction moments arising from the exoskeleton structure.

In contrast to the lower-limb joints, the elevated lumbar joint moments can be more directly attributed to compensatory strategies of the human body, as the exoskeleton does not provide actuation at the lumbar spine. Restricted ankle function further shifts responsibility for forward propulsion toward more proximal segments. With limited ankle push-off, ground reaction forces are transmitted through a relatively rigid limb configuration rather than being modulated by active ankle control. As a result, forward progression relies predominantly on hip-driven limb advancement, increased lumbar motion, and crutch support.

Together, these mechanisms contribute to the elevated joint moments observed during ARGO-assisted gait, with different joints affected through different biomechanical pathways.

5.2.3. Limitations in gait analysis

Participant- and measurement-related limitations

This study was conducted with a healthy participant, despite the ARGO Walker being intended for individuals with spinal cord injury. Although the participant was instructed to minimise lower-limb muscle activation, voluntary muscle use could not be fully eliminated.

As a result, active movement of the participant within the ARGO Walker may have occurred, meaning that part of the observed kinematic patterns could reflect active movement of the participant within the exoskeleton rather than motion of the exoskeleton itself. In addition, the estimated joint kinetics represent a combination of contributions from the human user and reaction moments associated with the ARGO Walker structure. Because the healthy participant has voluntary control of the lower limbs, it is possible that lower-limb muscle activity was used to partially reduce the mechanical demands on the upper body. Consequently, upper-body joint moments reported in this study may underestimate the demands that would be present in individuals with spinal cord injury, who lack voluntary lower-limb control.

Taken together, the reported joint moments should be interpreted as net moments of the combined human–exoskeleton system, which limits direct generalisation of the findings to the spinal cord injury population.

The accuracy of the marker placement could also be a limitation. Although markers were placed as accurately as possible, small displacements relative to the underlying anatomical landmarks are unavoidable and may introduce errors in the kinematics results. While the marker RMS error after inverse kinematics remained below 2 cm, deviations may still be present in the calculated joint angles and joint moments.

Furthermore, experimental limitations related to force plate availability limited the possibility to directly measure all gait events. Because only four force plates were available, two for both feet and two for both crutches, only a single heel strike per foot could be captured within a trial. Consequently, the 0–100% gait cycle normalisation was partly based on proxy events, which were based on the timing of peak hip flexion. This approach introduces uncertainty in the exact timing of gait events. For example, left toe-off occurred on the force plate after the second right heel strike and therefore beyond 100% of the analysed gait cycle, requiring its timing to be estimated from the subsequent cycle.

Another limitation is the potential influence of force plate targeting. Despite instructions to walk without

aiming for the force plates, the participant may have subconsciously adjusted foot and crutch placement to ensure contact, potentially affecting the gait pattern. In addition, because no additional plates were available to create a fully level walking surface, the crutches contacted a slightly lower surface during the second crutch-ground contact within the gait cycle. This height difference likely contributed to the increased lumbar flexion observed toward the end of the gait cycle in the kinematic data, as the participant had to lean further forward to achieve crutch contact with the ground. Together, these factors introduce variability in the measured kinematics and kinetics.

Limitations of the reference gait

Several methodological aspects need to be considered when interpreting the joint moments presented in this study. First, the healthy reference data used for comparison were collected at a substantially higher walking speed (0.88 m/s) than the ARGO-assisted gait (0.34 m/s). Since joint moments increase with walking speed, the reference curves likely overestimate the moments that would occur at the slower ARGO walking speed. As a result, the difference in joint moments between ARGO-assisted and healthy gait is likely underestimated in the present comparison.

Joint moments are also affected by participant-specific characteristics such as body mass and segment length. The participants in the reference dataset were generally comparable to the participant in this study in terms of sex (predominantly male), age, and body mass. Together with the ARGO Walker, the participant in this study had a slightly higher total mass ($\sim$80 kg including the exoskeleton) compared to the reference group ($\sim$73 kg), although this difference is relatively small. A more notable difference, however, is body height. The participant in this study was considerably taller (1.94 m) than the mean height of the reference dataset (1.71 m). Increased body height is relevant because longer body segments create larger moment arms, which can lead to higher joint moments. Therefore, height-related differences could contribute to elevated joint moments in this participant. Nonetheless, the influence of walking speed on joint moments is substantially larger than the influence of body height.

Furthermore, the reference dataset reflects unassisted, crutch-free walking, whereas ARGO-assisted gait involves continuous upper-body loading through the crutches. Crutch support reduces the vertical load on the lower limbs and changes the direction of external forces acting on the body. These differences in loading conditions must be taken into account when comparing the two gait cycles, as crutch use reduces the load on the lower limbs while shifting part of the generation of forward propulsion of the body from the legs to the upper body and the crutches. As a result, joint moment magnitudes and their timing may differ from unassisted gait.

Together, these considerations highlight that the healthy reference curves provide essential context, but cannot be interpreted as a direct normative baseline for ARGO-assisted gait.

5.3. Modelling the ARGO Walker in OpenSim

5.3.1. Overview

An OpenSim model of the ARGO Walker was developed to represent the combined human–exoskeleton system and to serve as a foundation for more detailed modelling in the future and subsequent simulation studies. The modelling approach was informed by direct inspection of the ARGO Walker and by the findings from the experimental gait analysis.

The model combines a generic human skeletal model with a simplified representation of the ARGO Walker. The exoskeleton segments were modelled as four rigid cylinders and are connected to the feet, knee and torso via bushing forces, representing the interfaces between the user and the device. The lower-limb segments of the exoskeleton are modelled as rigid structures, reflecting the locked-knee configuration of the ARGO Walker and thereby eliminating knee flexion during gait. Reciprocal hip motion is implemented using an opposing hip coupling mechanism to mimic the Bowden cable system that mechanically links left and right hip motion.

Given the exploratory nature of this study, the model was intentionally kept relatively simple to keep the model stable and computationally manageable. Consequently, the current model should be regarded as an initial representation of ARGO-assisted gait rather than a fully validated or detailed predictive model.

5.3.2. Evaluation of the ARGO Walker model

The current ARGO Walker model was evaluated by prescribing experimentally recorded motion-capture data and visually inspecting the relative motion between the exoskeleton and the human body across the gait cycle. Although, in reality, the ARGO Walker typically drives leg motion rather than following leg motion initiated by the user, this approach provides insight into the alignment and interaction between the exoskeleton and the user within the model. During evaluation, the ARGO Walker leg components were observed to move in synchrony with the lower limbs, showing the expected reciprocal forward motion pattern. However, deviations in alignment were also observed. In particular, the exoskeleton was not consistently aligned with the anatomical knee joint centres, and increased relative motion was observed at the foot segment and at hip level than what would have been expected. These deviations suggest that the interaction between the exoskeleton and the body is not yet reliably modelled in the current configuration, possibly due to uncertainties in both bushing placement and parameterisation.

5.3.3. Limitations of the current ARGO Walker model

Several of the observed alignment deviations can be attributed to modelling limitations. One important limitation is the absence of an active bushing force at pelvic height. This bushing was disabled because the large pelvic tilt excursions observed in the experimental data caused numerical instability when the pelvic bushing force was enabled. While this improves computational stability, it also removes the direct coupling between the pelvis and the ARGO Walker, resulting in increased relative motion between the ARGO Walker and the body at this level. In addition, the current bushing force parameters have not yet been experimentally calibrated. The stiffness and damping values were adopted from previous literature and manually tuned, but do not yet accurately reflect the mechanical properties of the physical ARGO Walker straps and interfaces. As a result, the interaction between the exoskeleton and the user may be represented with a different level of compliance in the model than in the physical ARGO Walker.

Another limitation is that some structural constraints present in the physical ARGO Walker are not yet fully represented in the model. In the physical exoskeleton, the two upper trunk components of the exoskeleton (R1 and L1) are connected by a rigid bar at the posterior side of the ARGO Walker, preventing independent motion between these components. In the current model, this rigidity is not implemented, allowing relative motion that would not occur in practice. This difference represents another aspect of the model that should be improved in future refinements.

Furthermore, the current OpenSim model relies on several simplifying assumptions. The exoskeleton segments were modelled as rigid bodies with simplified cylindrical geometry, and some elements, such as the foot segment, were not modelled separately. While these choices capture the gross mechanical behaviour of the ARGO Walker, they simplify the true mass distribution and neglect detailed geometry, which may influence the centre of mass location and inertial properties.

In addition, the reciprocal hip coupling was implemented by enforcing equal and opposite hip motion, assuming a perfectly smooth and symmetric mechanism. In reality, cable friction and slack are likely present, which may introduce small deviations from ideal reciprocal behaviour.

Despite these limitations, the current model forms a basis for further development. Through improvements to the model structure, combined with additional experimental data and improved parameter characterisation, it can be refined to enable simulations of ARGO-assisted gait in the future.

5.4. Future applications of the ARGO Walker model

5.4.1. Overview

The OpenSim model developed in this study represents an initial model for simulating ARGO Walker–assisted gait. Although further refinement of this model is required before realistic simulations can be performed, the model offers a foundation for evaluating how design modifications or assistive control strategies may influence gait performance and loading patterns.

5.4.2. Model refinement and extension

Future work should first focus on further improving the current model. An important extension involves calibrating the bushing parameters that represent human–exoskeleton interaction. This would require additional experimental data, including tracking of exoskeleton motion during walking and measurements of strap stiffness, to enable more accurate modelling of load transfer between the user and the device. This is discussed in more detail in Chapter 6, Outlook.

Further extensions may include introducing knee mobility, by modelling separate upper- and lower-leg segments to enable exploration of FES-assisted gait with knee flexion. Additional refinements could involve more detailed modelling of the reciprocating hip mechanism, including effects of slack and friction. Moreover, incorporating musculature in the lower limbs would enable simulations involving functional electrical stimulation, while modelling upper-body muscles would allow investigation of their active contribution to gait and upper-body loading. Finally, replacing the simplified cylindrical geometries with available CAD-based STL files from the SolidWorks model of the ARGO Walker could improve the accuracy of mass distribution, inertial properties, and the visual realism of the model.

5.4.3. Potential role of FES in RGO-assisted gait

A key goal of (A)RGO-assisted gait is to improve walking energy efficiency. Functional electrical stimulation may contribute by supporting active lower-limb motion during gait, thereby reducing the compensatory demands placed on proximal segments for limb advancement.

Existing clinical FES systems illustrate how electrical stimulation can be applied to support gait in individuals with gait impairments. The potential relevance of such systems in combination with the ARGO Walker is discussed further in Chapter 6 (Outlook).

Once the model has been further refined, it could be used to explore whether functional electrical stimulation can meaningfully reduce energy expenditure within the mechanical constraints of the ARGO Walker, prior to experimental implementation. However, as reported in previous studies discussed in the literature review in Appendix A, muscle fatigue remains a key limitation of FES-based assistance and should be carefully considered when assessing its applicability.

5.5. Study findings in the context of existing research

In Chapter 6 (Outlook), other studies are discussed that investigate exoskeleton-assisted gait in individuals with spinal cord injury, including modelling approaches in OpenSim. Besides, the EvoMove, which integrates functional electrical stimulation to support gait, is described.

Earlier research has investigated gait characteristics during ARGO-assisted walking between able-bodied individuals and persons with spinal cord injury to distinguish gait limitations imposed by the orthosis from those related to neurological impairment. Arazpour et al. [61] compared able-bodied individuals and persons with spinal cord injury and reported substantial reductions in walking speed, step length, cadence, and hip, knee, and ankle joint range of motion in both groups. Walking speed, stride length, and cadence were further reduced in the SCI group, while joint range of motion was lower but not consistently significantly different. Despite these quantitative differences, both groups exhibited qualitatively similar movement patterns. These findings indicate that gait parameters in individuals with spinal cord injury are likely to be reduced relative to those observed in the healthy participant included in this study, which should be considered in the model of the ARGO Walker for future OpenSim simulations.

In an earlier study, Arazpour et al. investigated the effect of trunk posture during ARGO-assisted walking in individuals with spinal cord injury [62]. By reducing trunk flexion through the use of a thoracolumbosacral orthosis (a trunk brace providing external support to the thoracic and lumbar spine), they reported improvements in temporal–spatial gait parameters as well as increased hip and ankle joint range of motion. Although energy consumption was not assessed in this study, the authors discussed these findings in the context of previously reported high upper-limb loading and energetic demands during RGO-assisted walking, and suggested that providing trunk extension through improvements in orthosis design may help reduce these demands. This aspect may therefore also be relevant when considering strategies to reduce energy expenditure in the ARGO Walker investigated in this study.

Beyond RGO-based approaches, other interventions aimed at restoring walking after spinal cord injury have also been reported. These include brain–spine interfaces [63, 64] and other neuromodulatory approaches, which are also addressed in the literature review in Appendix A. Although some studies report promising preliminary results, these approaches remain largely experimental and have so far been demonstrated in only a limited number of subjects. While different from RGO walking, they illustrate that alternative strategies for gait restoration after spinal cord injury are actively being explored and may become increasingly relevant in future research.

6

Outlook

This chapter discusses how the ARGO Walker model could be further refined and how, with these refinements, the model could be used for OpenSim simulations, such as tracking-based analyses, using OpenSim Moco, and the evaluation of interaction loads and potential integration of functional electrical stimulation (FES).

6.1. Refinement of the current model

6.1.1. Overview

As discussed in the previous chapter, the current ARGO Walker model requires further refinement before it can be used for realistic simulations. One key area for improvement consists of the definition of the human–exoskeleton interface, specifically the parameterisation of the bushing forces that represent mechanical coupling between the user and the device. The determination of appropriate bushing force parameters is therefore discussed in the following subsection.

6.1.2. Previous literature on determining bushing force parameters

The literature was examined to understand how other studies defined human–exoskeleton contact mechanics and determined bushing parameters.

Several studies used OpenSim's BushingForce to represent human–robot interactions, but the methods for choosing stiffness and damping parameters vary widely. Some studies assigned very simplified, manually selected values (e.g., a single translational DOF with arbitrarily chosen stiffness[65]). Other work chose full 6-DOF bushing parameters empirically in the OpenSim GUI to obtain firm contact between the human and exoskeleton models[66], without experimental calibration.

Moreover, one study attempted to inform these parameters using experimental measurements. A 2025 study by De Carvalho et al.[67] developed a computational framework to estimate hip, knee, and ankle joint loads during exoskeleton-assisted walking, and evaluated how different modelling assumptions for human–robot interaction influence these joint-force predictions. Among the four modelling approaches they compared, two incorporated OpenSim BushingForces. In this context, bushing elements were placed at the strap and pelvic-band locations of the ReWalk exoskeleton to represent the transmission of forces between the device and the user. Translational stiffness and damping parameters were tuned using experimental measurements from an instrumented exoskeleton knee bracket. The publication does not describe the specific procedure used to derive these parameters, and the resulting numerical values were not reported. Rotational stiffness and damping were set to zero, meaning that the bushings generated only compressive and shear forces but no rotational moments. The translational and rotational bushing force parameters were assumed to be the same at all exoskeletal straps and bands.

In the current ARGO Walker model, the bushing force components were implemented but could not yet be reliably parameterised. Accurate definition of these parameters requires experimental data that capture the relative motion and load transfer between the exoskeleton and the human body. Future experiments should therefore include motion capture markers placed on both the exoskeleton and the user, allowing relative displacements at strap and attachment locations to be quantified. In addition,

experimental characterisation of strap stiffness and damping properties would be required to inform translational and rotational bushing parameters. Such data would enable a more realistic representation of human–exoskeleton interaction forces and support the use of the model for simulations in OpenSim.

6.2. Simulation possibilities in OpenSim

6.2.1. Overview

OpenSim and the Moco framework enable both tracking-based and predictive simulation approaches for evaluating assistive strategies [68]. Tracking-based methods (e.g. MocoTrack, MocoInverse) could particularly be promising for ARGO-assisted gait, as they remain grounded in experimentally observed movement patterns. This makes them well suited for exploring specific modifications in the current walking pattern, such as introducing knee flexion through stimulation of the knee extensors and/or flexors, while respecting the mechanical constraints and feasible gait patterns imposed by the RGO. Figure 6.1 illustrates the type of optimisation workflows that Moco enables within OpenSim.

Figure 6.1: Overview of the OpenSim Moco optimisation workflow [68].

6.2.2. Previous literature

Previous OpenSim studies demonstrate how hybrid FES–exoskeleton concepts can be explored computationally prior to experimental implementation. De Sousa et al. (2019) used OpenSim to evaluate control strategies for a hybrid system combining hip actuation with FES-driven knee flexion and extension. Their simulations showed that predefined joint trajectories could be tracked, but also revealed instability in FES-driven knee control, particularly when knee flexion coincided with hip extension, highlighting challenges in coordinating FES with exoskeleton mechanics [69]. Makowski et al. (2022) applied a “muscle-first” control strategy and predefined kinematic objectives in an OpenSim model of the hybrid FES–exoskeleton system. By prioritising muscle activation and introducing a simplified fatigue model with reduced muscle force capacity, they demonstrated how declining muscle capacity shifts assistance demands from FES toward mechanical actuation [70]. In this study, muscle fatigue was represented using a simplified approach based on a fixed reduction in maximal muscle force. While this captures a general decline in force-generating capacity, it does not account for the physiological or time-dependent characteristics of muscle fatigue. More advanced fatigue formulations could therefore improve the realism of future simulations.

Together, these studies support the use of OpenSim-based simulations to investigate feasible stimulation targets and timing, while emphasising that FES effectiveness is constrained by muscle fatigue.

Beyond performance optimisation and making walking more energy efficient, estimating joint loading and human–exoskeleton interaction forces is also clinically relevant, particularly for individuals with SCI. Exoskeleton-assisted walking imposes upright weight-bearing loads on a musculoskeletal system that is often weakened by rapid post-injury bone loss below the neurological lesion [71, 72, 73, 74, 75, 76], increasing fracture risk. Fracture incidences of up to 10% during exoskeleton-assisted gait have been reported in individuals with SCI [67, 77, 78].

De Carvalho et al. (2025) demonstrated that OpenSim’s MocoInverse can be used to estimate internal joint reaction forces during exoskeleton-assisted walking by tracking measured kinematics and solving

for muscle and actuator contributions while accounting for ground reaction forces, exoskeleton torques, and human–device interaction forces via bushing elements [67]. Although their model was based on able-bodied muscle properties and could not be directly generalised to individuals with SCI, their work illustrates how simulation frameworks can provide valuable insight into joint loading patterns during exoskeleton-assisted gait.

6.2.3. Limitations of OpenSim simulations

While a refined ARGO Walker–human model could provide a valuable basis for future simulation studies in OpenSim, several limitations must be considered when interpreting simulation outcomes.

Moco simulations should be interpreted with caution, as optimisation results are highly sensitive to the objectives defined by the user in Moco. Different objectives, such as minimising muscle effort, joint moments, or joint loading, can yield similar kinematics while producing substantially different predicted assistance profiles [79]. In addition, the muscle models in OpenSim do not capture SCI-specific muscle physiology or the stimulation-to-force dynamics of FES, meaning that predicted activations cannot be directly translated to realistic stimulation parameters. Finally, the mechanical constraints of ARGO-assisted gait, including reciprocal hip coupling, restricted knee and ankle joints, and reliance on crutch support, must be taken into account when selecting an appropriate simulation approach. Although predictive Moco simulations respect these model constraints, they may still generate movement patterns that are mathematically feasible but not realistic or achievable for an ARGO user. For this reason, tracking-based approaches are considered more suitable for future work, as they ensure that simulated motions remain consistent with experimentally observed and feasible ARGO gait patterns.

6.3. External technological developments

If future simulations demonstrate the potential benefit of integrating functional electrical stimulation (FES) with the ARGO Walker, clinical implementation would be required to evaluate feasibility in practice. It is relevant to consider existing external technologies that combine mechanical assistance with muscle activation.

An example is EvoMotion[80], the developer of the EvoMove FES system. EvoMove applies surface electrical stimulation in combination with IMU-based motion detection to activate hip and leg muscles during walking in individuals with walking difficulties, including individuals with incomplete spinal cord injury. Functions such as foot clearance, limb progression, and standing stability could be supported, either independently or in combination with orthotic devices[80]. Figure 6.2 illustrates the muscle groups that can be targeted using this system.

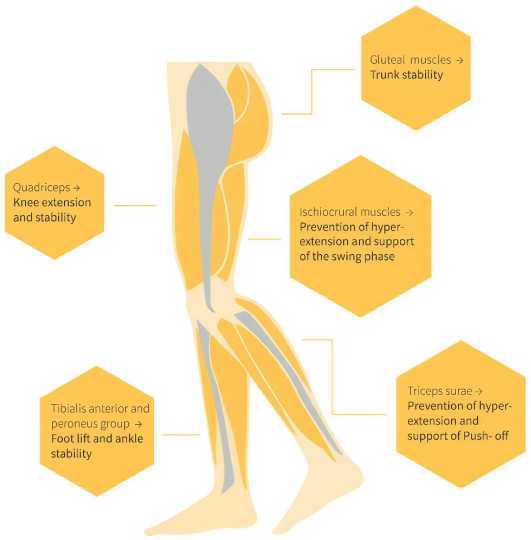

Figure 6.2: Muscle groups that can be stimulated superficially using the Evomove FES system to support gait [81].

Investigating whether technologies developed by such companies could be integrated with the ARGO Walker may represent a promising direction for future work. However, this lies beyond the scope of the present study and would only become relevant once simulation-based findings support the theoretical feasibility of such combined approaches.

7

Conclusion

ARGO Walker–assisted walking differs fundamentally from healthy gait due to the mechanical characteristics of the device. Mechanical constraints eliminate normal distal joint functions, resulting in a slow, stability-oriented gait that relies heavily on crutch support and increased contributions from proximal joints and the upper body.

The kinematic compensations were particularly expressed at the pelvis and trunk, with pronounced posterior pelvic tilt and increased lumbar flexion observed throughout the gait cycle. This altered movement strategy was accompanied by elevated joint moments, with large increases observed at the lumbar region, indicating substantially increased mechanical demands on the upper body. Joint moments were markedly increased at the hip and knee as well. Because distal joint strategies such as knee shock absorption and ankle push-off are limited or absent, stabilisation during weight acceptance relies on elevated knee extension moments, while forward limb advancement depends predominantly on flexion-directed hip moments to enable swing of a stiff lower limb.

An initial, strongly simplified OpenSim model capturing the main mechanical features of the ARGO Walker was developed and shown to reproduce the overall movement patterns observed during walking. However, misalignments between the human and exoskeleton were observed, indicating that further refinement is required before the model can be used for simulation-based analyses.

Overall, this work provides an initial simplified biomechanical model of ARGO Walker–assisted gait. With further refinement, the model may support future simulation studies to evaluate assistive strategies, such as functional electrical stimulation, and to assess design adaptations aimed at improving gait efficiency, reducing upper-body demands, and ultimately making exoskeleton-assisted walking accessible to a broader population of individuals with spinal cord injury.

References

[1] World Health Organization. *Spinal cord injury*. https://www.who.int/news-room/fact-sheets/detail/spinal-cord-injury. Accessed: 2025-02-24. 2023.

[2] Frederick M Maynard et al. “International Standards for Neurological and Functional Classification of Spinal Cord Injury”. In: *Spinal Cord* 35.5 (May 1997), pp. 266–274. ISSN: 1476-5624. DOI: 10.1038/sj.sc.3100432.

[3] M P Jensen et al. “Frequency and age effects of secondary health conditions in individuals with spinal cord injury: a scoping review”. In: *Spinal Cord* 51.12 (Oct. 2013), pp. 882–892. ISSN: 1476-5624. DOI: 10.1038/sc.2013.112.

[4] Rita J. van den Berg-Emons, Johannes B. Bussmann, and Henk J. Stam. “Accelerometry-Based Activity Spectrum in Persons With Chronic Physical Conditions”. In: *Archives of Physical Medicine and Rehabilitation* 91.12 (Dec. 2010), pp. 1856–1861. ISSN: 0003-9993. DOI: 10.1016/j.apmr.2010.08.018.

[5] Jonathan Myers, Matthew Lee, and Jenny Kiratli. “Cardiovascular Disease in Spinal Cord Injury: An Overview of Prevalence, Risk, Evaluation, and Management”. In: *American Journal of Physical Medicine and Rehabilitation* 86.2 (Feb. 2007), pp. 142–152. ISSN: 0894-9115. DOI: 10.1097/phm.0b013e31802f0247.

[6] William A. Bauman and Ann M. Spungen. “Invited Review Carbohydrate And Lipid Metabolism In Chronic Spinal Cord Injury”. In: *The Journal of Spinal Cord Medicine* 24.4 (Jan. 2001), pp. 266–277. ISSN: 2045-7723. DOI: 10.1080/10790268.2001.11753584.

[7] William C Duckworth et al. “Glucose Intolerance Due to Insulin Resistance in Patients with Spinal Cord Injuries”. In: *Diabetes* 29.11 (Nov. 1980), pp. 906–910. ISSN: 1939-327X. DOI: 10.2337/diab.29.11.906.

[8] A Scheel-Sailer et al. “Prevalence, location, grade of pressure ulcers and association with specific patient characteristics in adult spinal cord injury patients during the hospital stay: a prospective cohort study”. In: *Spinal Cord* 51.11 (Sept. 2013), pp. 828–833. ISSN: 1476-5624. DOI: 10.1038/sc.2013.91.

[9] Jonviea D. Chamberlain et al. “Excess burden of a chronic disabling condition: life lost due to traumatic spinal cord injury in a Swiss population-based cohort study”. In: *International Journal of Public Health* 64.7 (May 2019), pp. 1097–1105. ISSN: 1661-8564. DOI: 10.1007/s00038-019-01265-6.

[10] Gülçin Demirel et al. “Osteoporosis after spinal cord injury”. In: *Spinal Cord* 36.12 (Dec. 1998), pp. 822–825. ISSN: 1476-5624. DOI: 10.1038/sj.sc.3100704.

[11] Douglas E. Garland et al. “Osteoporosis after spinal cord injury”. In: *Journal of Orthopaedic Research* 10.3 (May 1992), pp. 371–378. ISSN: 1554-527X. DOI: 10.1002/jor.1100100309.

[12] Michael J. Castro et al. “Influence of complete spinal cord injury on skeletal muscle within 6 mo of injury”. In: *Journal of Applied Physiology* 86.1 (Jan. 1999), pp. 350–358. ISSN: 1522-1601. DOI: 10.1152/jappl.1999.86.1.350.

[13] A L Hicks et al. “The effects of exercise training on physical capacity, strength, body composition and functional performance among adults with spinal cord injury: a systematic review”. In: *Spinal Cord* 49.11 (June 2011), pp. 1103–1127. ISSN: 1476-5624. DOI: 10.1038/sc.2011.62.

[14] Oche Adam Itodo et al. “Physical activity and cardiometabolic risk factors in individuals with spinal cord injury: a systematic review and meta-analysis”. In: *European Journal of Epidemiology* 37.4 (Apr. 2022), pp. 335–365. ISSN: 1573-7284. DOI: 10.1007/s10654-022-00859-4.

[15] Thomas Platz et al. “Device-Training for Individuals with Thoracic and Lumbar Spinal Cord Injury Using a Powered Exoskeleton for Technically Assisted Mobility: Achievements and User Satisfaction”. In: *BioMed Research International* 2016 (2016), pp. 1–10. ISSN: 2314-6141. DOI: 10.1155/2016/8459018.

[16] Ana Ferri-Caruana et al. “Accelerometer assessment of physical activity in individuals with paraplegia who do and do not participate in physical exercise”. In: *The Journal of Spinal Cord Medicine* 43.2 (Dec. 2018), pp. 234–240. ISSN: 2045-7723. DOI: 10.1080/10790268.2018.1550597.

[17] P L Ditunno et al. “Who wants to walk? Preferences for recovery after SCI: a longitudinal and cross-sectional study”. In: *Spinal Cord* 46.7 (Jan. 2008), pp. 500–506. ISSN: 1476-5624. DOI: 10.1038/sj.sc.3102172.

[18] Tamar Semerjian et al. “Enhancement of Quality of Life and Body Satisfaction Through the Use of Adapted Exercise Devices for Individuals with Spinal Cord Injuries”. In: *Topics in Spinal Cord Injury Rehabilitation* 11.2 (Oct. 2005), pp. 95–108. ISSN: 1082-0744. DOI: 10.1310/bxe2-mtku-yl15-429a.

[19] Antonio Rodríguez-Fernández, Joan Lobo-Prat, and Josep M. Font-Llagunes. “Systematic review on wearable lower-limb exoskeletons for gait training in neuromuscular impairments”. In: *Journal of NeuroEngineering and Rehabilitation* 18.1 (Feb. 2021). ISSN: 1743-0003. DOI: 10.1186/s12984-021-00815-5.

[20] G Scivoletto et al. “A prototype of an adjustable advanced reciprocating gait orthosis (ARGO) for spinal cord injury (SCI)”. In: *Spinal Cord* 41.3 (Feb. 2003), pp. 187–191. ISSN: 1476-5624. DOI: 10.1038/sj.sc.3101417.

[21] M Massucci et al. “Walking with the Advanced Reciprocating Gait Orthosis (ARGO) in thoracic paraplegic patients: energy expenditure and cardiorespiratory performance”. In: *Spinal Cord* 36.4 (Mar. 1998), pp. 223–227. ISSN: 1476-5624. DOI: 10.1038/sj.sc.3100564.

[22] Janet Rae-Duprees. “A Stimulating New Direction for FES”. In: *IEEE Pulse* 13.6 (Nov. 2022), pp. 12–16. ISSN: 2154-2317. DOI: 10.1109/mpuls.2022.3227809.

[23] Rudi Kobetic et al. “Development of hybrid orthosis for standing, walking, and stair climbing after spinal cord injury”. In: *The Journal of Rehabilitation Research and Development* 46.3 (2009), p. 447. ISSN: 0748-7711. DOI: 10.1682/jrrd.2008.07.0087.

[24] Sanjeev Agarwal et al. “Long-term user perceptions of an implanted neuroprosthesis for exercise, standing, and transfers after spinal cord injury.” In: *Journal of Rehabilitation Research & Development* 40.3 (2003).

[25] Maureen C. Ashe et al. “Response to Functional Electrical Stimulation Cycling in Women With Spinal Cord Injuries Using Dual-Energy X-ray Absorptiometry and Peripheral Quantitative Computed Tomography: A Case Series”. In: *The Journal of Spinal Cord Medicine* 33.1 (Jan. 2010), pp. 68–72. ISSN: 2045-7723. DOI: 10.1080/10790268.2010.11689676.

[26] Shunji Hirokawa et al. “Energy expenditure and fatiguability in paraplegic ambulation using reciprocating gait orthosis and electric stimulation”. In: *Disability and Rehabilitation* 18.3 (Jan. 1996), pp. 115–122. ISSN: 1464-5165. DOI: 10.3109/09638289609166028.

[27] L Sykes et al. “Energy expenditure of walking for adult patients with spinal cord lesions using the reciprocating gait orthosis and functional electrical stimulation”. In: *Spinal Cord* 34.11 (Nov. 1996), pp. 659–665. ISSN: 1476-5624. DOI: 10.1038/sc.1996.119.

[28] Robert Voicu et al. “Influence of gait-synchronized functional electrical stimulation during exoskeleton-assisted ambulation on cardiorespiratory outcomes in individuals with incomplete spinal cord injury”. In: *Journal of Rehabilitation Medicine* 57 (Nov. 2025), jrm43423. ISSN: 1651-2081. DOI: 10.2340/jrm.v57.43423.

[29] EB Marsolais and Bennett G Edwards. “Energy costs of walking and standing with functional neuromuscular stimulation and long leg braces.” In: *Archives of physical medicine and rehabilitation* 69.4 (1988), pp. 243–249.

[30] Régine Brissot et al. “Clinical Experience With Functional Electrical Stimulation-Assisted Gait With Parastep in Spinal Cord–Injured Patients”. In: *Spine* 25.4 (Feb. 2000), pp. 501–508. ISSN: 0362-2436. DOI: 10.1097/00007632-200002150-00018.

[31] Grazia Cicirelli et al. “Human Gait Analysis in Neurodegenerative Diseases: A Review”. In: *IEEE Journal of Biomedical and Health Informatics* 26.1 (Jan. 2022), pp. 229–242. ISSN: 2168-2208. DOI: 10.1109/jbhi.2021.3092875.

[32] Musculoskeletal Key. *Hemiparetic Gait*. Accessed: 19 October 2025. Apr. 2017. URL: https://musculoskeletalkey.com/hemiparetic-gait/.

[33] Joseph Hamill, Kathleen M. Knutzen, and Timothy R. Derrick. *Biomechanical Basis of Human Movement*. 4th ed. Philadelphia, PA: Wolters Kluwer / Lippincott Williams & Wilkins, 2015. ISBN: 978-1-4511-7730-5.

[34] Claim Accident Services. *Spinal Cord Injury Levels*. Accessed: 2025-11-23. 2025. URL: https://claimaccident.ca/personal-injury-wrongful-death-claim-resources/spinal-cord-injury-levels/.

[35] Rüdiger Rupp. “Spinal cord lesions”. In: *Brain-Computer Interfaces*. Ed. by N.F. Ramsey and J. del R. Millán. Vol. 168. Handbook of Clinical Neurology. Elsevier, 2020, pp. 51–65. ISBN: 9780444639349. DOI: 10.1016/B978-0-444-63934-9.00006-8.

[36] Useok Jeong and Kyu-Jin Cho. “A Novel Low-Cost, Large Curvature Bend Sensor Based on a Bowden-Cable”. In: *Sensors* 16.7 (June 2016), p. 961. ISSN: 1424-8220. DOI: 10.3390/s16070961.

[37] Scott L. Delp et al. “OpenSim: Open-Source Software to Create and Analyze Dynamic Simulations of Movement”. In: *IEEE Transactions on Biomedical Engineering* 54.11 (Nov. 2007), pp. 1940–1950. ISSN: 0018-9294. DOI: 10.1109/tbme.2007.901024.

[38] David A. Winter. *Biomechanics and Motor Control of Human Movement*. 4th ed. Hoboken, NJ, USA: John Wiley & Sons, 2009. ISBN: 978-0-470-39818-0.

[39] OpenSim Documentation Team. *Getting Started with Inverse Kinematics*. Accessed: 19 October 2025. Stanford University, OpenSim Project. July 2018. URL: https://opensimconfluence.atlassian.net/wiki/spaces/OpenSim/pages/53090032/Getting+Started+with+Inverse+Kinematics.

[40] OpenSim Documentation Team. *Getting Started with Inverse Dynamics*. Accessed: 19 October 2025. Stanford University, OpenSim Project. 2024. URL: https://opensimconfluence.atlassian.net/wiki/spaces/OpenSim/pages/53090063/Getting+Started+with+Inverse+Dynamics.

[41] Qualisys AB. *Qualisys Track Manager (QTM)*. Accessed: 24 December 2025. 2025. URL: https://www.qualisys.com/software/qualisys-track-manager/.

[42] Kistler Group. *3D force plates for biomechanics and gait analysis*. Accessed: December 2025. 2025. URL: https://www.kistler.com/INT/en/3d-force-plate/C00000090.

[43] CGM2 Project Team. *Conventional Gait Model 2.5 Documentation*. Accessed: October 22, 2025. URL: https://pycgm2.netlify.app/cgm/cgm2.5/.

[44] Philipp Barzyk et al. “AI□smartphone markerless motion capturing of hip, knee, and ankle joint kinematics during countermovement jumps”. In: *European Journal of Sport Science* 24.10 (Aug. 2024), pp. 1452–1462. ISSN: 1536-7290. DOI: 10.1002/ejsc.12186.

[45] pyCGM2 Project. *Palpation Landmarks*. Accessed: 20 October 2025. URL: https://pycgm2.netlify.app/ressources/palpation/.

[46] Adrian K. M. Lai, Allison S. Arnold, and James M. Wakeling. “Why are Antagonist Muscles Co-activated in My Simulation? A Musculoskeletal Model for Analysing Human Locomotor Tasks”. In: *Annals of Biomedical Engineering* 45.12 (Sept. 2017), pp. 2762–2774. ISSN: 1573-9686. DOI: 10.1007/s10439-017-1920-7.

[47] Scott D. Uhlrich et al. “Muscle coordination retraining inspired by musculoskeletal simulations reduces knee contact force”. In: *Scientific Reports* 12.1 (July 2022). ISSN: 2045-2322. DOI: 10.1038/s41598-022-13386-9.

[48] Apoorva Rajagopal et al. “Full-Body Musculoskeletal Model for Muscle-Driven Simulation of Human Gait”. In: *IEEE Transactions on Biomedical Engineering* 63.10 (Oct. 2016), pp. 2068–2079. ISSN: 1558-2531. DOI: 10.1109/tbme.2016.2586891.

[49] OpenSim Creator Developers. *OpenSim Creator*. Accessed: 2025-12-01. 2025. URL: https://www.opensimcreator.com/.

[50] Míriam Febrer-Nafría et al. “Prediction of three-dimensional crutch walking patterns using a torque-driven model”. In: *Multibody System Dynamics* 51.1 (June 2020), pp. 1–19. ISSN: 1573-272X. DOI: 10.1007/s11044-020-09751-z.

[51] David Osgood, Vincent Cameron, and Bradley Christensen. *Mass Moment of Inertia*. Open access educational resource, accessed 19 December 2025. 2016. URL: https://eng.libretexts.org/Bookshelves/Engineering/Statics/Engineering_Statics_(Osgood)/07%3A_Moments_of_Inertia/7.04%3A_Mass_Moment_of_Inertia.

[52] OpenSim Team. *BushingForce Class Documentation*. Accessed: 2025-12-01. 2025. URL: https://simtk.org/api_docs/opensim/api_docs/classOpenSim_1_1BushingForce.html (visited on 12/01/2025).

[53] Adrian Sahetapy. “Effect of Cuff Compliance on Muscle Activation in a Passive Shoulder-Exotendon Suit”. Master’s thesis. Delft, The Netherlands: Delft University of Technology, 2024.

[54] M. M. Samson et al. “Differences in gait parameters at a preferred walking speed in healthy subjects due to age, height and body weight”. In: *Aging Clinical and Experimental Research* 13.1 (Feb. 2001), pp. 16–21. ISSN: 1720-8319. DOI: 10.1007/bf03351489.

[55] Joseph B. Webster and Benjamin J. Darter. “Principles of Normal and Pathologic Gait”. In: *Atlas of Orthoses and Assistive Devices*. Elsevier, 2019, 49–62.e1. ISBN: 9780323483230. DOI: 10.1016/b978-0-323-48323-0.00004-4.

[56] Jennifer Hicks. *Tutorial 1 – Intro to Musculoskeletal Modeling*. OpenSim Documentation. Mar. 2025. URL: https://opensimconfluence.atlassian.net/wiki/spaces/OpenSim/pages/53088700/Tutorial+1+-+Intro+to+Musculoskeletal+Modeling.

[57] OpenSim Documentation. *Gait 2392 and 2354 Models*. Accessed: 19 December 2025. Mar. 2024. URL: https://opensimconfluence.atlassian.net/wiki/spaces/OpenSim/pages/53086215/Gait+2392+and+2354+Models.

[58] Chand T. John et al. “Contributions of muscles to mediolateral ground reaction force over a range of walking speeds”. In: *Journal of Biomechanics* 45.14 (Sept. 2012), pp. 2438–2443. ISSN: 0021-9290. DOI: 10.1016/j.jbiomech.2012.06.037.

[59] Allison S. Arnold et al. “The role of estimating muscle-tendon lengths and velocities of the hamstrings in the evaluation and treatment of crouch gait”. In: *Gait & Posture* 23.3 (Apr. 2006), pp. 273–281. ISSN: 0966-6362. DOI: 10.1016/j.gaitpost.2005.03.003.

[60] Jonathan Camargo et al. “A comprehensive, open-source dataset of lower limb biomechanics in multiple conditions of stairs, ramps, and level-ground ambulation and transitions”. In: *Journal of Biomechanics* 119 (Apr. 2021), p. 110320. ISSN: 0021-9290. DOI: 10.1016/j.jbiomech.2021.110320.

[61] Mokhtar Arazpour et al. “Comparison of gait between healthy participants and persons with spinal cord injury when using the advanced reciprocating gait orthosis”. In: *Prosthetics & Orthotics International* 40.2 (Apr. 2016), pp. 287–293. ISSN: 0309-3646. DOI: 10.1177/0309364615592699.

[62] Mokhtar Arazpour et al. “The influence of trunk extension in using advanced reciprocating gait orthosis on walking in spinal cord injury patients: A pilot study”. In: *Prosthetics & Orthotics International* 39.4 (Aug. 2015), pp. 286–292. ISSN: 0309-3646. DOI: 10.1177/0309364614531010.

[63] Marco Capogrosso et al. “A brain–spine interface alleviating gait deficits after spinal cord injury in primates”. In: *Nature* 539.7628 (Nov. 2016), pp. 284–288. ISSN: 1476-4687. DOI: 10.1038/nature20118.

[64] Henri Lorach et al. “Walking naturally after spinal cord injury using a brain–spine interface”. In: *Nature* 618.7963 (May 2023), pp. 126–133. ISSN: 1476-4687. DOI: 10.1038/s41586-023-06094-5.

[65] SeyedHooman Hosseini-Zahraei et al. “A Simple OpenSim-Simulink Interface for Cascaded Zero-Force Control of Human-Robot Interaction in a Hip Exoskeleton Robot”. In: *2022 10th RSI International Conference on Robotics and Mechatronics (ICRoM)*. IEEE, Nov. 2022, pp. 55–60. DOI: 10.1109/icrom57054.2022.10025309.

[66] Andreas Christou et al. “Model-Based Optimization for the Personalization of Robot-Assisted Gait Training”. In: *IEEE Transactions on Medical Robotics and Bionics* 7.2 (May 2025), pp. 642–654. ISSN: 2576-3202. DOI: 10.1109/tmrb.2025.3550649.

[67] Gabriela B. De Carvalho et al. “Hip, knee, and ankle joint forces during exoskeletal-assisted walking: Comparison of approaches to simulate human-robot interactions”. In: *PLOS One* 20.8 (Aug. 2025). Ed. by Jyotindra Narayan, e0322247. ISSN: 1932-6203. DOI: 10.1371/journal.pone.0322247.

[68] Christopher L. Dembia et al. “OpenSim Moco: Musculoskeletal optimal control”. In: *PLOS Computational Biology* 16.12 (Dec. 2020). Ed. by Kenneth S. Campbell, e1008493. ISSN: 1553-7358. DOI: 10.1371/journal.pcbi.1008493.

[69] Ana Carolina C. de Sousa, João Pedro C.D. Freire, and Antonio P.L. Bo. “Integrating hip exosuit and FES for lower limb rehabilitation in a simulation environment”. In: *IFAC-PapersOnLine* 51.34 (2019), pp. 302–307. ISSN: 2405-8963. DOI: 10.1016/j.ifacol.2019.01.030.

[70] Nathaniel S. Makowski et al. “Biologically Inspired Optimal Terminal Iterative Learning Control for the Swing Phase of Gait in a Hybrid Neuroprosthesis: A Modeling Study”. In: *Bioengineering* 9.2 (Feb. 2022), p. 71. ISSN: 2306-5354. DOI: 10.3390/bioengineering9020071.

[71] Courtney M. Mazur et al. “Bone Mineral Loss at the Distal Femur and Proximal Tibia Following Spinal Cord Injury in Men and Women”. In: *Journal of Clinical Densitometry* 26.3 (July 2023), p. 101380. ISSN: 1094-6950. DOI: 10.1016/j.jocd.2023.101380.

[72] W. B. Edwards, T. J. Schnitzer, and K. L. Troy. “Bone mineral loss at the proximal femur in acute spinal cord injury”. In: *Osteoporosis International* 24.9 (Mar. 2013), pp. 2461–2469. ISSN: 1433-2965. DOI: 10.1007/s00198-013-2323-8.

[73] W. B. Edwards, T. J. Schnitzer, and K. L. Troy. “Bone mineral and stiffness loss at the distal femur and proximal tibia in acute spinal cord injury”. In: *Osteoporosis International* 25.3 (Nov. 2013), pp. 1005–1015. ISSN: 1433-2965. DOI: 10.1007/s00198-013-2557-5.

[74] M Dauty et al. “Supralesional and sublesional bone mineral density in spinal cord-injured patients”. In: *Bone* 27.2 (Aug. 2000), pp. 305–309. ISSN: 8756-3282. DOI: 10.1016/s8756-3282(00)00326-4.

[75] Prisca Eser et al. “Fracture threshold in the femur and tibia of people with spinal cord injury as determined by peripheral quantitative computed tomography”. In: *Archives of Physical Medicine and Rehabilitation* 86.3 (Mar. 2005), pp. 498–504. ISSN: 0003-9993. DOI: 10.1016/j.apmr.2004.09.006.

[76] P Eser et al. “Relationship between the duration of paralysis and bone structure: a pQCT study of spinal cord injured individuals”. In: *Bone* 34.5 (May 2004), pp. 869–880. ISSN: 8756-3282. DOI: 10.1016/j.bone.2004.01.001.

[77] Dany H. Gagnon et al. “Locomotor training using an overground robotic exoskeleton in long-term manual wheelchair users with a chronic spinal cord injury living in the community: Lessons learned from a feasibility study in terms of recruitment, attendance, learnability, performance and safety”. In: *Journal of NeuroEngineering and Rehabilitation* 15.1 (Mar. 2018). ISSN: 1743-0003. DOI: 10.1186/s12984-018-0354-2.

[78] Ian Benson et al. “Lower-limb exoskeletons for individuals with chronic spinal cord injury: findings from a feasibility study”. In: *Clinical Rehabilitation* 30.1 (Mar. 2015), pp. 73–84. ISSN: 1477-0873. DOI: 10.1177/0269215515575166.

[79] Ali Nikoo and Thomas K. Uchida. “Be Careful What You Wish for: Cost Function Sensitivity in Predictive Simulations for Assistive Device Design”. In: *Symmetry* 14.12 (Nov. 2022), p. 2534. ISSN: 2073-8994. DOI: 10.3390/sym14122534.

[80] Evomotion GmbH. *The Evomove® System — Evomotion*. 2025. URL: https://evomotion.de/en/the-evomove/ (visited on 11/28/2025).

[81] Evomotion GmbH. *Evomove® – brochure for functional electrical stimulation system (Flyer V4.1.0 EN)*. https://evomotion.de/wp-content/uploads/2025/03/Flyer_V4.1.0_EN_Digital.pdf. Accessed: 2025-11-28. 2025.

A

Literature Review

A literature review for the course TM30003.

Integration of Functional Electrical Stimulation in Passive and Semi-Passive Orthoses for Individuals with Spinal Cord Injuries: A Literature Review

A.L. (Linde) Zegwaard[a]

Supervisors: R. Osterthun[b], G. Smit[c], M.G.H. Wesseling[d]

[a]*Student MSc Technical Medicine, Delft University of Technology, Delft, The Netherlands,*
[b]*Department of Rehabilitation Medicine, Erasmus Medical Center, Rijndam Revalidatie, Rotterdam, the Netherlands*
[c]*Department of Biomechanical Engineering, Delft University*
[d]*Department of Orthopaedics and Sports Medicine, Erasmus Medical Center, Rotterdam, the Netherlands*

Abstract

Background: Walking restoration remains a high priority for individuals with spinal cord injury (SCI). Orthotic devices and exoskeletons have been developed to support walking, but often face limitations such as poor usability due to their heavy structures and limited user-driven control. Combining Functional Electrical Stimulation (FES) with passive or semi-passive orthoses may help overcome these limitations by actively engaging the user's own paralyzed muscles, potentially reducing reliance on heavy external actuators and providing additional health benefits. However, rapid muscle fatigue remains a major challenge, requiring effective control strategies and design solutions.

Methods: In February 2025, a systematic search of seven databases (Medline ALL, Embase, Web of Science, Cochrane Central, Scopus, IEEE Xplore, Google Scholar) was conducted for studies published after 2010 on FES combined with passive or semi-passive orthoses for gait support in SCI. Studies were screened based on predefined inclusion criteria. Data on orthosis design, FES parameters, and control strategies were extracted. In addition, reported outcomes on the studies were also evaluated.

Results: Twenty-one studies met the inclusion criteria. Fifteen simulation studies investigated fully passive FES–orthosis concepts, demonstrating that energy-storing and joint-locking mechanisms could reduce the muscle torque needed from FES, and that optimized FES controllers may improve stimulation timing, gait-phase transitions, and fatigue resistance. Six experimental studies tested semi-passive orthotic designs with limited actuation combined with FES in eight individuals with SCI. These trials demonstrated synchronized FES stimulation with orthotic support, enabling walking ranging from a few steps to six minutes, with benefits such as reduced spasticity. Limitations included rapid fatigue, tracking errors, and limited endurance, as well as the small, laboratory-based nature of the trials.

Conclusion: Passive and semi-passive FES–orthosis systems show potential to support stepping and short walking trials in individuals with SCI. While the studies highlight promising design and control strategies, experimental evidence remains scarce. Future work should focus on validating fatigue management approaches, refining adaptive control algorithms, and evaluating long-term feasibility and usability in clinical and real-world rehabilitation contexts.

Keywords: Functional Electrical Stimulation, Passive Orthosis, Hybrid Exoskeleton, Gait Support, Spinal Cord Injury.

1 Introduction

The spinal cord serves as the main pathway for transmitting for motor and sensory signals between the brain and the body. When damaged by trauma or disease, the conduction of the signals is affected, which is known as a condition called spinal cord injury (SCI). Paraplegia can result from SCI and is characterized by the impairment or loss of motor and/or sensory function in the thoracic, lumbar or sacral segments of the spinal cord. In paraplegia, arm function is preserved, while the trunk, legs and pelvic organs may be affected, depending on the level of injury[1].

Individuals with SCI experience a wide range of secondary health conditions, including pain, spasticity, and bladder and bowel dysfunction[2]. In addition, the sedentary lifestyle commonly observed in this population, due to paralysis which contributes to their reduced mobility compared to that of the able-bodied individual[3], further increases the risk of secondary health complications. These include cardiovascular disease[4], type 2 diabetes [5][6], pressure ulcers[7] and ultimately, reduced life expectancy[8]. Immobilization following SCI also frequently leads to osteoporosis[9][10] and muscle

atrophy[11]. Improving mobility may therefore play an important role in maintaining health and mitigating complications in this population.

The wheelchair remains the primary means of mobility for individuals with SCI and lower-limb paresis[12], and being in a wheelchair still allows for physical activity, particularly for the upper body, which can offer health benefits. Nevertheless, a 2008 survey showed that walking remains a top recovery priority, regardless of injury severity, time since injury, or age at onset for individuals with SCI[13]. Moreover, technologies that enable individuals with SCI to stand or walk have been shown to improve body image and sense of well-being[14].

Rehabilitation methods, such as body weight-supported treadmill training, orthoses, and robotic exoskeletons, allow individuals with SCI to practice walking movements in an upright position. However, current orthotic and exoskeletal systems still present limitations in terms of usability, effectiveness, and accessibility.

Many wearable exoskeletons are still heavy and bulky devices due to their rigid structures, actuators and batteries[15], which limits their practicality in daily life. Additionally, many systems rely on pre-defined movement trajectories[15], offering limited adaptability or user-driven control. As a result, users often become passive participants during training, rather than active contributors to the walking motion. Current systems often do not sufficiently engage the user's own musculature.

Functional Electrical Stimulation (FES) has been introduced to help solve some of the shortcomings of mechanical orthoses[16]. FES is a technology which uses electrical currents delivered through electrodes to induce muscle contractions, thereby activating one's own paralyzed muscles, which can replace the natural signal that should be coming from the brain[17]. In combination with orthotic devices, FES can help stabilize the body against collapse and provide the power for forward progression[16]. Furthermore, FES may be able to improve some of the physiologic problems that result from reduced mobility[18]. Reported health benefits include improving the ratio of high density and low density lipoproteins, reducing insulin resistance[19, 20], improving cardio- and pulmonary fitness[21], improving muscle mass and endurance[22], and preserving bone mass[23]. Additional benefits include improving circulation[24], reducing the likelihood of deep vein thrombophlebitis[25], and reducing spasticity[26].

One major limitation of FES, however, is the rapid onset of muscle fatigue. Consequently, FES-assisted walking in individuals with paraplegia requires high metabolic effort[27] and primarily remains experimental and for therapeutic exercise[28, 29].

However, optimizing FES control strategies and refining orthosis design could help reduce muscle fatigue and enhance the overall feasibility of these systems for therapeutic use.

This review provides an overview of how Functional Electrical Stimulation (FES) has been integrated with passive and semi-passive orthoses in existing studies, focusing on FES control strategies and design principles for orthotic gait support in individuals with spinal cord injury. In this context, passive orthoses refer to studies that apply FES in combination with mechanical or reciprocating orthoses and exoskeletons during walking, without powered actuators. Semi-passive orthoses refer to orthotic devices in which powered actuators are included as an addition to FES, operating with an assist-as-needed approach to compensate for performance loss due to muscle fatigue.
In 2012, del-Ama et al.[30] published a comprehensive review covering previous work on lower-limb exoskeletons integrated with FES, which they referred to as hybrid exoskeletons. Building on that foundation, the present review includes studies published from 2012 onwards, while also including relevant articles from 2010 and 2011. These studies are compared and categorized according to their control strategies and orthotic designs, providing insight into the current state of hybrid gait technologies.

2 Methods

2.1 Databases and search strategy

On February 17th, 2025, a comprehensive literature search was conducted in the following databases: Medline ALL, Embase, Web of Science, Cochrane Central Register of Controlled Trials, Scopus, IEEE Xplore and Google Scholar. The search query focused on studies researching orthoses and exoskeletons combined with FES for individuals with spinal cord injury. The search queries used for each database are provided in Appendix A. Only studies published from 2010 onwards were reviewed in this literature review, as a systematic review by del-Ama et al. already provides an overview of hybrid lower-limb exoskeletons from before 2012, including passive orthoses combined with functional electrical stimulation[30].

2.2 Study selection

This review included articles specifically addressing the application of FES in a orthotic device applied to the lower limbs for people with spinal cord injuries. Publications identified through the search were screened for relevance on the criteria formulated below. Screening was performed by a single reviewer, initially based on title and abstract, followed by an evaluation of the full text.

The formulated inclusion criteria were:
(1) Studies that apply functional electrical stimulation (FES) in combination with mechanical and reciprocating orthoses or exoskeletons during walking.
(2) Studies in which the orthoses are intended for individuals with spinal cord injury (SCI).

The formulated exclusion criteria were:
(1)Studies done on healthy participants, patients with stroke, cerebral palsy, or other neurological conditions that are not SCI.
(2) Studies that use FES as a therapy for muscle conditioning before walking or applied during cycling, rather than being directly integrated with orthoses or exoskeletons for gait assistence.
(3) Studies using FES only in combination with walking aids such as a walker, or similar assistive devices that do not involve mechanical orthoses or exoskeletons.
(4) Studies where brain-computer interfaces (BCIs) are used instead of FES to control movement.

(5) Studies applying FES to the upper body rather than the lower limbs.
(6) Studies where FES is exclusively used with an ankle-foot orthosis (AFO), without involvement of the knee joint or reciprocating or mechanical orthoses.
(7) Studies using implanted electrodes for FES or functional neuromuscular stimulation (FNS) where electrodes are surgically placed inside the body, instead of using surface electrodes.
(8) Studies integrating FES with powered actuators as the primary driving force in orthotic devices, instead of orthoses where FES is the main driving force, potentially supported by small actuators and following an assisted-as-needed approach for these actuators.
(9) Studies analyzing only non-walking movements, such as sit-to-stand transitions, stair climbing, or static balance exercises, without including any form of gait assessment.
(10) Studies of which the full text was not available in English.

2.3 Strategy for searching articles

As mentioned above, only studies published from 2010 onwards were included in the initial search. Although the primary focus was on articles from 2012 onwards, relevant publications from 2010 and 2011 that provide valuable information have also been incorporated into this review.

2.4 Data extraction

During the full-text review of all included studies, data were extracted on the type of exoskeleton or orthosis used, the muscles stimulated by FES, the applied FES parameters, and the control strategy for FES stimulation. Depending on the study type, additional parameters were collected: simulation tools, energy-storing mechanisms and joint-locking mchanisms in theoretical studies, and participant injury characteristics and motor placement in experimental studies.
Additionally, information on the study objectives and reported outcomes was extracted and evaluated.

3 Results

3.1 Search results and study characteristics

The study selection process is outlined in the PRISMA flow diagram, shown in Figure 1. In total, 1,877 articles were identified through the database search. After removing 1,341 duplicates and studies published before 2010, 535 articles remained for title and abstract screening. Subsequently, 228 articles were retrieved for full-text review, and 215 were excluded after full-text assessment Ultimately, 14 studies published from 2012 onwards met the eligibility criteria for inclusion in this literature review. Additionally, 7 relevant studies published before 2012 were included. This resulted in a final selection of 21 articles.
The initial focus of this article was on studies involving fully passive orthoses or exoskeletons combined with FES, tested during walking in individuals with spinal cord injury. However, no studies investigating fully passive orthoses in combination with FES that were tested in experimental settings on individuals with SCI were found, which led to a broadening of the initially defined inclusion criteria. This resulted in the inclusion of 21 articles, of which 15 explored the combination of passive orthotic devices and FES for spinal cord injury but were purely theoretical and not tested on individuals with SCI. Six studies investigated hybrid devices equipped with motors or actuators, in which FES was the main driving force for movement and the actuators primarily provided additional support rather than serving as the main source of motion. Only hybrid studies in which the orthosis was tested in individuals with spinal cord injury were included.
Table 1 and table 2 enlist the extracted data from these articles.

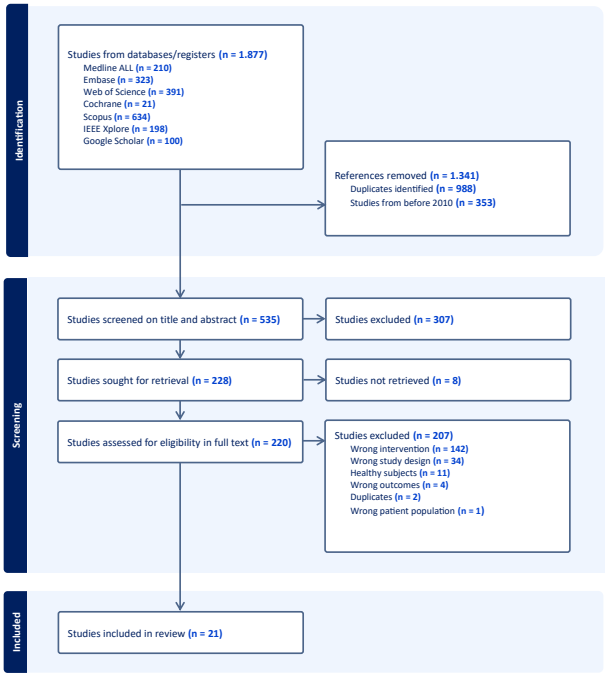

Figure 1: *PRISMA flow diagram of the study selection process*

3.2 Theoretical studies on fully passive FES-orthotic devices

In the theoretical studies, fully passive orthotic devices designed to support walking in individuals with spinal cord injury were investigated, although some designs incorporated miniature servo motors for locking and unlocking the hip and/or knee joints.

It was found that some of the included studies originated from the same research groups, leading to some similarity and continuity across studies. Four of included theoretical studies were authored by Sharma et al. and five were authored by Jailani et al, which resulted in related works that build upon one another.

3.2.1 Design of passive orthotic device

Since FES in individuals with SCI can lead to rapid muscle fatigue, as mentioned in the introduction, and the theoretical studies included in this review did not, or minimally, incorporate motors or actuators, researchers focused on the mechanical design of the orthotic devices to reduce muscle fatigue by providing passive support. The goal was to reduce the physical demand on the stimulated muscles

and support completion of the gait cycle, for which various strategies were explored in these studies, such as energy storage mechanisms and joint locking or control systems. This paragraph discusses those mechanisms in more detail. In table 1 the type of orthosis used in each study is specified under the column "Exoskeleton type".

Energy storage mechanisms Many of the included studies incorporated springs at the knee joints to enable passive energy storage. During FES-induced knee extension, potential energy is stored in the spring, which can then be released to assist with knee flexion during the initial swing phase. As can be seen in Table 1, some studies also implemented hip springs. For example, Gustafson et al.[31] used hip springs that are charged by upper body force and released passively to facilitate hip flexion. In the study by Boughner et al.[32], a hip equilibrium spring stores energy when another spring, a transfer spring, is released. This transfer spring stores energy during quadriceps activation for knee extension. The studies by Brown et al.[33], Ullah et al.[34], and Kangude et al.[35], explored alternative energy storage mechanisms, including gas springs, energy units, pneumatic systems and rubber bands, to support joint movement.

Joint locking mechanisms Theoretical studies included in this review also describe mechanisms for joint control based on locking and unlocking of the knee and hip joints. These mechanisms reduce the need for continuous FES application, thereby minimizing muscle fatigue and enhancing stability. They achieve this by allowing movement in one direction while locking the joint in the opposite direction, or by enabling selective locking in both directions, depending on the phase of the gait cycle.

The various mechanisms used for this are mentioned in Table 1 under the column "Joint Locking Mechanisms".

Joint locking control The control of joint locking mechanisms varies widely across studies, ranging from actively controlled systems with precise timing to passive or mechanically triggered designs. This paragraph categorizes the studies according to the type of control strategy employed.

Active electronically controlled mechanisms: In some of the included studies, the locking and unlocking of knee and hip joints are actively controlled using small, motorized components or microcontroller-based systems. For example, Boughner et al.[32] used miniature servo motors to actively unlock wrap spring brakes that are normally locked. The timing of locking and unlocking was coordinated with the gait phases to optimize energy use and prevent muscle fatigue. Similarly, Kangude et al.[35] applied Pulse Width Modulation (PWM)-controlled solenoids to unlock the wrap spring brakes of both the hip and knee joints, that are normally locked. Each brake was controlled by a microcontroller, with timing managed through open-loop step cycle control executed on a netbook worn by the user.

User-triggered control: Other systems rely on mechanical events or direct user input. In a study by Sharma et al.[36], a spring clutch mechanism was used for knee joint locking, controlled via force-sensitive resistors in the foot or a hand-operated switch. In the study by Gustafson et al.[31], joint locking was primarily coordinated through the user's upper body forces. Weight shifting and torso uprighting mechanically triggered spring loading and release, thereby managing joint transitions during the gait cycle. Ullah et al.[34] employed a unidirectional clutch mechanism, where joint motion was passively restricted based on angular velocity. When moving in the preferred direction, no resistance torque was applied, whereas movement in the locked direction generates a resistive torque equivalent to that of a spring-damper system, effectively preventing backward motion.

State and time-based control: Some studies employed predefined timing schemes. The most recent included study by Jailani et al.[37] describes the use of a finite state controller (FSC) to manage the hip and knee brakes. An FSC, or finite state machine, is a conceptual model composed of a defined set of states, along with input and output events that determine transitions between states and trigger corresponding actions. In this study, FSC is used not only for brake control, but also to coordinate FES and spring engagement throughout the gait cycle. The use of FSC for FES control is further elaborated in the section "FES control strategies".
Earlier studies by Jailani et al.[38, 39, 40, 41] used a timing block to control the knee brake by sending strobe signals at predefined moments, thereby initiating the swing phase and re-engaging the brake to support stance. For the hip, a state-based locking strategy is implemented in which the hip locking occurred at the point of maximum flexion during swing and remained fixed until the end of the swing phase, supporting stable gait.

Finally, some studies, such as those by Huq et al.[42], Brown et al.[33], and Sharma et al.[43], included mechanical brakes in their designs but did not specify how these were controlled.

3.2.2 FES configuration and control

This paragraph elaborates on the FES stimulation parameters and control strategies proposed in the included studies, providing insight into how FES was configured and coordinated to support gait.

Targeted muscle groups and movements The quadriceps is the most consistently targeted muscle group across the included studies, and the only one stimulated in all theoretical models. Some studies mention additional specific muscles, while others refer more generally to the stimulation of the hip and knee flexors and extensors, as shown in Table 1 under the column "Muscles stimulated (muscles)." In the brackets, the intended movement of the stimulated muscles is indicated. Across all studies where the quadriceps was stimulated, the intended movement was knee extension, mainly required during the stance phase. Some studies reported that quadriceps stimulation produced more energy than needed for extension. This excess energy was stored in the spring mechanisms of the exoskeleton to be released later in the gait cycle, for example, to support hip or knee flexion[33] or hip extension[35]. In some cases, it was only noted that the energy was

stored for later use, without specifying which movement it exactly contributed to[32, 34, 42]. Furthermore, in all Sharma studies [36, 43, 44, 45], FES was applied to hip and knee flexors and extensors to generate the movements required for step initiation, leg swing, and general joint motion during walking. However, the studies did not specify in detail which exact movements each muscle contributed to.
Some studies provide further detail on surface electrode placement. For example, Gustafson et al.[31] describe two large surface electrodes placed on the leg, one of which is positioned over the quadriceps motor point near the hip socket, and one just above the knee. Kangude et al.[35] also report specific placements, using 2×4 inch uni-patch electrodes positioned 6 cm proximal to the kneecap and on the upper thigh about 2 cm from the right midline.
Only a few studies specify the number of stimulation channels. For instance, Kangude et al[35] used single-channel, uni-phasic, charge-balanced stimulation of the quadriceps.

FES parameters This section describes the stimulation parameters used across studies, such as frequency and pulse width, that are defined prior to walking. An overview of the parameters per study can be seen in Table 1 under the column "FES parameters". Not all included studies provided details on stimulation parameters. Specifically, Brown et al.[33] and Sharma et al.[43] did not report these settings. Among the remaining studies, reporting varied: some provided specific values (stimulation frequency)[42, 38, 39, 40, 41], others reported calculated target torques to achieve a desired step length and cycle time (e.g., 15 Nm by Gustafson et al.[31] and Boughner et al.[32], and 7 Nm by Ullah et al.[34]), and some described stimulation intensity in arbitrary units[36, 44, 45]. The studies that reported a specific value for FES parameters, explained how the parameter pulse width was modulated while keeping the stimulation frequency fixed (25 Hz for Huq et al.[42] or 33 Hz for Jailani et al.[38, 39, 40, 41]). Studies that dynamically adjusted stimulation parameters during walking are further discussed in the section "FES control strategies".

FES control strategies FES control strategies refer to the methods used to determine when muscles are stimulated during the gait cycle and how stimulation is regulated or adjusted over time. These strategies range from simple rule-based activation, such as triggering stimulation when a joint angle crosses a predefined threshold, to advanced, adaptive control systems optimized that aim to minimize muscular fatigue and improve gait performance. Based on the included studies, the control strategies can be broadly categorized into feedforward control, closed-loop control, and optimization-based control.

Feedforward control: Feedforward control involves predefined rules or timings that trigger muscle stimulation without using real-time feedback. For example, Gustafson et al.[31] applied stimulation based on predefined thresholds, e.g. when the hip reached full flexion, and thereby initiating knee extension. This approach relies on known gait events and fixed thresholds. Brown et al.[33] employed a similar strategy in which stimulation was triggered at fixed points within the gait cycle. Ullah et al.[34] also used a phase-based open-loop system in which stimulation was applied during a specific phase to initiate knee extension. In the study by Boughner et al.[32], stimulation was applied only during knee extension; once full extension was achieved, the knee joint was mechanically locked and stimulation turned off to reduce muscle fatigue. Kangude et al.[35] similarly used a step cycle control system that followed a preprogrammed sequence of events, without real-time adaptation based on feedback.

Closed-loop control: In contrast, closed-loop control strategies dynamically adjust stimulation parameters in response to sensor feedback. These systems are often more complex but allow for greater adaptability and precision. Huq et al.[42] tested two closed-loop strategies to regulate knee extension, using either a Proportional-Integral-Derivative (PID) controller or a Fuzzy Logic Controller (FLC). These controllers aim to adjust stimulation in real time to ensure that joint movements follow the intended trajectory as accurately and smoothly as possible.
The first strategy involved continuous tracking of a reference trajectory. This reference trajectory could be derived either from the passive oscillation of the spring brake orthosis (SBO) or could be adapted iteratively from previous steps through a cycle-to-cycle control approach, where stimulation patterns are refined over successive gait cycles. The PID or FLC controller modulates the stimulation intensity or stimulation pulse-width in real time based on the difference between the actual and desired knee joint angle trajectory.
The second strategy was a part-time closed-loop controller that activated at a defined time after the start of the swing, aiming to reach a target (e.g., full knee extension) without following an entire trajectory. This approach was simpler and focused on achieving a specific target rather than continuously adapting to dynamic inputs. Both strategies were implemented using either PID or FLC. Their control parameters were optimized using Genetic Algorithms (GA). GA helped identify optimal controller parameters to improve motion accuracy and minimize fatigue. Results indicated that cycle-to-cycle control was more effective at reaching target joint angles, while FLC minimized overshoot and PID reduced muscle fatigue.
Similarly, the studies by Jailani et al.[38, 39, 40, 41] employed PID or FLC systems to modulate stimulation pulse width based on knee joint angle error, while keeping stimulation frequency fixed. In their most recent study[37], Jailani et al. introduced a Finite State Controller (FSC) strategy, which was designed and implemented in MATLAB Simulink and integrated with a dynamic walking model for output analysis. The FSC manages transitions between gait phases and consists of a set of states, with transition functions that respond to input events and trigger corresponding outputs. This event-triggered approach coordinates the activation of brakes, FES, and energy-storing springs, ensuring that a transaction from one state to another only takes place if a predefined event occurs.

Optimization-based control: A third group of studies applied optimization-based control, in which stimulation profiles, joint trajectories and arm reaction forces are computed using mathematical models and cost functions. In

a series of simulation studies by Sharma et al.[36, 44, 45], stimulation intensity was modeled as abstract, time-varying inputs for each agonist-antagonist muscle pair. Only one muscle from each agonist-antagonist pair was stimulated at a time to reduce co-activation and delay fatigue. In the optimization framework that used MATLAB's fmincon optimization tool, for each step, stimulation and force profiles were defined at discrete time points, and linear interpolation was used to create smooth, continuous trajectories across the gait cycle. In this optimization tool, a cost function minimized excessive muscle activation, arm reaction forces, and deviations from a target gait trajectory. The total cost function, or objective function, was distributed across three gait phases: initial double support (DSP), single support (SSP), and final DSP, and was defined as:

$$\Pi = \int_{t_0}^{t_1} F_w^2 \, dt + \int_{t_1}^{t_2} \left(F_w^2 + u_{h_f}^2 + u_{h_e}^2 + u_{k_f}^2 + u_{k_e}^2 \right) dt + \int_{t_2}^{t_f} F_w^2 \, dt$$

,where where u_i (where $i \in \{h_f, h_e, k_f, k_e\}$) are the muscle stimulation variables of hip flexors, hip extensors, knee flexors, knee extensors, F_w is arm reaction force, and t_0, t_1, t_2 and t_f define the start and end points of each gait phase, respectively.
Biomechanical constraints ensured realistic joint angles, swing leg clearance, and step durations. Active stimulation was only applied during the SSP, while the orthosis provided stability during stance. This framework aimed to generate energy-efficient, fatigue-minimizing gait patterns suitable for FES-assisted walking in individuals with spinal cord injury.

Lastly, the remaining study by Sharma et al.[43] does not propose an explicit FES control strategy but addresses the sensor limitation by introducing a nonlinear state-dependent coefficient (SDC) estimator for robust real-time estimation of lower-limb angles using noisy intertial measurement unit (IMU) data. The resulting kinematic estimates can enhance the accuracy and timing of FES application and thereby support the implementation of other various control strategies.

3.2.3 Aims and simulation outcomes of the studies

The theoretical studies mainly focused on two aspects: improving exoskeleton design and developing advanced FES control strategies to support gait after SCI. Some studies focused on redesigning exoskeletons to be lighter, improve joint control[33], and enable standing or stepping[31], often incorporating energy-storing or joint-locking mechanisms. Others targeted the reduction of muscle torque requirements, for example by adapting step size while maintaining toe clearance[34]. Other studies concentrated on advanced control strategies, as described in previous sections, with the goal of optimizing stimulation timing, gait trajectories, and robustness. Across these approaches, recurring aims were the reduction of muscle fatigue, lowering of metabolic energy cost, and the achievement of stable gait patterns.
Simulation outcomes generally suggested that the proposed concepts could be technically feasible. Studies ensured in their models that predicted torques and step lengths remained within achievable ranges, and studies indicated that quadriceps torque could be reduced through adapted step size[34] or the use of energy-storing mechanisms. Optimized controllers and algorithms were shown to produce gait trajectories, improve gait-phase transitions, and reduce both muscle activations and reliance on upper-body effort. Some studies also reported design-specific findings, such as springs that best matched reference trajectories[38] or control methods that achieved smoother knee movements[37] and more accurate timing of knee flexion[38]. However, details about overall gait quality were mostly not provided, since none of the studies have yet been experimentally validated. The conclusions consistently emphasized that these results remain limited to simulations.
The studies suggest that although many approaches demonstrated improvements compared to earlier models or concepts, further development and prototype testing are required to validate whether the predicted benefits can translate into functional gait in practice.

3.3 Experimental studies on semi-passive FES-orthotic devices

During the literature search, it was noted that many recent studies integrated motor or actuator support into the orthotic devices to compensate for muscle fatigue. Therefore, such studies were considered for inclusion, provided that the motor or actuator served only as an addition to FES, rather than being the primary source of gait generation. The additional motor or actuator support was provided only to compensate for performance loss due to muscle fatigue as a result of applying FES. Only studies that were tested on participants with spinal cord injury were included.
It was found that several of the included studies originated from the same research groups, resulting in noticeable similarities and continuity across publications. For instance, in the two studies by Iyer et al.[46] and Sun et al.[47], all three researchers Iyer, Sun, and Lambeth were involved. In the most recent study from 2024, authored by Lambeth et al.[48], both Iyer and Sharma contributed. Notably, Sharma had also been involved in the 2018 study by Alibeji et al.[49] This overlap in authors reflects some continuity in research focus and methodology across these studies.

3.3.1 Motor placement

In four of the six included experimental studies, motors were placed bidirectionally at the hip and knee joints[48, 46, 47, 49]. In the study by del-Ama et al.[50], active actuators were placed only at the knee joints as the Kinesis orthosis, a bilateral knee-ankle-foot-orthosis (KAFO), does not include actuation at the hips. In the 2012 study by Kurokawa et al.[51], actuators were positioned at the ankle and hip joints, with no motorized assistance at the knees. The specific joint movements supported by the motors are described in the section "Targeted muscle groups and movements". Alongside motor assistance and FES, most studies also used additional walking aids, such as a walker or crutches, to provide trunk stability and balance support.

3.3.2 FES configuration

Targeted muscle groups and movements Among the four studies with bidirectional motors at the hip and

knee, three tested the device only on the left leg, with FES applied to the quadriceps of that leg[46, 47, 48].The intended effect of FES was to support knee extension while reducing motor torque demand. In these setups, the contralateral leg was fully driven by motors, and in the stimulated leg, hip and knee flexion and extension were also assisted by the motors to minimize quadriceps fatigue. The remaining study with bidirectional motors at both hip and knee joints applied FES to quadriceps and hamstrings on both sides [49]. This configuration aimed to generate knee flexion and extension, with torque distributed between motors and FES. In the study by Kurokawa et al.[51], multiple lower limb muscles were stimulated: the gastrocnemius and soleus (triceps surae) during late stance to produce ankle plantarflexion for push-off and to assist knee flexion at the start of swing; the tibialis anterior and extensor digitorum longus during swing to generate ankle dorsiflexion for foot clearance; and the quadriceps during stance for knee stabilization. In addition to FES, a servo-motor at the hip provided forward progression, and an ankle actuator supported push-off when muscle performance declined.In this study, no powered knee joints were included, so stance stability relied on the mechanical support of the orthosis, while walking trials were conducted within parallel bars for additional balance assistance. In the study by del-Ama et al.[50], which used a KAFO, the quadriceps and knee flexors were stimulated by FES to generate knee flexion and extension. Actuators at the knee joints were placed to assist these movements.

FES parameters In half of the experimental studies, a separate pre-walking experiment was conducted before the walking tests were performed[50, 46, 47]. In the study by del-Ama et al.[50], a stimulation test was performed to evaluate the muscular response and to familiarize the patient with the stimulation. Similarly, Iyer et al.[46] and Sun et al.[47] conducted seated knee extension experiments prior to the overground walking trials. In the study by Iyer et al.[46], this test was used to examine the controller's performance under fatigue and to validate its adaptive behavior prior to walking. In contrast, the aim of the seated test in the study by Sun et al.[47] was to investigate FES-induced muscle fatigue and to validate ultrasound-based fatigue measurements.
This section focuses specifically on the FES parameters used during the walking experiments. As summarized in Table 2, only three studies, by Lambeth et al.[48], Alibeji et al.[49], and Kurokawa et al.[51], reported their stimulation parameters of FES for overground walking. Alibeji et al.[49] and Kurokawa et al.[51] both provided specific information on the FES parameters used during walking, which can be seen in Table 2. In the study by Lambeth et al.[48], the stimulation amplitude was adaptively scaled using a normalized controller input within a subject-specific amplitude range. The minimum and maximum values of this range were determined per participant but not reported. Other FES parameters, such as frequency and pulse width, were also not specified in this study.

3.3.3 FES and motor control strategies

Between the studies, the control strategies vary widely between them. This paragraph categorizes the studies according to the type of control strategy employed.

Model Predictive Control: Model Predictive Control (MPC) is a control technique which uses a mathematical model to predict future system behavior and determines optimal control actions. In three of the included studies that use MPC, it is used to calculate the optimal distribution of effort between the electrical motor and FES.
Two out of the three studies that use MPC, from Lambeth et al.[48] and Iyer et al.[46], used ultrasound (US) imaging for fatigue measurements. However, the results of the ultrasound images were only used for real-time adjustments of the hybrid control in one of the two studies.
In the study by Lambeth et al.[48], ultrasound images were collected before and after each trial to quantify quadriceps fatigue progression. These measurements were used to evaluate fatigue progression but did not inform the control strategy during the experiment itself. Instead, during walking, fatigue was estimated using a musculoskeletal model within the Model Predictive Control (MPC) framework. This model incorporates real-time data on joint position, velocity, and muscle activation, and the fatigue estimates are derived from predefined model parameters. In this study, the MPC cost function prioritized position and velocity tracking over fatigue compensation, leading to increased FES dosage over time as muscle efficiency decreased.
For enhancing stability during walking, a RISE (Robust Integral of the Sign of the Error) controller is used, which is a feedback controller that corrects for tracking errors and unexpected disturbances in real time, ensuring a smooth knee movement. In the study by Lambeth et al.[48], the importance of fatigue tracking is demonstrated, suggesting that future implementations should place greater emphasis on real-time fatigue adaptation to improve muscle recovery and reduce power consumption.
In the other study by Iyer et al.[46], real-time ultrasound imaging was used to monitor FES-related muscle contractility and fatigue, due to direct visualization of muscle fibers. Changes in muscle strain served as biomarkers of FES-induced fatigue. To integrate these measurements into the control strategy, a sample-data observer (SDO) structure is proposed, which incorporates the real-time US measurement into a pre-existing mathematical fatigue model. This is embedded within a MPC framework, allowing the hybrid exoskeleton to adjust FES intensity and motor torque based on muscle fatigue during each stride. In the experiment in this study, the MPC algorithm was implemented on the left knee during knee flexion and extension of the swing phase, while the right knee and both hips were controlled by a RISE controller.
The remaining study, from Sun et al.[47], applied tube-based nonlinear MPC, which maintains system trajectories within a bounded region, combined with a Lyapunov-based terminal controller to ensure feasibility and stability even when muscle reaction changes or FES becomes less effective. Additionally, a nonlinear feedback controller was included to handle discrepancies between actual and desired knee joint angles. In this study, the control strat-

egy is also optimized based on fatigue, which is estimated using a predictive model. Unlike the studies by Lambeth et al.[48] and Iyer et al.[46], fatigue was not measured in the muscles but estimated based on literature.

Finite State Machine: Two studies, of del-Ama et al.[30] and Alibeji et al.[49], used Finite State Machine (FSM) for the control strategy, which divides the gait cycle into gait phases and activates the appropriate control rules for each phase.
In the study by Alibeji et al.[49], a Finite-State Machine is used to determine which trajectories and synergy activations, muscle coordination patterns, of the gait cycle is used, that is, either half right step state, full left step, or full right step. Between these active states, a standby state is activated by default, in which the motors at the joints hold their positions and the synergy activations are set to zero. Within each active state, an extended, adaptive synergy-based controller with dynamic postural synergies is used to distribute the control effect to the hybrid actuation structure, FES and the motors.
These dynamic postural synergies are artificially generated through an optimization process. Each time-invariant synergy is designed to produce a specific lower-limb posture, for example hip extension or knee flexion. A synergy represents a fixed combination of muscle activations that work together to achieve a functional action. When several of these postural synergies are combined using time-varying activation weights, the controller is able to reconstruct smooth, coordinated walking movements, particularly for generating the swing phase of gait.
To address several challenges inherent to a hybrid FES-exoskeleton system, additional control mechanisms were incorporated. A Dynamic Surface Control (DSC) scheme was used to improve robustness in the presence of model uncertainties and mixed actuator dynamics. An electromechanical delay (EMD) compensation term was added to correct for the time lag between FES activation and muscle force generation, ensuring better timing. Additionally, a model-based fatigue estimate scaled the feedforward control to reduce reliance on fatigued muscles and shift effort to the exoskeleton motors. It is important to note that in this study by Alibeji et al., the clinical overground walking trial was conducted only with FES in combination with a walker, supported by a separate theoretical simulation study with a powered exoskeleton model. Thus, both a physical experiment and a theoretical experiment were performed separately.
In the study of del-Ama et al.[50], the control strategy is managed by a Finite State Machine that synchronizes FES and robotic actuation during the different phases of the gait cycle. During stance phase, a high stiffness is applied by the exoskeleton through a stiffness modulation strategy, stabilizing the knee. In the swing phase, stiffness is reduced to promote knee flexion driven by FES. Force sensing resistors are used to monitor floor contact, which in dicates the beginning of the stance phase, while custom force sensors measure interaction torques, which represents the force exchange between FES and the exoskeleton. As muscle fatigue develops, muscle performance decreases, leading to an increase in interaction torque. A muscle fatigue estimator, based on these interaction torque measurements, can trigger a fatigue compensation strategy by reducing the FES stimulation rate and increasing robotic assistance. This adaptive control prioritizes muscle activation while providing robotic support when muscles cannot achieve the target flexion angle for effective swing of the leg.

Predefined gait patterns with real-time feedback: The control strategy of the study from Kurokawa et al.[51] is based on a predefined gait pattern with real-time feedback. To maintain synchronization with the predefined gait cycle, foot switches detect events within the stride cycle, triggering adjustments in stimulation timing to match the expected walking pattern. Additionally, real-time feedback is obtained through the M-wave, an electrical response measured directly from the muscles, which is used to monitor muscle output and adjust FES intensity when necessary.

3.3.4 Aims and experimental outcomes of the studies

Two of the six studies focused primarily on quadriceps fatigue and how this could be integrated into the control strategy [48, 46]. Lambeth et al.[48] concluded that their model predictive control approach did not sufficiently prioritize fatigue, resulting in fatigue. Iyer et al.[46] reported short walking trials of about 10 steps in which their ultrasound-based control strategy was implemented, demonstrating feasibility but without extensive gait outcomes. The remaining studies tested different hybrid control strategies in walking trials. Sun et al.[47] confirmed walking feasibility with their tube-based NMPC approach, although issues such as early heel contact and tracking errors were observed. Alibeji et al.[49] demonstrated quasi-static walking with well-timed stimulation and minimal fatigue, but provided limited detail on walking performance. Del-Ama et al.[50] reported that their participant successfully completed a six-minute walking test without adverse effects, indicating tolerability of the hybrid cooperative control strategy. Finally, Kurokawa et al.[51] showed that after three months of training, walking time improved from less than five to more than five minutes, with reduced effort and fewer spasticity episodes. They emphasized, however, that continuous monitoring of fatigue is required to further improve gait quality, which was not described in detail.

Article	Exoskeleton Type	Simulation Tool	Energy Storing Mechanism	Joint Locking Mechanisms	Muscles Stimulated (movement)	FES Parameters	FES Control Strategy
Gustafson 2024 [31]	Pseudo-passive exoskeleton	CREO Parametric	Knee and hip springs	Knee and hip brakes	Quadriceps(knee extension)	τ_{stim}=15 Nm	Feedforward control
Brown 2022 [33]	Energy-storing exoskeleton (ESE)	N.A.	Gas springs	Bidirectional clutch mechanisms for knee and hip	Quadriceps(knee extension)	N.R.	Feedforward control
Ullah 2020 [34]	Energy storing orthosis (ESO)	Simscape Multibody	Energy units at hip and knee	Unidirectional clutch mechanisms for knee and hip	Quadriceps(knee extension)	τ_{stim}=7 Nm	Feedforward control
Boughner 2014 [32]	ESO	SimMechanics and MATLAB	Hip, knee and energy transfer spring	Knee and hip wrap spring brakes	Quadriceps(knee extension)	τ_{stim}=15 Nm	Feedforward control
Sharma 2014 [43]	Orthosis	CVX convex optimization MATLAB toolbox	N.A.	Knee brake	Hip and knee flexors and extensors(hip and knee flexion and extension)	N.R.	N.A.
Sharma 2014 [36]	Knee-ankle-foot orthosis (KAFO)	N.A.	N.A.	Inbuilt spring clutch mechanism for knee	Hip and knee flexors and extensors(hip and knee flexion and extension)	In arbitrary units	Optimization-based control
Huq 2012 [42]	Spring brake orthosis (SBO)	vN4D and MATLAB/Simulink	Knee spring	Knee brake	Quadriceps(knee extension)	PW modulation with f=25Hz	Closed-loop control
Sharma 2012 [44]	KAFO	Optimization toolbox MATLAB	N.A.	Knee brake	Hip and knee flexors and extensors(hip and knee flexion and extension)	In arbitrary units	Optimization-based control
Sharma 2011 [45]	KAFO	MATLAB Optimization	N.A.	Knee brake	Hip and knee flexors and extensors(hip and knee flexion and extension)	In arbitrary units	Optimization-based control
Jailani 2011 [37]	SBO	Vn4D and MATLAB/Simulink	Knee spring	Knee and hip brake	Quadriceps(knee extension)	N.R.	Closed-loop control
Jailani 2011 [38]	SBO	Vn4D and MATLAB/Simulink	Knee spring	Knee and hip brake	Quadriceps(knee extension)	PW modulation with f=33Hz	Closed-loop control
Jailani 2010 [39]	SBO	Vn4D and MATLAB/Simulink	Knee spring	Knee and hip brake	Quadriceps(knee extension)	PW modulation with f=33Hz	Closed-loop control
Jailani 2010 [40]	SBO	Vn4D and MATLAB/Simulink	Knee spring	Knee and hip brake	Quadriceps(knee extension)	PW modulation with f=33Hz	Closed-loop control
Jailani 2010 [41]	SBO	Vn4D and MATLAB/Simulink	Knee spring	Knee and hip brake	Quadriceps(knee extension)	PW modulation with f=33Hz	Closed-loop control
Kangude 2010 [35]	ESO	N.A.	Pneumatic system and rubber bands	Hip and knee brakes	Quadriceps(knee extension)	N.R.	Feedforward control

Table 1: *Data extraction of theoretical studies on fully passive FES-orthotic devices*

Notes: N.A.=not applicable, N.R.=not reported, PW=pulse width, τ_{stim} = stimulation torque generated by FES, f = stimulating frequency

Article	Aim of study	Outcomes	Conclusions
Gustafson 2024 [31]	Simulate an exoskeleton using upper-body input and FES of the quadriceps with energy storage.	Required torques are within achievable range; Step lengths 275–450 mm and speeds of 0.18–0.23 m/s.	Can enable standing and stepping exercise in simulation after SCI; performance is comparable to powered exoskeletons.
Brown 2022 [33]	Redesign a FES-exoskeleton for lighter weight and improve joint control, enabling standing and walking.	40% weight reduction of exoskeleton (estimated now to be 10.2 kg); hip and knee movement range meets intended design; joint torques are not tested.	The new design is expected to reduce muscle fatigue and device weight. Joint lock design is still in development.
Ullah 2020 [34]	Reducing torque required from the quadriceps by reducing the step size while maintaining the condition of toe clearance.	Estimated quadriceps torque requirement is reduced from 23 Nm to 7 Nm for a 49 cm step length.	Smaller step sizes can lower FES torque demands while preserving toe clearance.
Boughner 2014 [32]	Determine the feasibility of a new exoskeleton design, focusing on the novel hip and knee joint mechanisms, to guide further development.	Design and static analysis met specifications for size, weight, and required locking torque. Predicted step cycle time of 2.7 s with 15 Nm quadriceps torque.	Concept seems feasible for accomplishing gait.
Sharma 2014 [43]	Develop a nonlinear estimation algorithm for estimating lower limb segment angles during walking in a FES-exoskeleton.	SDC-based estimator (IMU-based) showed improved performance compared to an EKF-like estimator, with faster convergence; robust to model uncertainties and IMU noise/bias.	The proposed SDC-based nonlinear estimator can accurately estimate lower limb segment angles in simulation and may be useful for controlling hybrid FES–orthosis systems.
Sharma 2014 [36]	Determine optimal control inputs, joint trajectories, step length and walking speed for an FES–orthosis walking system, using dynamic optimization without relying on able-bodied gait data.	Optimal step length 0.43–0.46 m; steady-state angular velocity 0.25–0.35 rad/s. Absence of dorsiflexion led to 20° hip/knee flexion overshoot and higher hip torques vs. able-bodied gait.	The models yielded optimal gait parameters and showed deviations from able-bodied gait. The frameworkmay guide stimulation profiles or serve as reference trajectories for closed-loop control.
Huq 2012 [42]	To develop closed-loop control schemes for FES-induced knee extension in SBO, and to evaluate their ability to minimize muscle fatigue using GA and MOGA optimization.	Cycle-to-cycle control achieved full extension. PID: smoother stimulation, leading to reduced fatigue. FLC: accurate tracking. Part-time closed-loop also effective.	The control approaches are feasible for controlling FES-induced knee extension. FLC offers better accuracy, PID reduces muscle fatigue.
Sharma 2012 [44]	Develop a walking model for FES-orthosis walking that incorporates a finite double support phase and use this model to design new optimal gait trajectories that reduce muscle fatigue and metabolic energy consumption.	The new model produced convergent optimal gait trajectories after 3 steps, with reduced muscle activations and arm reaction forces.	A finite DSP model combined with a single support model generated stable and efficient hybrid FES–brace gait patterns in simulation. It can guide the design of gait strategies aimed at reducing muscle fatigue and metabolic cost, potentially.
Sharma 2011 [45]	Develop a walking model for a FES-based KAFO to design gait trajectories that reduce muscle fatigue and lower metabolic energy consumption.	Simulations of 10 steps produced feasible gait trajectories with minimizing both muscle activations and upper-body effort.	The model can generate efficient gait patterns for hybrid FES–brace walking without relying on able-bodied gait data. This approach is promising for control strategies that limit fatigue and energy cost.
Jailani 2011 [37]	Improve a SBO-FES-assisted walking system by implementing FSC to automatically manage the transitions between gait phases.	FSC improved timing of knee and hip brakes. Knee trajectories and stimulation profiles between FSC and manual control showed similarities, but FSC ensured more consistent and accurate gait phase transitions.	FSC ensured accurate timing with gait phase switching. The method is simple, practical for implementation, and robust to disturbances. FSC may be integrated with FLC in future applications to regulate knee extension.
Jailani 2010 [41]	To replace the withdrawal reflex and aiming for stable gait and reduced muscle torque demands compared to walking without SBO.	Simulations showed PID enabled correct timing of quadriceps stimulation. Quadriceps torque is reduced by 11.5% and hamstring torque is eliminated vs. walking without SBO.	SBO replaces withdrawal reflex through spring–brake mechanism for hip and knee flexion. PID control achieved stable gait with reduced muscle torque compared to walking without SBO.
Kangude 2010 [35]	To design and bench-test a prototype of a FES-integrated ESO, aiming to reduce muscle fatigue and improve stability.	Bench tests showed brakes exceeded target torque (60 vs. 40 Nm) and pneumatic storage matched predictions (9.6 J vs. 10 J). Pre-clinical test (1 T12 SCI) confirmed safe standing, good fit, and torque within design limits.	The prototype is mechanically feasible, meets key design goals, and is safe for standing. Slightly reduced energy storage due to brace deformation, but suitable for future walking trials.

Table 2: *Summary extraction of theoretical studies on fully passive FES-orthotic devices*

Notes: SDC=state-dependent coefficient, IMU=intertial measurement unit, EKF=extended Kalman filter, SBO=spring brake orthosis, GA=genetic algorithm, MOGA=multi-objective generatic algorithm, FLC=fuzzy logic controller, PID=proportional-integral-derivative controller, KAFO=knee-ankle-foot orthosis, FSC=finite state controller, ESO=energy-storing orthosis.
Three earlier studies by Jailani et al.[38, 39, 40] were not included in this table, as they preceded and largely overlapped in aims and outcomes with the 2011 study by Jailani et al.[38].

Article	Exoskeleton Type	Subjects	Muscles Stimulated (movement)	Motor placement	FES Parameters	FES Control Strategy
Lambeth 2024 [48]	INDEGO, Ekso Bionics	1 subject with SCI	Quadriceps(knee extension)	Bidirectional motors at hip and knee joints	Subject-specific range for FES amplitude	Model Predictive Control
Iyer 2024 [46]	INDEGO (Ohio, USA)	2 subjects with SCI	Quadriceps(knee extension)	Bidirectional motors at hip and knee joints	N.R.	Model Predictive Control
Sun 2023 [47]	INDEGO, Ekso Bionics	1 subject with iSCI (T10, AIS C)	Quadriceps(knee extension)	Bidirectional motors at hip and knee joints	N.R.	Model Predictive Control
Alibeji 2018 [49]	N.R.	1 subject with iSCI (T10, AIS A)	Quadriceps and hamstrings(knee flexion and extension)	Bidirectional motors at hip and knee joints	f=35Hz, t_p=400 µs	Finite State Machine
Del-Ama 2015 [50]	Kinesis: bilateral KAFO	1 subject with iSCI (L4, AIS D)	Quadriceps and hamstrings(knee flexion and extension)	Active actuators at knee hinges	N.R.	Finite State Machine
Kurokawa 2012 [51]	Custom-built walking assistive system	2 subjects with iSCI (C5)	Gastrocnemius, soleus(ankle plantairflexion and knee flexion), tibialis anterior, extensor digitorum longus(ankle dorsiflexion) and quadriceps(knee extension)	Actuator at ankle and hip	f_{burst}=5kHz, t_s=2.4 ms, f=20 Hz	Predefined gait patterns with real-time feedback

Table 3: *Data extraction of experimental studies on semi-passive FES-orthotic devices*

Notes: AIS=ASIA (American Spinal Injury Association) Impairment Scale, iSCI=incomplete SCI, N.A.=not applicable, N.R.=not reported, f_{burst} = burst frequency, f = stimulating frequency, t_s = stimulating duration, t_p = pulse width.

Article	Aim of study	Outcomes	Conclusions
Lambeth 2024 [48]	To evaluate quadriceps fatigue in a hybrid exoskeleton with MPC, comparing FES-only (with exoskeleton), exoskeleton-only, and hybrid conditions.	Muscle efficiency increased in exoskeleton-only (+0.218), but decreased in FES-only (–0.250) and hybrid MPC (–0.281), showing hybrid fatigue comparable to FES-only. Hybrid MPC increased FES use by 33%, closely linked to declining efficiency (R^2=0.96). Hybrid-MPC reduced mean motor torque by 9.6% compared to exoskeleton-only.	Hybrid MPC maintained joint performance but prioritized movement over fatigue, leading to fatigue comparable to FES-only. Future control should better account for fatigue.
Iyer 2024 [46]	To test real-time ultrasound of quadriceps strain for detecting FES-induced fatigue and use this to optimize shared control by adjusting FES–motor allocation during walking.	Ultrasound fatigue estimates differed <7% from dynamometer (golden standard). The ultrasound feedback made MPC more sensitive to fatigue, reducing FES dosage, increasing motor support, and lowering power use while maintaining knee tracking.	Real-time ultrasound fatigue detection was validated and integrated into MPC for hybrid control. Shown in continuous leg extension and walking ($\geq$ 10 steps/trial). Walking quality not reported.
Sun 2023 [47]	To develop a robust NMPC strategy for limb tracking and fatigue regulation in a hybrid exoskeleton, by optimally distributing FES-motor effort.	NMPC maintained knee tracking by shifting effort from FES to motor as fatigue increased. In post-fatigue trials, FES dropped ∼29% and motor rose ∼13%. Walking feasibility was shown, but SCI participant had higher tracking errors due to insufficient hip motor torque, causing early heel contact.	Tube-based NMPC redistributed control to manage fatigue and reduce FES use, potentially delaying fatigue in longer use. Walking feasibility was confirmed, though insufficient hip motor torque leaded to early heel contact and higher tracking errors.
Alibeji 2018 [49]	To develop and test a muscle synergy–inspired control strategy to coordinate FES and exoskeleton motors, for multi-joint gait.	In simulation and in a participant with incomplete SCI, synergy-based control improved tracking and reduced motor energy use vs. motor-only. Walking trials with a simplified synergy-based version, showed well-timed stimulation; minimal fatigue due to preserved voluntary control.	Synergy-based control coordinated FES and motors for quasi-static walking, addressing redundancy, actuator dynamics, electromechanical muscle delay, and fatigue. Simulation and experiment confirmed feasibility for hybrid neuroprostheses.
Del-Ama 2015 [50]	To assess feasibility of hybrid cooperative control in the exoskeleton, adapting FES and robotic assistance to manage fatigue, electromechanical delays, and pathological gait.	The participant completed the 6MWT without adverse effects. After one day of training, he could operate Kinesis. The hybrid controller compensated for limited left-knee extension and excessive right-knee flexion during stance, and fatigue detection adapted stimulation intensity effectively.	The cooperative control was well tolerated and compensated bilateral pathological gait patterns by autonomously increasing knee flexor stimulation and robotic stiffness.
Kurokawa 2012 [51]	To assess quasi-passive reciprocal FES walking and evaluate M-wave based force feedback for stabilising muscle output and address fatigue.	In the subject, FES improved ankle dorsiflexion and foot clearance, due to increased hip and knee flexion. After 3 months' training, walking time improved from <5 to >5 min with less effort; spasticity episodes reduced.	Quasi-passive FES walking was feasible; selective soleus/gastrocnemius stimulation improved gait. M-wave feedback showed potential for fatigue management, but continuous monitoring of fatigue is needed to fully address fatigue in clinical use.

Table 4: *Summary extraction of experimental studies on semi-passive FES-orthotic devices*

Notes: MPC=model predictive control, NMPC=non-linear model predictive control, 6MWT=6-minute walking test

4 Discussion

4.1 Summary of results

This review provides an overview of the different design concepts and control strategies proposed in studies that integrate FES with passive or semi-passive orthotic devices to support gait in individuals with SCI. Fully passive orthoses relying solely on FES remain theoretical and have not been clinically tested. In contrast, hybrid systems combining FES with actuators show some preliminary results in small trials, suggesting they might help maintain gait patterns while also compensating for muscle fatigue.

4.1.1 Mechanical design

The studies focusing on fully passive orthotic devices were all theoretical and addressed mechanical design strategies to minimize the reliance on FES and thereby reduce the likelihood of rapid muscle fatigue. To achieve this, two key design features were frequently explored: energy storage mechanisms and joint locking systems.
For energy storage, the most common approach involved integrating springs at the knee and hip joints. These springs store energy during muscle-induced extension and release it to facilitate and assist flexion during the swing phase. This passive support helps reduce the activation needed from the stimulated muscles.
Regarding joint locking and unlocking, various mechanisms were proposed that allow the joints to move freely in one direction while locking them in the opposite direction during specific phases of the gait cycle, such as during stance, to provide stability and minimize unnecessary muscle activation. Correct timing of locking and unlocking is critical to ensure safe and effective support throughout the gait cycle.
To control these locking systems, the reviewed studies described three main approaches. First, actively controlled mechanisms, where small servo motors, PWM-controlled solenoids, or microcontrollers are used to operate the brakes electronically. Second, user-triggered control, where the locks are engaged or disengaged based on user actions such as pressing a hand switch, shifting upper body weight, or changes in joint angular velocity. Third, state- and time-based control, in which predefined timing schemes or a Finite State Controller (FSC) coordinate the activation of brakes in sync with the gait phases.
While these mechanical strategies present promising ways to support gait with minimal stimulation from FES, none have been validated in walking trials with individuals with SCI.

4.1.2 FES configuration and control strategies

In addition to mechanical design, effective FES configuration and control are essential to synchronize muscle activation with orthosis mechanics and to manage muscle fatigue.

FES parameters Among the included studies, various FES parameter settings were described. However, the way these were reported differed widely, making comparisons challenging. Some studies specified target joint torques to be generated by FES, others provided stimulation intensities in arbitrary units, and a few reported detailed parameters such as frequency and pulse width. In the experimental studies, explicit parameter reporting was also inconsistent, with some studies describing subject-specific ranges and others providing specific values.

FES control strategies With respect to control strategies, three categories are distinguished in this review for theoretical studies and the hybrid systems separately, so six categories in total.
FES control strategies in theoretical studies: In the theoretical studies, control strategies were generally categorized as feedforward control, closed-loop control, or optimization-based control. Feedforward control involved predefined thresholds or fixed events within the gait cycle to trigger muscle stimulation, often implemented as a preprogrammed sequence without real-time adaptation. Closed-loop control strategies, on the other hand, dynamically adjusted stimulation parameters in response to sensor feedback using Proportional-Integral-Derivative (PID) controllers, Fuzzy Logic Controllers (FLC), Genetic Algorithms (GA), or Finite State Controllers (FSC). These approaches aimed to improve tracking accuracy and adapt stimulation to variations in joint motion. Optimization-based control relied on mathematical models and cost functions to compute optimal stimulation profiles, joint trajectories, and arm reaction forces aimed at producing energy-efficient, fatigue-minimizing gait patterns.
FES control strategies in experimental studies: For the hybrid systems, three categories were identified. Model Predictive Control (MPC)is a technique that uses a mathematical model to predict future system behavior and compute optimal distributions of effort between FES and motor assistance. In some studies, ultrasound imaging was incorporated to estimate muscle fatigue, with one study using these measurements in real time to adjust control actions, while another used ultrasound to quantify fatigue progression for later analysis, and in which they applied a predictive model estimating fatigue progression. A second control strategy employed in experimental studies was the use of a Finite State Machine (FSM), which divides the gait cycle into phases and activates appropriate control rules to coordinate FES and motor engagement accordingly. Finally, one study implemented predefined gait patterns combined with real-time feedback, where muscle output was monitored through M-wave measurements.

4.2 Interpretation and practical implications

When interpreting the reviewed studies, it becomes clear that integrating FES with passive or semi-passive orthoses appears technically feasible, but the evidence remains at an early stage. Theoretical studies primarily explored design concepts and control strategies in simulation. These models demonstrated that energy-storing mechanisms, joint-locking systems, and advanced control approaches could reduce muscle torque demands [33, 41, 42, 44, 45] and generate more optimal gait trajectories [44, 45]. Optimization- and control-based methods further showed potential to improve stimulation timing, enable smoother gait-phase transitions [37], and reduce

muscle fatigue [37, 42]. Although these results suggest feasibility, they were all derived from models, leaving their clinical results uncertain. Experimental studies confirmed that integrating FES with semi-passive orthoses is feasible in practice, but under specific and controlled conditions. In some studies, participants were able to complete short walking trials, ranging from about 10 steps to six minutes, demonstrating that stimulation could be synchronized with orthotic support to enable repeated stepping. Some clinically relevant outcomes were also reported, such as successful completion of a six-minute walk test without adverse effects using the Kinesis hybrid cooperative control strategy [50], and reductions in effort and spasticity after three months of training two to three times per week, after which walking duration increased from less than five to more than five minutes using their developed hybrid FES walking system [51]. At the same time, several limitations were consistently observed, including rapid muscle fatigue that was not sufficiently prioritized in the control strategy [48], tracking errors [47], limited endurance, and the frequent absence of detailed gait quality assessments. Moreover, most studies involved single participants, very short walking distances, and highly controlled laboratory environments, limiting the generalizability of the findings to rehabilitation practice. Compared to the earlier review by del-Ama et al. in 2012[30], recent research has made progress in refining control strategies and addressing fatigue-related challenges, but robust clinical evidence remains limited. The reviewed studies indicate that FES can contribute meaningfully to gait when combined with mechanical support, particularly in generating knee extension with FES, while orthotic structures provide stability during stance. However, the translation from promising simulations and proof-of-concept trials to robust clinical applications remains hindered by muscle fatigue, small sample sizes, and the complexity of coordinating stimulation with mechanical assistance. Future research should therefore prioritize larger-scale experimental validation, including systematic assessments of gait quality, endurance, and long-term usability. If these challenges are addressed, combining FES with lightweight orthotic devices may offer a cost-effective and accessible alternative to fully powered exoskeletons, with the additional benefit of promoting active muscle engagement.

4.3 Strengths and limitations

A key strength of this review is its comprehensive and systematic search strategy across multiple databases, which ensured broad coverage and systematic screening of relevant literature and an up-to-date overview of the field. In addition, by focusing specifically on studies that integrate FES with passive or semi-passive orthotic devices for gait support in individuals with SCI, this review covers a clear and clinically relevant niche that has been less studied than fully powered exoskeletons.

However, there are also some limitations to consider. Some potentially relevant studies have been excluded, such as those investigating hybrid exoskeletons that combine FES with motorized components but do not explicitly apply a muscle-first approach. Similarly, studies involving healthy participants or purely theoretical work on muscle-first systems were not included, even though they might offer useful technical insights. Another limitation is that all study selection and data extraction were performed by a single reviewer, which may introduce a risk of selection bias or overlooked details. Finally, the heterogeneity among the included studies, in terms of control strategies, the reporting of FES parameters, and experimental conditions, makes it difficult to directly compare outcomes or to determine which specific strategies might hold the greatest potential for improving gait in individuals with SCI.

4.4 Future recommendations

Future research should focus on conducting clinical trials with SCI participants to evaluate the feasibility, usability, and practical limitations of FES-assisted passive and hybrid orthotic systems, particularly regarding muscle fatigue. Several studies emphasize the disadvantages of FES, such as limited control over muscle activation and rapid fatigue of muscles, which have motivated the development of hybrid systems in these studies with motorized components to address these challenges more effectively[52, 53, 54].

In a review by Karimi et al.[55], several additional practical limitations of current hybrid exoskeletons are highlighted, including difficulties in optimally placing electrodes, inconsistent stimulation, and the time-consuming process of donning and doffing orthoses with the electrodes attached. Cross-stimulation of unintended muscle groups has also been reported. These considerations underline the importance of assessing whether newly proposed systems overcome these issues and of testing such improvements under realistic conditions.

Additionally, emerging technologies such as brain-computer interfaces (BCIs), spinal cord stimulation, artificial intelligence applications and other neuromodulation approaches are increasingly being explored to support gait rehabilitation for individuals with SCI. Some of these techniques are already being combined with FES. For example in a study by King et al.[56], an electroencephalogram (EEG)-based BCI is developed to control a FES system for overground walking and assessed in an individual with paraplegia due to SCI. A recent review by Tao et al.[57] further highlights the progress of AI research, discussing intelligent robots and limb exoskeletons for rehabilitation training, as well as the integration of BCIs, neuromodulation, and noninvasive electrical stimulation with AI for motor function recovery.

Exploring these innovations alongside FES could broaden the field and offer new opportunities to improve walking function and independence for people with SCI.

Future work should focus on integrating emerging control techniques, intelligent sensing, and powered actuation where needed, to balance muscle engagement and external assistance optimally.

5 Conclusion

This review summarized existing concepts that integrate Functional Electrical Stimulation (FES) with passive and semi-passive orthotic devices for gait support in individuals with spinal cord injury (SCI). The included studies illustrate a range of design principles and control strategies aimed at reducing muscle torque demands, mitigating

fatigue, and enabling functional stepping. Fully passive FES–orthosis systems remain limited to theoretical models, which consistently suggest technical feasibility but lack experimental validation. Approaches that combine FES with actuators have been tested in small pilot studies, showing that synchronization of stimulation with mechanical support is possible and can enable short walking trials, from a few steps to functional tests such as the six-minute walk test. These findings indicate that FES can meaningfully contribute to gait generation, particularly supporting knee extension with FES, while orthotic structures provide stance stability.

At the same time, challenges remain. Muscle fatigue, limited endurance, the complexity of coordinating stimulation with mechanical assistance, as well as the small and laboratory-based nature of existing trials, currently hinder translation to clinical practice. To move towards clinical translation, larger-scale trials and improving adaptive control strategies must be prioritized. FES-assisted orthotic devices could then offer a cost-effective and more accessible alternative to fully powered exoskeletons, combining functional gait support with the added benefit of promoting active muscle engagement and additional physical and mental health benefits.

References

[1] Maynard FM, Bracken MB, Creasey G, Jr JFD, Donovan WH, Ducker TB, et al. International Standards for Neurological and Functional Classification of Spinal Cord Injury. Spinal Cord. 1997 May;35(5):266–274. Available from: http://dx.doi.org/10.1038/sj.sc.3100432.

[2] Jensen MP, Truitt AR, Schomer KG, Yorkston KM, Baylor C, Molton IR. Frequency and age effects of secondary health conditions in individuals with spinal cord injury: a scoping review. Spinal Cord. 2013 Oct;51(12):882–892. Available from: http://dx.doi.org/10.1038/sc.2013.112.

[3] van den Berg-Emons RJ, Bussmann JB, Stam HJ. Accelerometry-Based Activity Spectrum in Persons With Chronic Physical Conditions. Archives of Physical Medicine and Rehabilitation. 2010 Dec;91(12):1856–1861. Available from: http://dx.doi.org/10.1016/j.apmr.2010.08.018.

[4] Myers J, Lee M, Kiratli J. Cardiovascular Disease in Spinal Cord Injury: An Overview of Prevalence, Risk, Evaluation, and Management. American Journal of Physical Medicine and Rehabilitation. 2007 Feb;86(2):142–152. Available from: http://dx.doi.org/10.1097/phm.0b013e31802f0247.

[5] Bauman WA, Spungen AM. Invited Review Carbohydrate And Lipid Metabolism In Chronic Spinal Cord Injury. The Journal of Spinal Cord Medicine. 2001 Jan;24(4):266–277. Available from: http://dx.doi.org/10.1080/10790268.2001.11753584.

[6] Duckworth WC, Solomon SS, Jallepalli P, Heckemeyer C, Finnern J, Powers A. Glucose Intolerance Due to Insulin Resistance in Patients with Spinal Cord Injuries. Diabetes. 1980 Nov;29(11):906–910. Available from: http://dx.doi.org/10.2337/diab.29.11.906.

[7] Scheel-Sailer A, Wyss A, Boldt C, Post MW, Lay V. Prevalence, location, grade of pressure ulcers and association with specific patient characteristics in adult spinal cord injury patients during the hospital stay: a prospective cohort study. Spinal Cord. 2013 Sep;51(11):828–833. Available from: http://dx.doi.org/10.1038/sc.2013.91.

[8] Chamberlain JD, Buzzell A, Gmünder HP, Hug K, Jordan X, Moser A, et al. Excess burden of a chronic disabling condition: life lost due to traumatic spinal cord injury in a Swiss population-based cohort study. International Journal of Public Health. 2019 May;64(7):1097–1105. Available from: http://dx.doi.org/10.1007/s00038-019-01265-6.

[9] Demirel G, Yilmaz H, Paker N, Önel S. Osteoporosis after spinal cord injury. Spinal Cord. 1998 Dec;36(12):822–825. Available from: http://dx.doi.org/10.1038/sj.sc.3100704.

[10] Garland DE, Stewart CA, Adkins RH, Hu SS, Rosen C, Liotta FJ, et al. Osteoporosis after spinal cord injury. Journal of Orthopaedic Research. 1992 May;10(3):371–378. Available from: http://dx.doi.org/10.1002/jor.1100100309.

[11] Castro MJ, Apple DF, Staron RS, Campos GER, Dudley GA. Influence of complete spinal cord injury on skeletal muscle within 6 mo of injury. Journal of Applied Physiology. 1999 Jan;86(1):350–358. Available from: http://dx.doi.org/10.1152/jappl.1999.86.1.350.

[12] Platz T, Gillner A, Borgwaldt N, Kroll S, Roschka S. Device-Training for Individuals with Thoracic and Lumbar Spinal Cord Injury Using a Powered Exoskeleton for Technically Assisted Mobility: Achievements and User Satisfaction. BioMed Research International. 2016;2016:1–10. Available from: http://dx.doi.org/10.1155/2016/8459018.

[13] Ditunno PL, Patrick M, Stineman M, Ditunno JF. Who wants to walk? Preferences for recovery after SCI: a longitudinal and cross-sectional study. Spinal Cord. 2008 Jan;46(7):500–506. Available from: http://dx.doi.org/10.1038/sj.sc.3102172.

[14] Semerjian T, Montague S, Dominguez J, Davidian A, de Leon R. Enhancement of Quality of Life and Body Satisfaction Through the Use of Adapted Exercise Devices for Individuals with Spinal Cord Injuries. Topics in Spinal Cord Injury Rehabilitation. 2005 Oct;11(2):95–108. Available from: http://dx.doi.org/10.1310/bxe2-mtku-yl15-429a.

[15] Rodríguez-Fernández A, Lobo-Prat J, Font-Llagunes JM. Systematic review on wearable lower-limb exoskeletons for gait training in neuromuscular impairments. Journal of NeuroEngineering and Rehabilitation. 2021 Feb;18(1). Available from: http://dx.doi.org/10.1186/s12984-021-00815-5.

[16] Kobetic R, To CS, Schnellenberger JR, Audu ML, Bulea TC, Gaudio R, et al. Development of hybrid orthosis for standing, walking, and stair climbing after spinal cord injury. The Journal of Rehabilitation Research and Development. 2009;46(3):447. Available from: http://dx.doi.org/10.1682/jrrd.2008.07.0087.

[17] Rae-Duprees J. A Stimulating New Direction for FES. IEEE Pulse. 2022 Nov;13(6):12–16. Available from: http://dx.doi.org/10.1109/mpuls.2022.3227809.

[18] Forrest GP, Smith TC, Triolo RJ, Gagnon J, DiRisio D, Miller ME, et al. Use of the Case Western Reserve/Veterans Administration neuroprosthesis for exercise, standing and transfers by a paraplegic subject. Disability and Rehabilitation: Assistive Technology. 2011 Nov;7(4):340–344. Available from: http://dx.doi.org/10.3109/17483107.2011.629328.

[19] Phillips SM, Stewart BG, Mahoney DJ, Hicks AL, McCartney N, Tang JE, et al. Body-weight-support treadmill training improves blood glucose regulation in persons with incomplete spinal

cord injury. Journal of Applied Physiology. 2004 Aug;97(2):716–724. Available from: http://dx.doi.org/10.1152/japplphysiol.00167.2004.

[20] Griffin L, Decker MJ, Hwang JY, Wang B, Kitchen K, Ding Z, et al. Functional electrical stimulation cycling improves body composition, metabolic and neural factors in persons with spinal cord injury. Journal of Electromyography and Kinesiology. 2009 Aug;19(4):614–622. Available from: http://dx.doi.org/10.1016/j.jelekin.2008.03.002.

[21] Johnston TE, Smith BT, Mulcahey MJ, Betz RR, Lauer RT. A Randomized Controlled Trial on the Effects of Cycling With and Without Electrical Stimulation on Cardiorespiratory and Vascular Health in Children With Spinal Cord Injury. Archives of Physical Medicine and Rehabilitation. 2009 Aug;90(8):1379–1388. Available from: http://dx.doi.org/10.1016/j.apmr.2009.02.018.

[22] Ragnarsson KT. Functional electrical stimulation after spinal cord injury: current use, therapeutic effects and future directions. Spinal Cord. 2007 Sep;46(4):255–274. Available from: http://dx.doi.org/10.1038/sj.sc.3102091.

[23] Ashe MC, Eng JJ, Krassioukov AV, Warburton DER, Hung C, Tawashy A. Response to Functional Electrical Stimulation Cycling in Women With Spinal Cord Injuries Using Dual-Energy X-ray Absorptiometry and Peripheral Quantitative Computed Tomography: A Case Series. The Journal of Spinal Cord Medicine. 2010 Jan;33(1):68–72. Available from: http://dx.doi.org/10.1080/10790268.2010.11689676.

[24] Nash MS, Jacobs PL, Montalvo BM, Klose KJ, Guest RS, Needham-Shropshire BM. Evaluation of a training program for persons with SCI paraplegia using the Parastep®1 ambulation system: Part 5. Lower extremity blood flow and hyperemic responses to occlusion are augmented by ambulation training. Archives of Physical Medicine and Rehabilitation. 1997 Aug;78(8):808–814. Available from: http://dx.doi.org/10.1016/s0003-9993(97)90192-1.

[25] Katz R, Green D, Sullivan T, Yarkony G. Functional electric stimulation to enhance systemic fibrinolytic activity in spinal cord injury patients. Archives of physical medicine and rehabilitation. 1987;68(7):423-6.

[26] Agarwal S, Triolo RJ, Kobetic R, Miller M, Bieri C, Kukke S, et al. Long-term user perceptions of an implanted neuroprosthesis for exercise, standing, and transfers after spinal cord injury. Journal of Rehabilitation Research & Development. 2003;40(3).

[27] Marsolais E, Edwards BG. Energy costs of walking and standing with functional neuromuscular stimulation and long leg braces. Archives of physical medicine and rehabilitation. 1988;69(4):243-9.

[28] Brissot R, Gallien P, Le Bot MP, Beaubras A, Laisné D, Beillot J, et al. Clinical Experience With Functional Electrical Stimulation-Assisted Gait With Parastep in Spinal Cord–Injured Patients. Spine. 2000 Feb;25(4):501–508. Available from: http://dx.doi.org/10.1097/00007632-200002150-00018.

[29] Agarwal S, Kobetic R, Nandurkar S, Marsolais EB. Functional Electrical Stimulation For Walking In Paraplegia: 17-Year Follow-Up Of 2 Cases. The Journal of Spinal Cord Medicine. 2003 Mar;26(1):86–91. Available from: http://dx.doi.org/10.1080/10790268.2003.11753666.

[30] del Ama AJ, Koutsou AD, Moreno JC, de-los Reyes A, Gil-Agudo n, Pons JL. Review of hybrid exoskeletons to restore gait following spinal cord injury. The Journal of Rehabilitation Research and Development. 2012;49(4):497. Available from: http://dx.doi.org/10.1682/jrrd.2011.03.0043.

[31] Gustafson KJ, Durfee WK. A Muscle-Powered Exoskeleton for Weight-Bearing Exercise After a Spinal Cord Injury. In: 2024 10th IEEE RAS/EMBS International Conference for Biomedical Robotics and Biomechatronics (BioRob). IEEE; 2024. p. 1849–1854. Available from: http://dx.doi.org/10.1109/BioRob60516.2024.10719756.

[32] Boughner KJ, Durfee WK. Preliminary design of an energy storing orthosis for providing gait to people with spinal cord injury. In: 2014 36th Annual International Conference of the IEEE Engineering in Medicine and Biology Society. IEEE; 2014. p. 2581–2584. Available from: http://dx.doi.org/10.1109/EMBC.2014.6944150.

[33] Brown E, Ullah YF, Gustafson K, Durfee W. Preliminary Design of Musclae-Powered Exoskeleton for Users with Spinal Cord Injury. In: 2022 Design of Medical Devices Conference. DMD2022. American Society of Mechanical Engineers; 2022. p. N/A. Available from: http://dx.doi.org/10.1115/DMD2022-1013.

[34] Farhat Ullah Y, Durfee WK. Identification of Low Torque Step Sizes for the Design of a Single-Channel Muscle-Powered Hybrid Orthosis for People With Spinal Cord Injury. In: 2020 Design of Medical Devices Conference. DMD2020. American Society of Mechanical Engineers; 2020. p. N/A. Available from: http://dx.doi.org/10.1115/DMD2020-9092.

[35] Kangude A, Burgstahler B, Durfee W. Engineering evaluation of the energy-storing orthosis FES gait system. In: 2010 Annual International Conference of the IEEE Engineering in Medicine and Biology. IEEE; 2010. p. 5927–5930. Available from: http://dx.doi.org/10.1109/IEMBS.2010.5627550.

[36] Sharma N, Mushahwar V, Stein R. Dynamic Optimization of FES and Orthosis-Based Walking Using Simple Models. IEEE Transactions on Neural Systems and Rehabilitation Engineering. 2014 Jan;22(1):114–126. Available from: http://dx.doi.org/10.1109/TNSRE.2013.2280520.

[37] Jailani R, Tokhi MO, Gharooni SC, Jogtaei M. Finite State Control of FES-Assisted Walking with

Spring Brake Orthosis. In: 2011 UkSim 13th International Conference on Computer Modelling and Simulation. IEEE; 2011. p. 183–188. Available from: http://dx.doi.org/10.1109/UKSIM.2011.43.

[38] Jailani R, Tokhi MO, Gharooni SC, Ibrahim BSKK. FES-assisted walking with spring brake orthosis: Simulation studies. Applied Bionics and Biomechanics. 2011;8:115-26. Affiliations: Dept. of Automatic Control and System Engineering, University of Sheffield, UK; Faculty of Electrical Engineering, Universiti Teknologi MARA, Malaysia.

[39] Jailani R, Tokhi MO, Gharooni SC. Spring brake orthosis for FES-assisted walking with wheel walker. In: Computational Intelligence in Business and Economics. World Scientific; 2010. p. 677–685. Available from: http://dx.doi.org/10.1142/9789814324441_0079.

[40] Jailani R, Tokhi MO, Gharooni SC. Fuzzy logic control of knee extension for FES-assisted walking with spring brake orthosis. In: 2010 IEEE International Conference on Systems, Man and Cybernetics. IEEE; 2010. p. 379–385. Available from: http://dx.doi.org/10.1109/ICSMC.2010.5641745.

[41] Jailani R, Tokhi MO, Gharooni SC, Hussain Z. PID Control of Knee Extension for FES-Assisted Walking with Spring Brake Orthosis. In: 2010 Fourth Asia International Conference on Mathematical/Analytical Modelling and Computer Simulation. IEEE; 2010. p. 261–266. Available from: http://dx.doi.org/10.1109/AMS.2010.59.

[42] Huq MS, Tokhi MO. Genetic algorithms based approach for designing spring brake orthosis – Part II: Control of FES induced movement. Applied Bionics and Biomechanics. 2012;9(4):317-31. Available from: https://doi.org/10.3233/ABB-2012-0058.

[43] Sharma N, Dani A. Nonlinear estimation of gait kinematics during functional electrical stimulation and orthosis-based walking. In: 2014 American Control Conference. IEEE; 2014. p. 4778–4783. Available from: http://dx.doi.org/10.1109/ACC.2014.6859342.

[44] Sharma N, Stein R. Gait planning and double support phase model for functional electrical stimulation-based walking. In: 2012 Annual International Conference of the IEEE Engineering in Medicine and Biology Society. IEEE; 2012. p. 1904–1907. Available from: http://dx.doi.org/10.1109/EMBC.2012.6346325.

[45] Sharma N, Stein R. Optimal trajectory planning for a constrained functional electrical stimulation-based human walking. In: 2011 Annual International Conference of the IEEE Engineering in Medicine and Biology Society. IEEE; 2011. p. 603–607. Available from: http://dx.doi.org/10.1109/IEMBS.2011.6090134.

[46] Iyer A, Sun Z, Lambeth K, Singh M, Cleveland C, Sharma N. Real-Time Ultrasound Imaging of a Human Muscle to Optimize Shared Control in a Hybrid Exoskeleton. IEEE Transactions on Robotics. 2024;40:4322–4336. Available from: http://dx.doi.org/10.1109/TRO.2024.3443668.

[47] Sun Z, Iyer A, Lambeth K, Cleveland C, Sharma N. Knee extension tracking and fatigue regulation results using a robust MPC approach in a hybrid exoskeleton. Control Engineering Practice. 2023 Dec;141:105717. Available from: http://dx.doi.org/10.1016/j.conengprac.2023.105717.

[48] Lambeth K, Iyer A, Sharma N. Quantifying Functional Electrical Stimulation-Induced Fatigue via Ultrasound for Hybrid Neuroprosthesis-Based Walking. In: 2024 10th IEEE RAS/EMBS International Conference for Biomedical Robotics and Biomechatronics (BioRob). IEEE; 2024. p. 1617–1622. Available from: http://dx.doi.org/10.1109/BioRob60516.2024.10719933.

[49] Alibeji NA, Molazadeh V, Moore-Clingenpeel F, Sharma N. A Muscle Synergy-Inspired Control Design to Coordinate Functional Electrical Stimulation and a Powered Exoskeleton: Artificial Generation of Synergies to Reduce Input Dimensionality. IEEE Control Systems. 2018 Dec;38(6):35–60. Available from: http://dx.doi.org/10.1109/MCS.2018.2866603.

[50] del Ama AJ, Gil-Agudo Á, Rovira JLP, Moreno JC. A Pilot Study on the Feasibility of Hybrid Gait Training with Kinesis Overground Robot for Persons with Incomplete Spinal Cord Injury. In: Neurotechnology, Electronics, and Informatics. Springer International Publishing; 2015. p. 19–27. Available from: http://dx.doi.org/10.1007/978-3-319-15997-3_2.

[51] Kurokawa N, Yamamoto N, Tagawa Y, Yamamoto T, Kuno H. Development of hybrid FES walking assistive system - Feasibility study. In: The 2012 International Conference on Advanced Mechatronic Systems; 2012. p. 93-7.

[52] Ha KH, Murray SA, Goldfarb M. An Approach for the Cooperative Control of FES With a Powered Exoskeleton During Level Walking for Persons With Paraplegia. IEEE Transactions on Neural Systems and Rehabilitation Engineering. 2016 Apr;24(4):455–466. Available from: http://dx.doi.org/10.1109/TNSRE.2015.2421052.

[53] Kirsch NA, Alibeji NA, Redfern M, Sharma N. Dynamic Optimization of a Hybrid Gait Neuroprosthesis to Improve Efficiency and Walking Duration: A Simulation Study. In: Converging Clinical and Engineering Research on Neurorehabilitation II. Springer International Publishing; 2016. p. 687–691. Available from: http://dx.doi.org/10.1007/978-3-319-46669-9_113.

[54] Hosseinpour S, Ozgoli S, Nekoukar V. Improving energy consumption in Exoped® Lower-limb Exoskeleton by means of Functional Electrical Stimulation. In: 2018 6th RSI International Conference on Robotics and Mechatronics (IcRoM). IEEE; 2018. p.

310–314. Available from: http://dx.doi.org/10.1109/ICRoM.2018.8657585.

[55] Karimi MT. What are the next steps in designing an orthosis for paraplegic subjects? International Journal of preventive medicine. 2012;3(3):145.

[56] King CE, Wang PT, McCrimmon CM, Chou CC, Do AH, Nenadic Z. The feasibility of a brain-computer interface functional electrical stimulation system for the restoration of overground walking after paraplegia. Journal of NeuroEngineering and Rehabilitation. 2015 Sep;12(1). Available from: http://dx.doi.org/10.1186/s12984-015-0068-7.

[57] Tao G, Yang S, Xu J, Wang L, Yang B. Global research trends and hotspots of artificial intelligence research in spinal cord neural injury and restoration—a bibliometrics and visualization analysis. Frontiers in Neurology. 2024 Apr;15. Available from: http://dx.doi.org/10.3389/fneur.2024.1361235.

Appendix A: Search queries per database

Medline

(Exoskeleton Device / OR Orthotic Devices / OR (exoskeleton* OR orthos* OR orthotic*).ab,ti,kw.) AND (Electric Stimulation Therapy / OR ((electr* ADJ3 (stimulat* OR therap*)) OR electrostimulat* OR fes OR electrotherap*).ab,ti,kw.) AND (Gait / OR Walking / OR Walking Speed / OR Mobility Limitation / OR Locomotion / OR Psychomotor Performance / OR (gait* OR walking OR locomot* OR functional* OR mobiliz* OR ambulat* OR (motor* ADJ3 performan*) OR treadmill* OR kinematic*).ab,ti,kw. OR (fes).ti.) AND (Spinal Cord Injuries / OR Paraplegia / OR Quadriplegia / OR ((spinal-cord ADJ3 (trauma* OR injur*)) OR paraplegi* OR tetrapleg* OR quadripleg* OR ((Lower-Limb* OR Lower-extremit* OR leg OR legs) ADJ3 Paraly*)).ab,ti,kw.) NOT (news OR congres* OR abstract* OR book* OR chapter* OR dissertation abstract*).pt. NOT (exp animals/ NOT humans/) AND english.la.

Embase

(exoskeleton/de OR 'exoskeleton (rehabilitation)'/exp OR orthosis/de OR 'hip-knee-ankle-foot orthosis'/de OR 'knee-ankle-foot orthosis'/de OR 'knee orthosis'/de OR 'leg orthosis'/de OR 'walking orthosis'/de OR 'gait orthosis'/de OR orthotics/de OR (exoskeleton* OR orthos* OR orthotic*):Ab,ti,kw) AND ('functional electrical stimulation'/de OR electrostimulation/de OR electrotherapy/de OR 'gait rehabilitation electrical stimulation system'/de OR ((electr* NEAR/3 (stimulat* OR therap*)) OR electrostimulat* OR fes OR electrotherap*):ab,ti,kw) AND (gait/de OR walking/de OR 'walking speed'/de OR treadmill/de OR 'walking difficulty'/de OR 'gait orthosis'/de OR 'functional electrical stimulation'/de OR locomotion/de OR mobilization/de OR 'motor performance'/de OR kinematics/de OR (gait* OR walking OR locomot* OR functional* OR mobiliz* OR ambulat* OR (motor* NEAR/3 performan*) OR treadmill* OR kinematic*):ab,ti,kw OR (fes):ti) AND ('spinal cord injury'/exp OR paraplegia/exp OR quadriplegia/de OR ((spinal-cord NEAR/3 (trauma* OR injur*)) OR paraplegi* OR tetrapleg* OR quadripleg* OR ((Lower-Limb* OR Lower-extremit* OR leg OR legs) NEAR/3 Paraly*)):Ab,ti,kw) NOT [conference abstract]/lim NOT ([animals]/lim NOT [humans]/lim) AND [english]/lim

Web of science

(TS=(exoskeleton* OR orthos* OR orthotic*)) AND (TS=((electr* NEAR/2 (stimulat* OR therap*)) OR electrostimulat* OR fes OR electrotherap*)) AND (TS=(gait* OR walking OR locomot* OR functional* OR mobiliz* OR ambulat* OR (motor* NEAR/2 performan*) OR treadmill* OR kinematic*) OR TI=(fes)) AND (TS=((spinal-cord NEAR/2 (trauma* OR injur*)) OR paraplegi* OR tetrapleg* OR quadripleg* OR ((Lower-Limb* OR Lower-extremit* OR leg OR legs) NEAR/2 Paraly*))) NOT DT=(Meeting Abstract OR Meeting Summary) AND LA=(English)

Cochrane

((exoskeleton* OR orthos* OR orthotic*):Ab,ti,kw) AND (((electr* NEAR/3 (stimulat* OR therap*)) OR electrostimulat* OR fes OR electrotherap*):ab,ti,kw) AND ((gait* OR walking OR locomot* OR functional* OR mobiliz* OR ambulat* OR (motor* NEAR/3 performan*) OR treadmill* OR kinematic*):ab,ti,kw OR (fes):ti) AND (((spinal-cord NEAR/3 (trauma* OR injur*)) OR paraplegi* OR tetrapleg* OR quadripleg* OR ((Lower-Limb* OR Lower-extremit* OR leg OR legs) NEAR/3 Paraly*)):Ab,ti,kw)
("conference abstract":kw OR Trial registry record:pt)
#1 NOT #2

Scopus

(TITLE-ABS-KEY(exoskeleton* OR orthos* OR orthotic*)) AND (TITLE-ABS-KEY((electr* W/2 (stimulat* OR therap*)) OR electrostimulat* OR fes OR electrotherap*)) AND (TITLE-ABS-KEY(gait* OR walking OR locomot* OR functional* OR mobiliz* OR ambulat* OR (motor* W/2 performan*) OR treadmill* OR kinematic*) OR TITLE(fes)) AND (TITLE-ABS-KEY((spinal-cord W/2 (trauma* OR injur*)) OR paraplegi* OR tetrapleg* OR quadripleg* OR ((Lower-Limb* OR Lower-extremit* OR leg OR legs) W/2 Paraly*))) AND NOT DOCTYPE(ab) AND LANGUAGE(English)

IEEE xplore

(exoskeleton OR orthosis OR orthotic) AND ("electrical stimulation" OR "electro therapy" OR electrostimulatation OR electrotherapy) AND (gait OR walking OR locomotion OR functional) AND ("spinal-cord trauma" OR "spinal-cord injury" OR paraplegia OR tetraplegia OR quadriplegia)

Google scholar

exoskeleton—orthosis—orthotic 'electrical stimulation—therapy'—electrostimulatation—electrotherapy gait—walking—locomot
'spinal-cord trauma—injury'—paraplegia—tetraplegia—quadriplegia